DOE/BC/14600-36
Distribution Category UC-122

Chemical Composition Profiles During Alkaline Flooding at Different Temperatures and Extended Residence Time

Topical Report

By
Roshanak Aflaki
Lyman L. Handy

DOE/BC/14600--36
DE93 000107

December 1992

Work Performed Under Contract No. DE-FG22-90BC14600

Prepared for
U.S. Department of Energy
Assistant Secretary for Fossil Energy

Thomas B. Reid, Project Manager
Bartlesville Project Office
P. O. Box 1398
Bartlesville, OK 74005

Prepared by
University of Southern California
Petroleum Engineering Department
Department of Chemical Engineering
Los Angeles, CA 90089-1211

Table of Contents

LIST OF TABLE

LIST OF FIGURES

ABSTRACT

During steamfloods, due to gravity override, steam moves to the upper portion of the reservoir and a hot water zone is formed in the lower portion of the reservoir. Therefore, a large portion of the oil may not be recovered in the lower portion of the reservoir. Injection of caustic along with the steam was proposed to reduce the interfacial tension between the oil phase and the water phase in the hot water zone. In order for caustic to be effective in reducing interfacial tension (IFT) between the water phase and the oil phase, it must preserve the pH above an effective level. The major consideration involved in practical applications of caustic flooding has been whether or not caustic effectively sweeps the major portion of the reservoir. Caustic loses pH and alkalinity through its interaction with the reservoir rock and brine. To evaluate caustic as an enhanced oil recovery (EOR) agent, it is necessary to determine the extent of the caustic/rock interaction and the rate of the reactions involved. Due to the complexities of these reactions, the published theoretical work is oversimplified and extrapolations to reservoir scales are erroneous. The published theoretical models have not considered all the possible caustic/rock interactions or incorrect rate of reactions have been assumed. Furthermore, the core flooding experiments were performed in short residence times, therefore, the

state of final equilibrium was never established. At the state of final equilibrium, all the reactions between the rock surface and the solutions are in equilibrium and no further loss of pH or alkalinity takes place.

The objective of this work was to investigate whether or not caustic sweeps the major portion of the reservoir efficiently during an alkaline flood process. It was also the objective of this work to study the state of final equilibrium during a caustic flood through determination of the pH and chemical composition profiles along the porous medium. For this purpose, a long porous medium which provided extended residence times was required. It was necessary to set up the porous medium such that the changes in the pH and chemical composition of the solution could be monitored. Four Berea sandstone cores (8" in length and 1" in diameter) placed in series provided the desired length and the opportunity for sampling in-between cores. This enabled establishment of pH and chemical composition profiles. The experiments were run at temperatures up to 180°C, and the flow rates varied from 4.8 to 0.2 ft/day. The samples were analyzed for pH and for Si and Al concentrations.

The results show that caustic consumption is insignificant for temperatures up to 100°C. Above 100°C consumption increases and is accompanied by a significant decrease in pH. The sharp decline in pH also coincides with a sharp decline in concentration of silica in solution. The results also show that alumina is removed from the solution and solubility of alumina ultimately reaches zero.

Sharp silica and pH declines take place even in the absence of any alumina in solution. As a result, removal of silica from solution is attributed to the irreversible caustic/rock interaction. This interaction is in the form of chemisorption reactions in which silica is adsorbed onto the rock surface consuming hydroxyl ion. Once these reactions are satisfied, caustic breakthrough occurs at a high pH. However, significant pore volumes of caustic must be injected for completion of the chemisorption.

Chapter 1

INTRODUCTION

Alkaline flooding was proposed as a recovery method for acidic oil reservoirs as early as 1917 by Squires[1], Nutting[2] in 1925 and Atkinsons[3] in 1927. The proposed recovery mechanisms are:

- Emulsification with entrainment,
- Emulsification with entrapment,
- Emulsification with coalescence,
- Wettability reversal,
- Oil phase swelling,
- Disruption of rigid films, and
- Low interfacial tensions.

Figure 1.1 shows a schematic of an alkaline recovery process. The acid oil reacts with alkali to produce the water soluble anionic surfactant A^-. This anionic surfactant reduces the interfacial tension (IFT) between the oil phase and the water phase. Therefore, in order for a crude to be a candidate for alkaline flooding, it must have a high acid number, and the hydrolyzed acid must be interfacially active. The number of different emulsifiers in a single crude oil may range into the hundreds or even higher. These emulsifiers are primarily oil

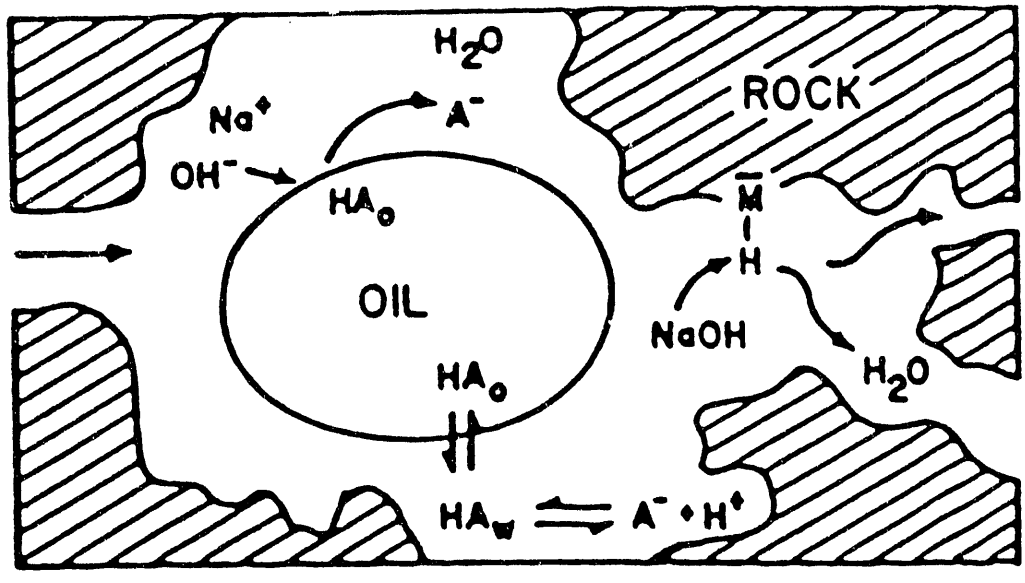

Figure 1.1 Schematic of alkali recovery process.

soluble carboxylic acids that are converted to the sodium soap in contact with caustic solution.

In 1977, the use of caustic for improving oil recovery in steamfloods was proposed.[4] During steamfloods, due to gravity override, steam moves to the upper portion of the reservoir and a hot water zone is formed in the lower portion of the reservoir. Therefore, a large portion of the oil may not be recovered in the lower portion of the reservoir. Injection of caustic along with the steam was proposed to reduce IFT between the oil phase and water phase in the hot water zone.

A number of field tests and laboratory studies have been conducted on various aspects of caustic flooding and have been reviewed by Mayer et al.[5] The results of these works are not in agreement. In some of these studies it was concluded that caustic can not maintain an effective pH through a significant portion of the reservoir while in others the opposite conclusion were reached. These controversies were attributed to the site-specific nature of alkaline flooding.

The loss of alkali within the reservoir is the most detrimental factor in the effectiveness of the process. The mechanisms which result in a loss of alkali include the following:[6]

- Surface exchange and hydrolysis which cause a delay in caustic breakthrough,
- Congruent and incongruent dissolution, and

- Insoluble hydroxide formation by reaction with hardness ions in the reservoir brine and from the rock surface.

The rate of dissolution of silica depends on the deviation from the equilibrium and it should decrease with time. Caustic flooding can be effective if pH is maintained above the minimum level required for interfacial tension reduction in a large portion of the reservoir. The alkalinity above the minimum effective alkalinity is defined as the useful alkalinity.

In the previous dynamic experimental work on caustic flooding, final equilibrium was not established due to the short residence time.[8] The objective of the present work is to study the variation of pH and chemical composition of injected caustic solution as a function of distance along the porous medium in a long system with an extended residence time. This enables us to examine the state of the final equilibrium, the distance from the injection point that the caustic stays effective and the interaction of the caustic with clays and other minerals.

Chapter 2

CAUSTIC CONSUMPTION BY ROCK

2.1. Ion Exchange

When a soluble oxide is added to an electrolyte solution hydrolysis occurs and complex formation of the surface atoms and dissociation of surface groups take place. These reactions are fast and reversible. Equilibrium is attained in a short time. The equilibrium depends on the dissociation constants of the surface OH group in contact with the electrolyte solution. On a silica surface, fast reactions take place in which hydrogen is replaced by sodium ion. Charged sites are changed to Si-OH groups or hydroxides upon addition of water. Addition of water results in a negative surface and a diffuse layer of positive ions. These two regions are called the electrical double layer. Therefore, the surface charge can be investigated by studying the double layer and the distribution of the potential determining ions, which are hydrogen and hydroxyl ions. The surface hydroxyl group, depending on solution pH, can go through either basic or acidic dissociation.

The pH at which the surface is undissociated is called the point of zero charge. Below this pH basic dissociation occurs and the surface develops a positive charge. Above this pH the opposite takes place. Silica goes though

acidic dissociation above the pH of 4. However, below pH of 4, dissociation does not take place. Therefore, it can be concluded that the silica surface does not go through basic dissociation. Sodium-hydrogen ion exchange on the surface depends on solution pH and electrolyte concentration.

It has been shown that ion exchange causes a delay in caustic breakthrough.[6,8,9,10] This is accompanied by a lag in surfactant generation which can make alkaline flooding uneconomic.

The sodium-hydrogen ion exchange reaction can be generalized as follows:[6,9,10,11]

$$MOH + Na^{+} \rightleftharpoons MONa + H^{+} \qquad (2.1)$$

$$H^{+} + OH^{-} \rightleftharpoons H_2O \qquad (2.2)$$

The mineral exchange site is represented by *M*. The above equation can be applied to the surface of silica, clays and other oxides.

Another type of ion exchange at the surface of the mineral is sodium-divalent ion exchange which may form an insoluble hydroxide or silicates:[12]

$$2Na^{+} + (MO)_2Ca \rightleftharpoons 2MONa + Ca^{+2} \qquad (2.3)$$

$$Ca^{+2} + 2OH^{-} \rightleftharpoons Ca(OH)_2 \qquad (2.4)$$

$$Ca^{+2} + H_2SiO_4^{-2} \rightleftharpoons CaH_2SiO_4\ (s) \qquad (2.5)$$

Hardness ions present in reservoir brine promote hydroxyl ion uptake according to the following reaction:[11]

$$2MOH + Ca^{+2} + 2OH^- \rightleftharpoons (MO)_2Ca + 2H_2O \qquad (2.6)$$

The ion exchange follows a Langmuir type isotherm which can be written as:[6,8,9,11]

$$\frac{n}{k_eC} = \frac{n_{max}}{(1 + k_eC)} \qquad (2.7)$$

where n is the difference between the hydrogen and hydroxyl ion adsorption. n_{max} is the hydrogen exchange capacity. k_e is the exchange equilibrium constant in units of inverse concentration.

The ion exchange reaction 2.1 indicates that increasing *NaCl* concentration increases the amount of ion exchange. The results of Saneie's[24] simulated model also show that an increase in *NaCl* concentration increases OH^- consumption. Consequently, the pH breakthrough volume increases. Dehghani[8] in his work concluded the opposite. This apparent disagreement is the result of his procedure and the interpretation of the data. In his work the cores were saturated with brine solution prior to caustic injection. Some exchange sites had reacted before the flood started. Therefore, the amount of ion exchanged measured by the core flood experiment did not include the total and exchange was underestimated.

Whereas, in Saneie's model, no initial *NaCl* in solution was present.

Ion exchange is enhanced by increasing temperature and pH.[8,9] The lag in caustic breakthrough caused by ion exchange, can be minimized if the Na^+ concentration of the injected fluid is increased. However, it has been noted that the interfacial tension (IFT) between the oil phase and the water phase increases with increasing Na^+ concentration above a certain level.[13] The proposed mechanism for this behavior is the formation of an undissociated salt which causes surface active species to partition into the oleic phase.[14] At an optimum Na^+ concentration the IFT between the oil phase and the water phase is minimum. In order to increase the optimum Na^+ concentration, Nelson et al.[15] proposed the use of a cosurfactant. Preflushing the reservoir with brine can also reduce ion exchange and insoluble hydroxide formation.

2.2. Rock Dissolution

In a series of experiments Holt and King[16] discovered that when powdered quartz was added to water the concentration of $Si(OH)_4$ increased rapidly at first but very slowly, thereafter. They concluded that 16% of a monolayer on the crystal surface is in the form of adsorbed silicic acid which they referred to as a high solubility layer. The layer is removed by alkali and is reformed by adsorption from silicic acid solution even if the concentration is well below that of a saturated solution. The solubility-time curve shown on Figure 2.1 consists

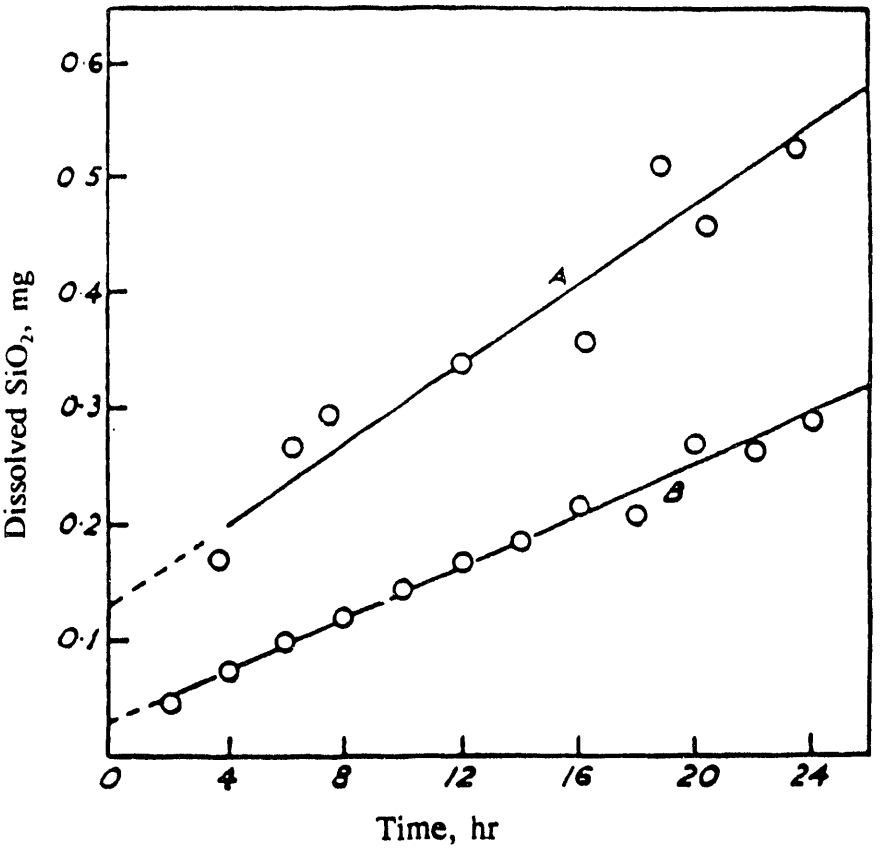

Figure 2.1 Rate of dissolution of silica powder in 0.1N sodium hydroxide, (A) Original powder, (B) Alkali-extracted powder. (Reference: 16)

of two portions. The first is the "high solubility" phase, and is due to the dissolution of the adsorbed silicic acid layer, and the second portion represents the attack of water on the true silica lattice. The second phase is very slow and the rate depends largely on the pH.

Stober[17] proposed the following mechanism for the interaction of the silica surface and the $Si(OH)_4$:

1. At the surface, *Si-O-Si* bonds are split by hydrolysis, averaging two bonds per tetrahedra, to form a hydrated silicic acid molecule adsorbed on the surface;
2. The $Si(OH)_4$ is desorbed into solution;
3. $Si(OH)_4$ is adsorbed onto the surface at equilibrium as the reverse process occurs, followed by condensation and addition of SiO_2 to the surface.

Therefore, solubility of silica depends on the final concentration of $Si(OH)_4$ which depends on the competition between silica passing into solution as $Si(OH)_4$ and $Si(OH)_4$ readsorbing on the surface blocking further dissolution. As was mentioned earlier, the solubility of silica is greatly affected by the pH of the solution. At neutral pH (pH between 6 and 7) all of the silica is in the form of silicic acid and the dissociation of quartz can be written as follow:

$$SiO_2 + H_2O \rightleftharpoons Si(OH)_4 \qquad (2.8)$$

Therefore equilibrium is established when the solution reaches the limiting concentration of $Si(OH)_4$.

Kopeykin and Mikhaylov[18] extended the above equation for higher pH. At pH above 7, ionization of silicic acid occurs. This causes a reduction in silicic acid concentration in solution and to re-equilibrate more silica will be dissolved and pass into solution as silicic acid. Using the following equations and appropriate equilibrium constants, Southwick[19] calculated the total solubility of quartz:

$$H_4SiO_4 \rightleftharpoons H_3SiO_4^- + H^+ \qquad (2.9)$$

$$H_3SiO_4^- \rightleftharpoons H_2SiO_4^{-2} + H^+ \qquad (2.10)$$

$$H_2SiO_4^{-2} \rightleftharpoons HSiO_4^{-3} + H^+ \qquad (2.11)$$

$$HSiO_4^{-3} \rightleftharpoons SiO_4^{-4} + H^+ \qquad (2.12)$$

$$H_2SiO_3 + H_2O \rightleftharpoons H_4SiO_4 \qquad (2.13)$$

$$H_2SiO_3 \rightleftharpoons HSiO_3^- + H^+ \qquad (2.14)$$

$$HSiO_3^- \rightleftharpoons SiO_3^{-2} + H^+ \qquad (2.15)$$

$$2HSiO_3^- \rightleftharpoons Si_2O_5^{-2} + H_2O \quad (2.16)$$

$$HSi_2O_5^- \rightleftharpoons Si_2O_5^{-2} + H^+ \quad (2.17)$$

$$Si_2O_5^{-2} + H_2O \rightleftharpoons HSi_2O_6^{-3} + H^+ \quad (2.18)$$

Similar calculations were performed for amorphous silica by applying an appropriate limiting $Si(OH)_4$ concentration.

The rate of dissolution and the mechanism of dissolution are discussed by Iler.[20] To evaluate the rate and mechanism of dissolution, factors affecting them, such as temperature and pH, should enter the calculations. The proposed mechanism of dissolution by Iler is shown in Figure 2.2.

The dissolution process requires a catalyst that can be chemisorbed, thereby increasing the coordination number of the silica to more than four. Chemisorption of the catalyst causes the weakening of the oxygen bond to the underlying silicon atoms. The dissolution of silica in water can be looked upon as a depolymerization through hydrolysis. At neutral pH, the apparent solubility of silica is the concentration $Si(OH)_4$ reaches at steady state as in a depolymerization-polymerization reaction. In alkaline solutions the hydroxyl ion acts as the catalyst as shown in Figure 2.2. The first step in dissolution is the adsorption of OH^- ion, which acts as the catalyst. Then, a silicon atom goes into solution as a silicate ion. If the pH is much below 11, the silicate ion is

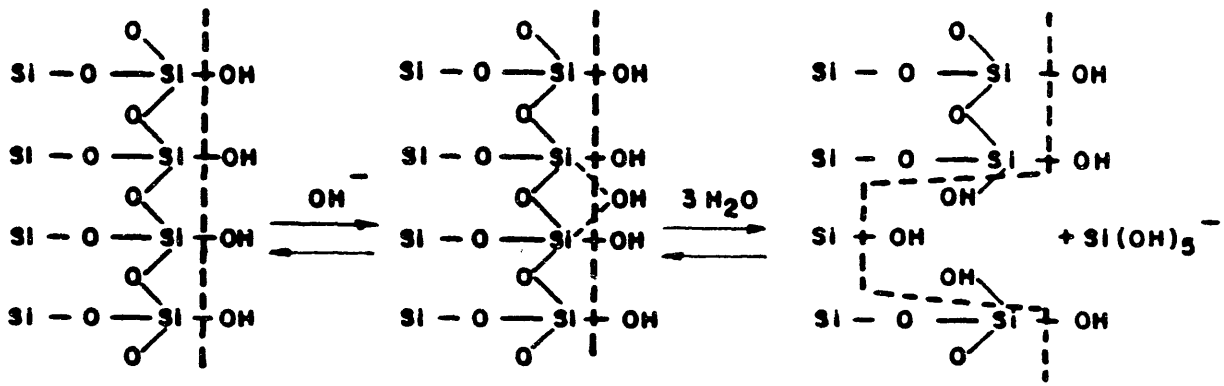

Figure 2.2 Proposed mechanism of dissolution of silica in water in the presence of hydroxyl ions. (Reference: 20)

hydrolyzed to $Si(OH)_4$ and OH^- is released. The process is repeated until the silicate "solubility" limit is attained. The "solubility" limit is achieved when the limiting $Si(OH)_4$ concentration is attained. Above pH of 11 the $Si(OH)_4$ is converted to silicate ions and the solution becomes unsaturated with respect to $Si(OH)_4$. Therefore, the silica continues to dissolve. At high pH a higher rate of dissolution has been observed.[8]

Temperature has the greatest effect on the solubility and the rate of dissolution of silica. The results obtained by Goto[21] indicate that the solubility of silica increases as temperature increases. Dehghani[8] observed a larger pH drop and, consequently, larger consumption of hydroxyl ions at higher temperatures, which was attributed to more silica dissolution. Sydansk[22] in a series of caustic core floods observed a higher silica content in the effluent at higher temperature, suggesting more silica dissolution.

Due to the possible presence of certain metal impurities and, especially, the presence of an adsorbed layer on the crystal surface of silica, reported solubility data can be misleading. Until the outstanding investigation by Van Lier[23], speculations were that quartz might exhibit no true solubility in water at room temperature. Van Lier found that cleaned quartz has a well-defined solubility in water, which can be described by the equation:

$$\log c = 0.151 - \frac{1162}{T} \qquad (2.19)$$

where c is the molar concentration of $Si(OH)_4$ and T is absolute temperature in °K. Solubility calculated from the above equation is 11 ppm at room temperature. Dehghani[8] used the above equation along with the silica ionization reactions and their constants to construct distribution curves for different silicate species as a function of hydroxyl ion concentration. An example of these plots is shown in Figure 2.3. Another factor affecting the solubility of silica is particle size. Solubility of silica is higher when the radius of the curvature of the surface is smaller or the specific surface area is greater.[20]

The effect of salt on the rate of dissolution has not been investigated in great details. However, it is believed that *NaCl* increases the rate of solution of quartz in water.[20]

Recently, detailed modeling of silica dissolution has been attempted by Saneie.[24] In developing a quantitative model for quartz dissolution, she used Strelko's[25] dissolution mechanism and Stober's[26] model. Silica dissolution was described as a two step reaction. The first step is the rapid formation of a complex. The second step is the breaking of the *Si-O* bond, which is the rate-determining step. Figure 2.4 shows the steps considered in her work. Her results show that the kinetics of silica dissolution can be approximated by a first-order reaction only for low concentrations. The rates of hydroxyl ion consumption and silica dissolution increase proportionally to the specific surface area. Temperature increase results in a significant increase in consumption and

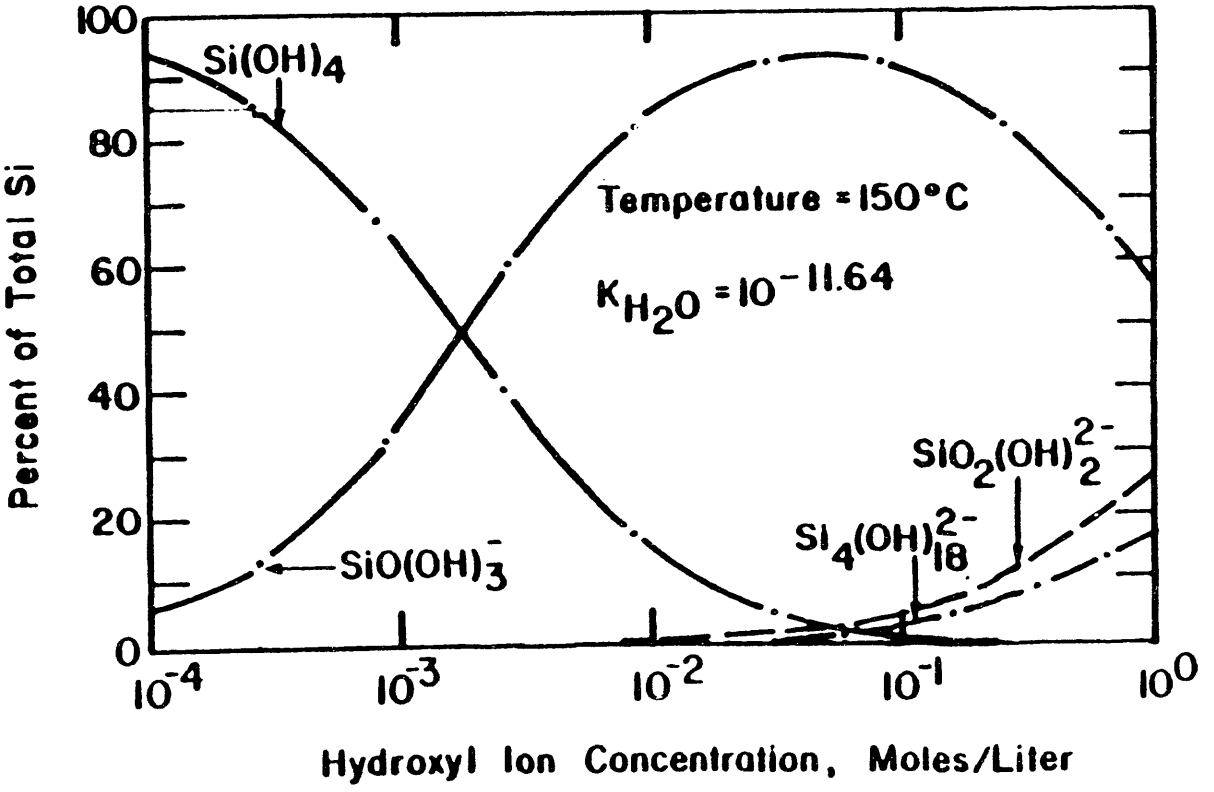

Figure 2.3 Distribution of different silicate species as a function of hydroxyl ion concentration.

(Reference: 8)

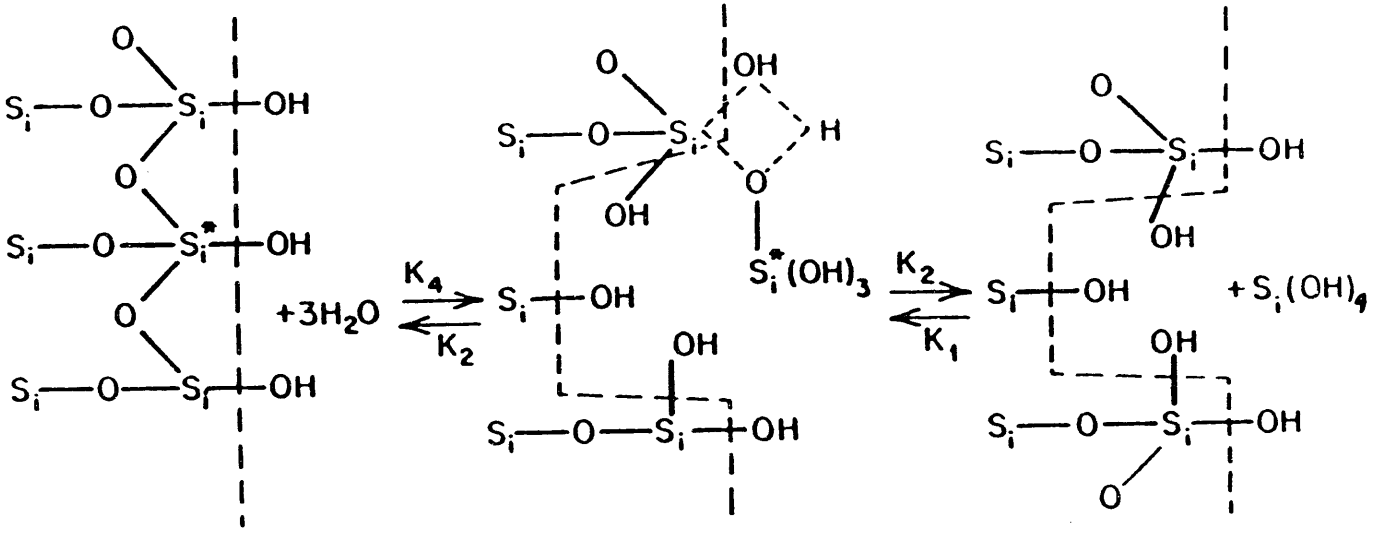

Figure 2.4 Two step silica dissolution mechanism. (Reference: 24)

decrease the final equilibrium pH. However, it does not affect the total dissolved silica significantly. One of her typical simulated results on the alkaline flood process is shown in Figure 2.5 . In this figure, pH and sodium ion concentration variations along the porous medium are plotted. The alkaline flood process is characterized by a plateau region near the injection end where ion exchange has been completed. The Na^+ concentration in this region is equal to the injected. The pH drops sharply at the injection end until equilibrium is attained, then it stays constant. The rate of advance of the region decreases with an increase in the ion exchange constant.

Silica dissolution was believed to be the major source of the caustic consumption which would make the process of alkaline flooding infeasible. Southwick[19] introduced the concept of useful alkalinity. Alkalinity is defined as the amount of hydrogen ion required to neutralize a basic solution to the break-point pH in a titration curve. "Useful alkalinity" is defined as the amount of alkalinity present above a critical pH. Critical pH is the minimum pH required for effective oil displacement. A series of static bottle tests with analyses of the equilibrated solutions, showed that the dissolved silica produce buffered alkaline solutions. Therefore, due to buffering, the loss of "useful alkalinity" is significantly less than the loss of hydroxyl ion concentration. Consequently, if the equilibrated solution maintains a pH above the critical pH, useful alkalinity will be sufficient to generate in situ surfactant. An example of titration curves

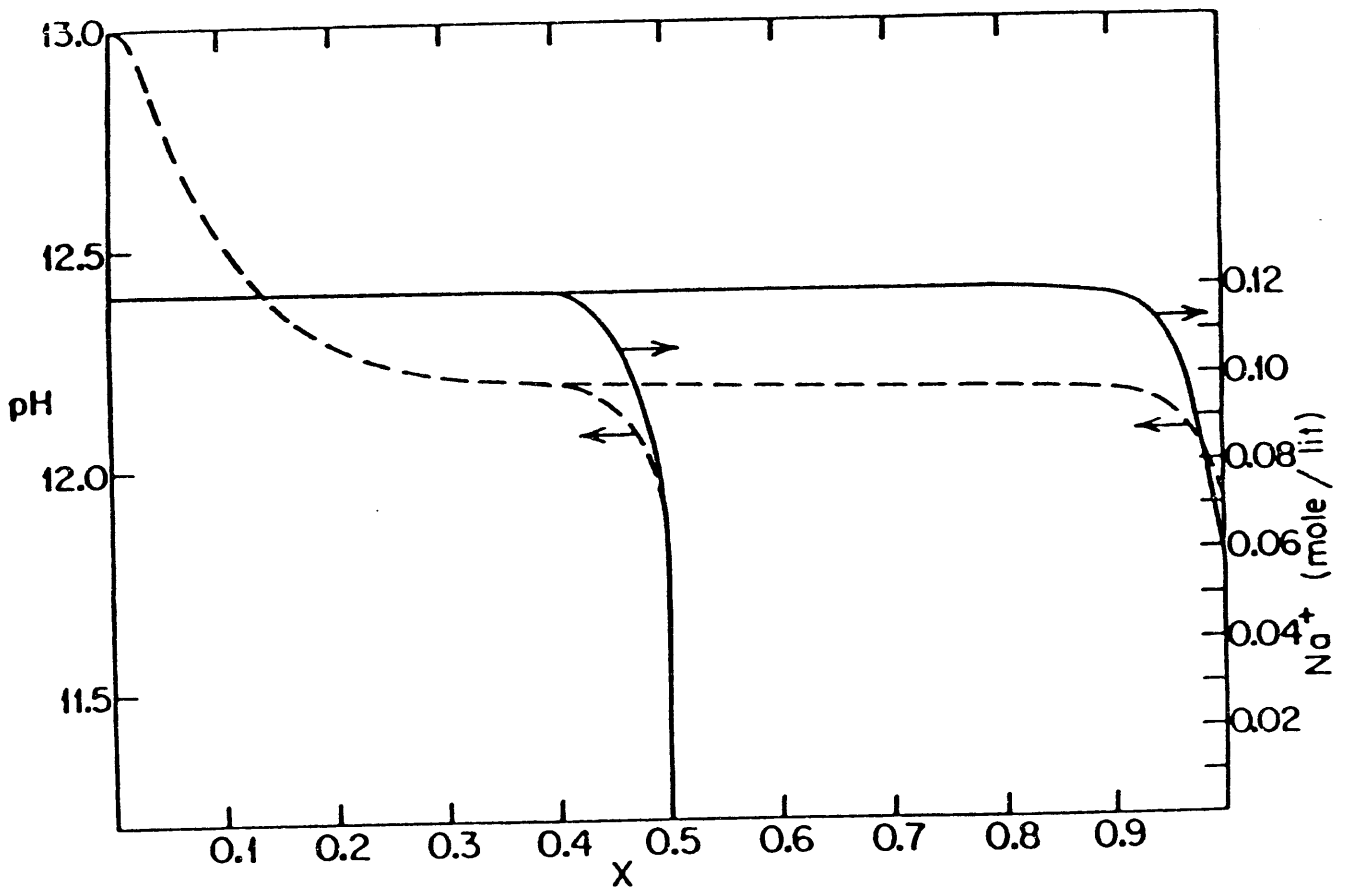

Figure 2.5 pH and sodium ion concentration profile for 0.1 N injected caustic concentration and 0.02 mol/lit NaCl.

(t = 0.5 and 1 pore volume, L/q = 400 days, a_m = 1 m^2/gr, $k_r/k_w = 10^3$).(Reference: 24)

for a sodium hydroxide solution and an equilibrated solution of sodium hydroxide with quartz are shown in Figure 2.6.

2.3. Consumption By Clay/Caustic Interaction

Clays are a major source of consumption in alkaline flooding. Their contribution to consumption through ion exchange is discussed in 2.1. Clays also consume alkali through the dissolution reaction. Ehrlich and Wygal[27] conducted experimental work to determine the caustic consumption by reservoir rock. Their batch results indicated that consumption was the highest for montmorillonite followed by illite and kaolinite. However, it should be realized that the batch results included both consumption by ion exchange and dissolution. The hydroxyl ion consumption due to ion exchange can not be differentiated from that due to dissolution in batch experiments. The amounts of consumption by dissolution for quartz, amorphous silica, kaolinite and montmorillonite were measured by Bunge et al.,[6] using *Si* concentration as an indicator. Therefore, consumption by ion exchange was excluded. Their results indicate that on a surface area basis the consumption by amorphous silica is higher than consumption by quartz, followed by kaolinite and, then by montmorillonite. Sydansk[22] performed caustic core floods on a series of sandstones of different mineralogy. The sandstones contained different amounts of clay. The results showed that sandstones with lower clay content were associated with less dissolution interaction. The scanning

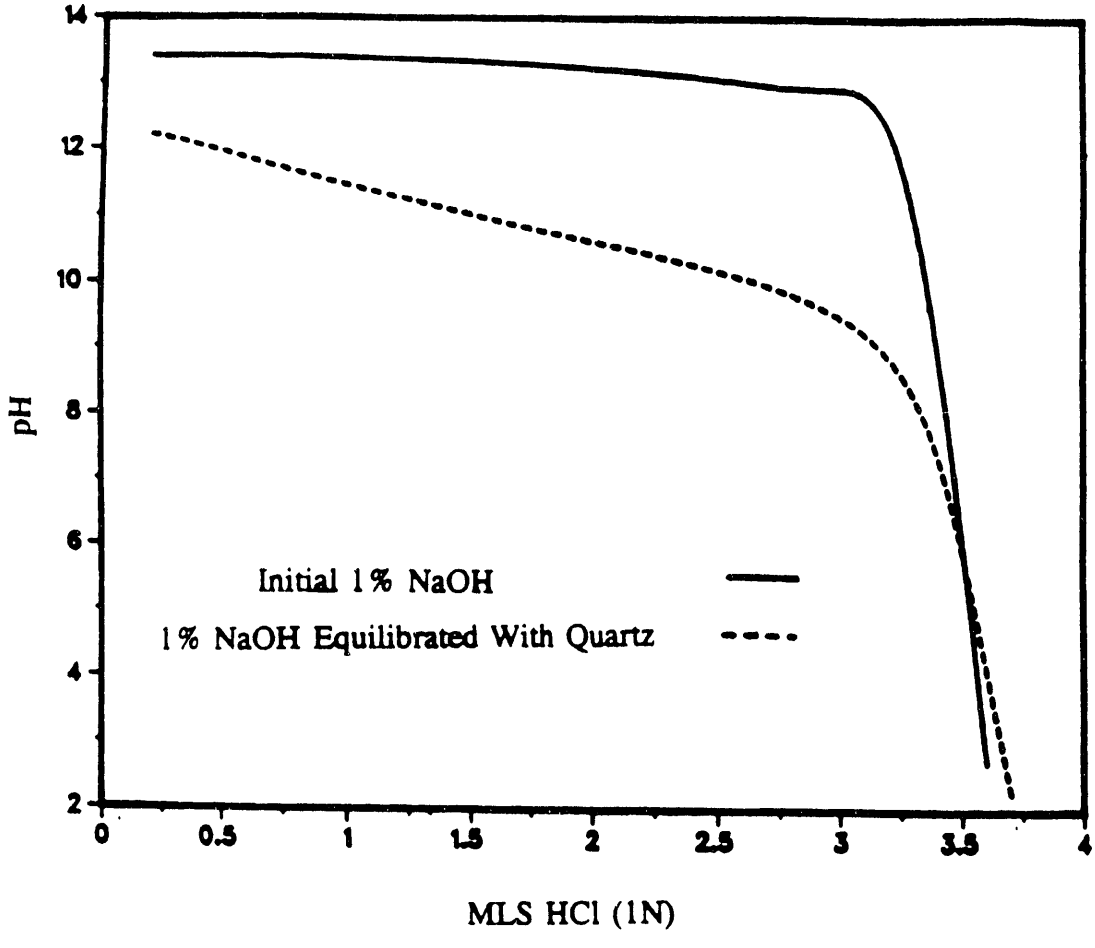

Figure 2.6 Titration curve for 15 ml of (-) 1% NaOH, and (---) the solution formed from the storage of 1% NaOH with quartz at 167°F for 110 days. (Reference: 19)

electron microscopy (SEM) results indicated that clays and large specific area silica minerals are dissolved preferentially, while framework sand grains and cementing minerals are not dissolved significantly. The SEM and X-ray diffraction (XRD) work indicated precipitation of a new mineral that belongs to the zeolite family. Mohnot[28] conducted static tests to study the alkali-mineral reactions. His results also show that kaolinite clay consumes a significantly higher amount of "useful alkalinity" than montmorillonite, illite or quartz sand. Alkali consumption by kaolinite consists of a rapid drop in alkalinity due to reversible ion exchange followed by a slow irreversible reaction. The *Si*, *Al* and alkalinity measurements of the filtrate showed that, even when no further changes in *Si* and *Al* concentration were noticed, the pH and the alkalinity continued to drop. This was attributed to the formation of new minerals which are mostly zeolites. The formation of new minerals consumes alkalinity along with silica.

Thornton et al.[29] also performed a series of bottle tests to evaluate the kaolinite-alkali reaction. Using experimental data on assumed reactions, they developed a simplified model to predict the consumption of alkali by kaolinite. The model could predict the results of the batch test on Kern River sand. However, it failed to predict hydroxide loss in a slim-tube experiment with 99% quartz and 1% kaolinite.

Diallo et al.[30] reported experimental dissolution results for quartz, kaolinite, and their mixtures in 0.1N *NaOH* at 70°C. They pointed out that the

experiments were short term and the pH changes were negligible. No data on either pH or alkalinity were reported. It was concluded that the addition of soluble alumina or aluminum bearing minerals, such as kaolinite and α-alumina, suppresses the silica solution rates from quartz. Also the addition of soluble silicon from quartz reduces the solution concentration of aluminum and silicon produced from kaolinite.

Recently, Johnson[31] studied the reaction of kaolinite with 0.1N *NaOH* at 70°C, 100°C and 120°C for periods up to 5000 hrs. His results show a significant increase in caustic consumption with increasing temperature. The rate of caustic consumption was approximately 5 times greater at 120°C than at 100°C. It was also concluded that the formation of a particular mineral, which they referred to as zeolite Na-PC, was the major cause of irreversible alkaline consumption.

Chapter 3

EXPERIMENTAL DESCRIPTION

3.1. Materials

The brine used in all the experiments were 2.0 weight percent brine in deareated, distilled water. 0.1N sodium hydroxide solutions were prepared by diluting certified, Fisher Scientific, 1.0 N sodium hydroxide solutions. The pHs of the caustic solutions were measured with a pH meter calibrated with buffers of known pH. The buffer solutions were prepared following instructions in the Handbook of Analytical Chemistry.[32] The distilled water used in making the buffer solutions was also deareated.

All the experiments were conducted on fired Berea Sandstone cores 1" in diameter and 8" in length. The cores were fired at about 600°C for 24 hours to stabilize clay minerals and minimize core plugging. For each experiment new sets of fresh cores were used. Table 3.1 shows a typical composition of Berea sandstone obtained by X-ray diffraction.[33]

3.2. Apparatus

A schematic diagram of the apparatus is shown in Figure 3.1. The system consisted of two fluid reservoirs, a filter, a constant rate pump, pressure gauges,

Table 3.1

Mineral Composition of Fired Berea Sandstone

Mineral	**Bulk Percentage**
Quartz	83
K-feldspar	8
Calcite	Trace
Plagioclase	Trace
Dolomite	2
Kaolinite	5
Illite	2

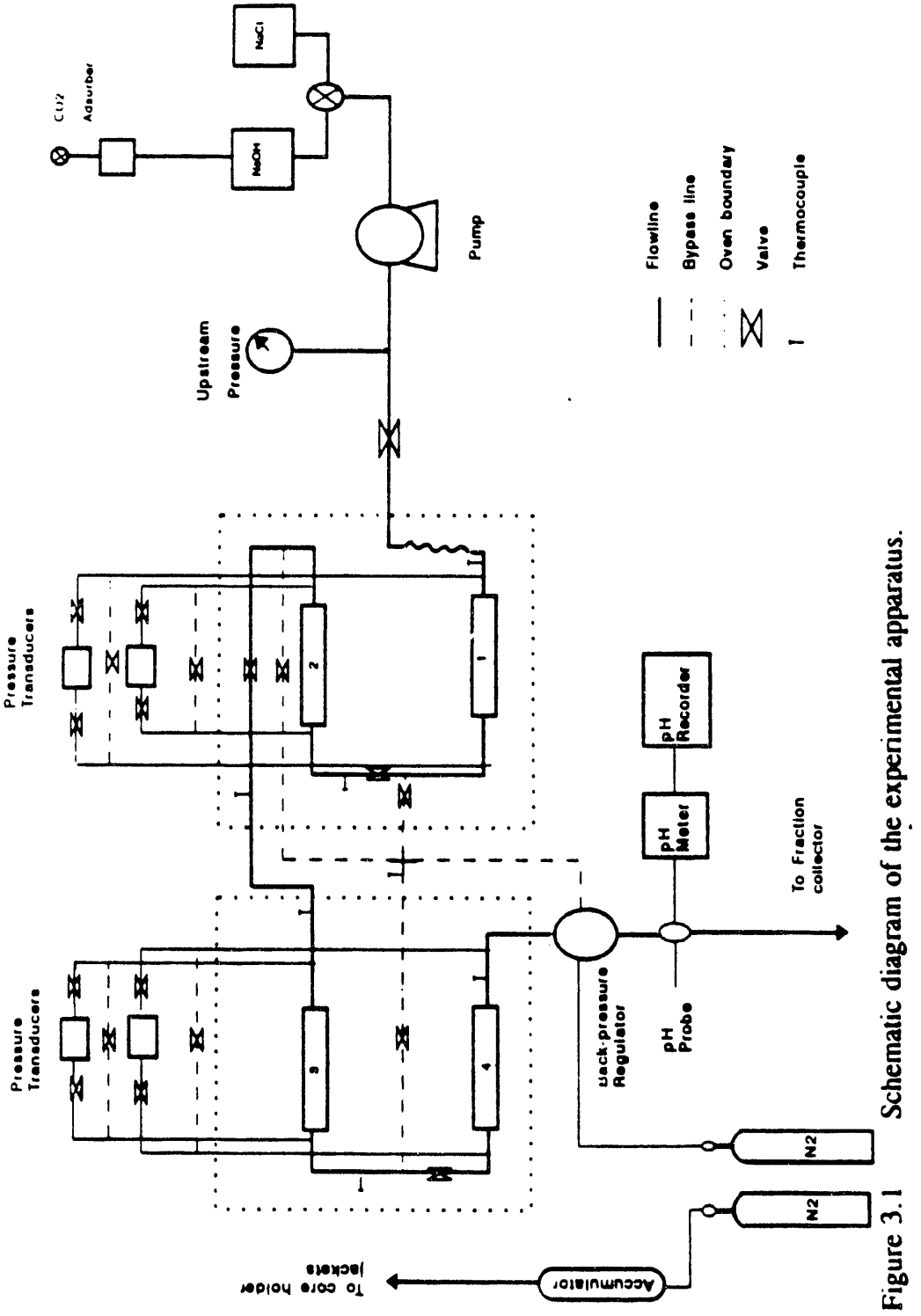

Figure 3.1 Schematic diagram of the experimental apparatus.

heat exchangers, thermocouples and temperature readout, 4 core holders, 2 constant temperature ovens with temperature control, 4 differential pressure transducers with demodulator, a chart recorder, an automatic fraction collector and a hydraulic overburden pressure supplier.

Polyethylene fluid reservoirs were placed in an elevated level to feed the pump. A stainless steel, 7 micron filter was used to filter the fluid prior to entering the pump. A constant rate, non-pulsating, high pressure liquid chromatography (HPLC) pump was used to pump the fluids. The pump was manufactured by Perkin-Elmer and had a single piston with a built-in pulse adsorber. The upstream pressure was monitored with a Heise gauge. A similar gauge was used to monitor the downstream pressure. A coil type heat exchanger with sufficient length was used to heat up the injected fluids and to the test temperature, before entering the first core. Cores were placed in the core holders. The core holders were designed for high-temperature, high pressure and for consolidated sandstone cores, 1" in diameter and 8" in length. Each core holder consisted of core holder jacket, two end fittings and two end plugs. The core holder jacket was a hollow cylinder 2" O.D., 1.5" I.D. and 13.75" in length. The core holder jacket was threaded at the ends for end fittings to be screwed in. Figure 3.2 is the diagram of the jacket. The diagram of the end fittings is shown in Figure 3.3. The O-rings on the end fitting were Viton and were designed to prevent leakage of the overburden fluids into the cores. Each

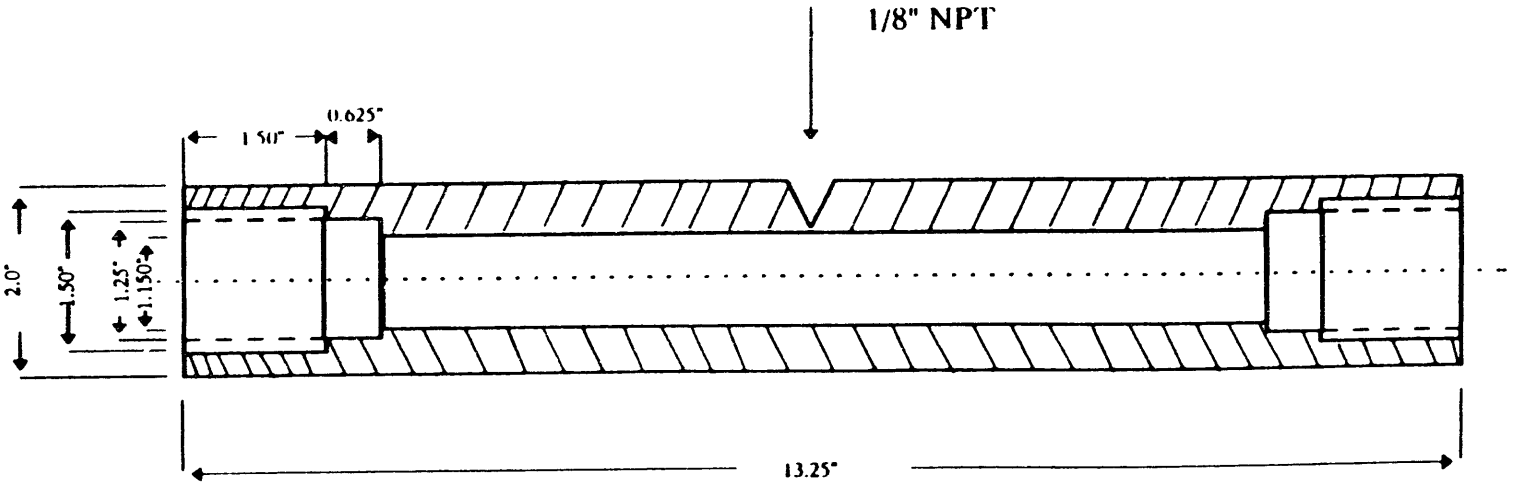

Figure 3.2 Schematic diagram of the core holder jacket.

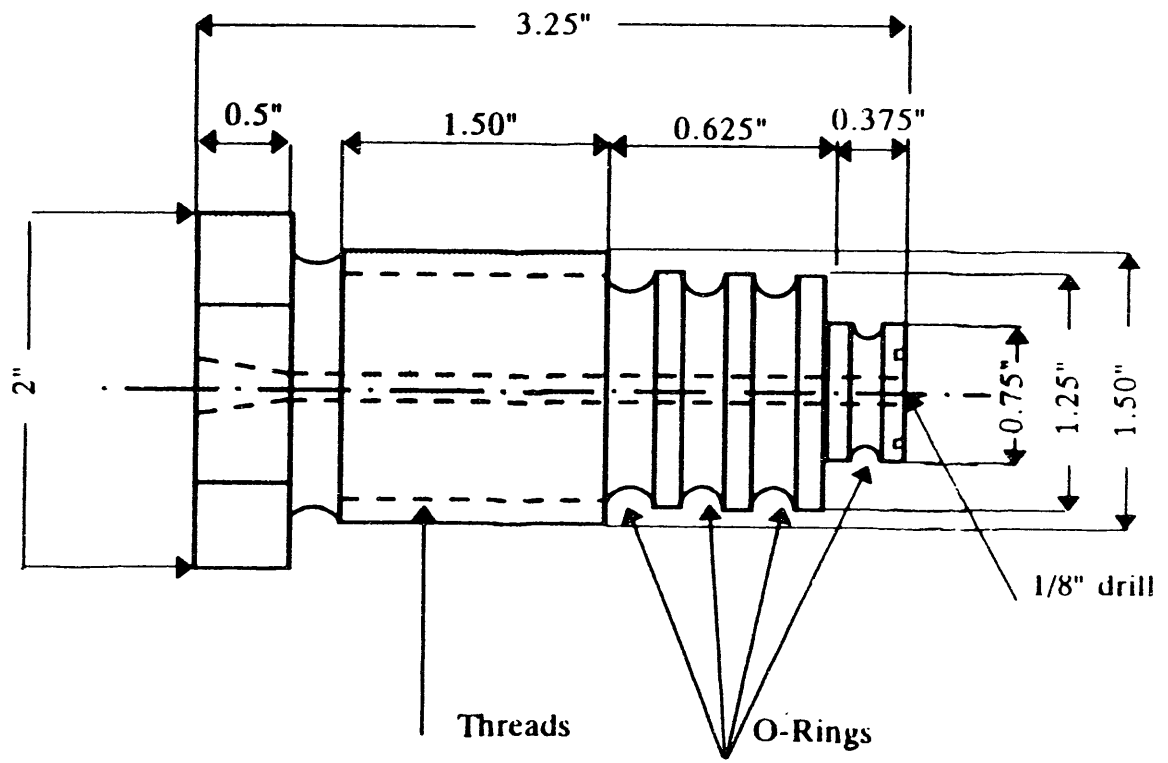

Figure 3.3 Schematic diagram of the end fitting.

end plug fitted to the end fittings on one side and pressed against the core face on the other side. The core and the two end plugs were placed on either end of the core were placed in a Teflon, heat-shrinkable sleeve. The Viton O-ring on the end of the plugs formed a bond between the end plug and the Teflon cover and stopped the leakage of overburden fluid into the cores. The circular and the radial grooves on the end plug allowed an even distribution of fluid at the inlet face of the core. The diagram of the end plug and the assembly of the core holders are shown in Figure 3.4 and Figure 3.5. Four core holders were placed in series. By-pass lines made sampling of fluids between cores possible. The heat exchangers, core holders and by-pass lines were contained in constant temperature ovens made by Blue-M. T-type thermocouples were used to monitor the temperature at different points along the flow path to insure isothermal conditions. The flow line between the two ovens was insulated and wrapped with a heating tape that connected to a variable-autotransformer. The heat loss in this segment of the flow path was monitored by thermocouple and was compensated by additional heat provided by the heating tape. The pressure drops across the cores were monitored with differential pressure transducers by Validyne. A pressure range of 0-5 psid was selected for the transducers. A flow line connected the upstream and downstream of each transducer with a switching valve. When the valve was in an open position a zero differential pressure was sensed by the transducer which allowed for zero calibration. This also provided

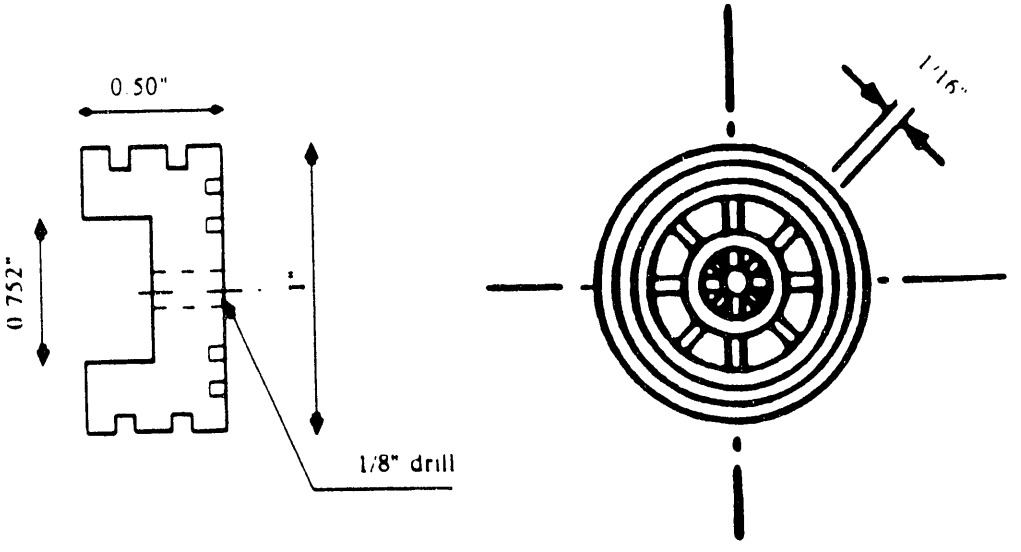

Figure 3.4 Schematic diagram of the end plug.

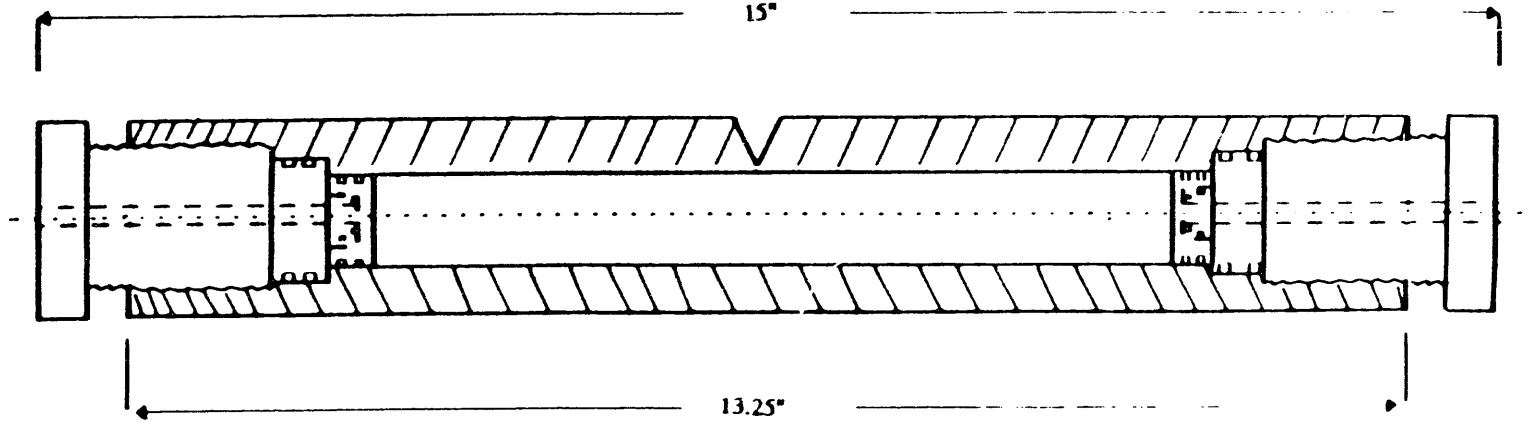

Figure 3.5 Schematic diagram of the core and core holder assembly.

a safeguard against over pressuring and damaging the transducer diaphragm. Since the flow rates were low, a condenser was not needed and the fluids cooled down by the time they reached the back pressure regulator. In order to keep the fluids in a liquid state, a back pressure in excess of the saturation pressure was held against the system. The cores were subject to a confining pressure which simulated overburden pressure and also prevented the flow of fluid between the Teflon sleeve and the core. This was done by pushing water into the space between the Teflon cover and the core holder jacket using an accumulator driven by nitrogen. The fluid pH was measured by a Fisher Scientific, in-line pH probe made with a polymer body. The pH probe was connected to a pH meter and a recorder. The pH probe had a working temperature only up to 70°C. Therefore, the pH was measured outside of the oven after the fluid passed through the back pressure regulator. The effluent fluid was collected in an automatic fraction collector loaded with graduated cylinders. The collected samples were used for chemical analyses. 1/8" O.D. inconel 600 tubing was used for all the flow lines to prevent corrosion problems caused by caustic at elevated temperatures. All the valves and fittings used were high pressure, high temperature stainless steel.

3.3. Experimental Procedures

3.3.1. Core Mounting

A high temperature core mounting technique discussed by others was tried initially.[8,33] The fresh core sample was placed in a Teflon, heat-shrinkable sleeve with plugs in place. The Teflon sleeve was etched with Tetra-Etch. A high-temperature sealant was applied overlapping the ends of the sleeve and around the end plugs to provide the bond required between the Teflon sleeve and the plugs. Hot air was blown by a heat-gun around the sleeve to shrink it onto the core and end plugs while they were clamped together. The heat was applied evenly around the core to prevent trapping of air bubbles between the core and the sleeve. This technique failed every time it was used and the overburden fluid leaked into the core. The failure was due to the sealant and to the use of an improper sleeve. The sealant was made up of a silicone which dissolved in sodium hydroxide at high temperatures. This caused a gap between the sleeve and the end plug and consequently the leakage of the overburden fluid. The more serious problem was caused by the Teflon sleeve. The Teflon sleeve used in the previous work[8] had a working temperature up to 400°F and the shrinkage range of 1.25" to 0.89" I.D. The continuous exposure of the sleeve to heat during the experiment caused a further tendency to shrink. However, due to the incompressibility of the core, shrinkage was not possible. This cause a longitudinal crack in the sleeve. The problem was solved by using a Teflon, heat-shrinkable sleeve that had a working

temperature up to 600°F. The heat from a heat-gun was not sufficient to shrink the new sleeve. A high temperature oven was used for this purpose. The new sleeve needed longer time for exposure to heat for adequate shrinkage. Consequently, the sealant dried up before the sleeve shrunk completely. To replace the sealant, two Viton O-rings were placed on each end plug. Once the sleeve shrunk, it compressed on the O-ring making the required bond between the end plug and the sleeve. These modifications stopped the leak of the overburden fluid into the cores. A holder was designed to clamp the core and the end plugs with the sleeve around them. The schematic diagram of the holder is shown in Figure 3.6. Then, cores, the end plugs and the sleeve on the holder were assembled. They were placed in the oven and the temperature was set at 650°F. With this technique the sleeve shrunk evenly and no air bubbles were trapped. The cores were then mounted in their core holders by placing them in the core holder jackets and tightening the end fittings. The new mounting technique was successful and experiments ran up to two months at high temperatures without any problem.

3.3.2. Procedure

After mounting the core inside the core holder, the porosity of each core was measured separately by using Boyle's Law. CO_2 was injected to replace the air present in the core. The cores were evacuated and then saturated with brine

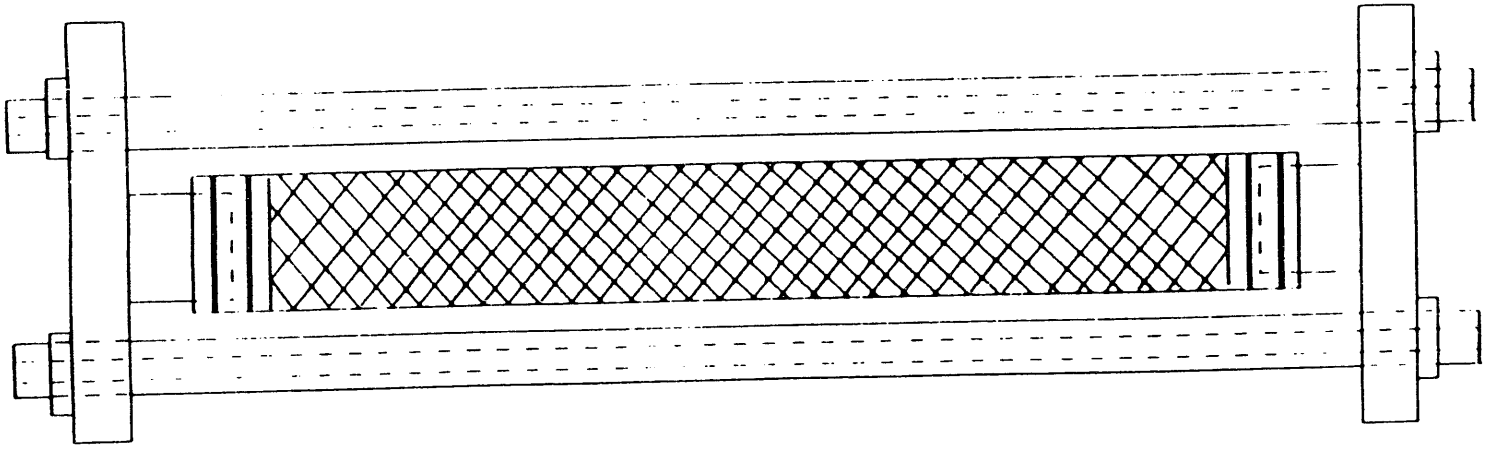

Figure 3.6 Schematic diagram of the core mounting holder.

solution. After all the flow lines and the transducer lines were filled with brine, the cores were placed in the ovens. Overburden pressure and back pressure were applied. Ovens were then turned on and the system was brought to the test temperature. Several pore volumes of brine were injected to insure complete saturation and divalent ion exchange. The absolute permeabilities of the cores to brine were measured by measuring the pressure drop across each core at different flow rates. The pump was then set to the initial flow rate and caustic injection was started. The pH was measured and recorded continuously. The pH meter was calibrated against buffer solutions of known pH periodically. Once no further change in the effluent end pH was observed, the effluent was produced from the end of the third core, using the by-pass lines. After the pH stabilized, samples were collected to be analyzed for *Si, Al* and other elements. The effluent was then produced from the end of the second core and, following the same procedure as above, the effluent was produced from the end of the first core. After taking all the necessary data for the fluids being produced from the ends of all four cores at steady state, the initial flow path was established and the effluent was produced from the end of the fourth core. The flow rate was then reduced to increase the residence time. When steady state had been established at the new rate, samples were taken from the end of the 4th, 3rd, 2nd and the first core and the pHs were measured. The total volume of the samples collected from in-between cores did not exceed 0.15 pore volumes. This amount is insignificant

compared to the total pore volumes injected during the experiments. In addition, to sample in-between the cores, the flow downstream of where the sample was taken must have been interrupted. For instance, if the sample was taken in-between the 3rd and the 4th core (effluent of the 3rd core), the flow to the 4th core was interrupted. As a result, in some experiments samples were not taken at the end of the first core, in order to minimize the time that caustic injection would be interrupted. Only at the last step of rate reduction were samples taken at the end of the first core, since afterwards the experiment was terminated. The temperature was raised for those experiments which were initially at lower temperature following the establishment of the steady state. At the steady state samples were taken from the end of each core following the same procedure as above. It should be noted that in all the experiments the changes in temperature or flow rate were applied in such a way that they would cause an increase in the amount of dissolution. After termination of the experiments, samples from different parts of the cores were analyzed for *Si*, *Al* and other elements such as *Fe* and *Mg*.

3.3.3. Sample Analysis

The fluid samples were analyzed for *Si*, *Al*, *Mg* and *Zn*. The Si concentration in solution is a measure of the amount of sandstone dissolution.

The two widely used methods for *Si* concentration measurement are silicomolybdic colorimetric method and atomic absorption.

Dissolved silica reacts with molybdate in mineral acid medium to form an intensely yellow-colored heteropoly acid $H_8[Si(Mo_2O_7)_6]$. The silicomolybdate method involves the reaction of ammonium molybdate with silica and phosphates. Phosphates also react with molybdate in acid medium to give the yellow heteropoly acid $H_7[P_2(Mo_2O_7)_6]$. Citric acid is added to destroy the interference caused by phosphate. This analytical method does not distinguish between the various silicate species which actually exist in solution. The measured *Si* concentration, which is the sum of all forms of silicate species, is defined as total SiO_2. A major drawback in applying this method is that silicates in the form of polymers react very slowly with molybdate and they can not be detected. Therefore, the validity of the analytical results largely depends on the state of aggregation of dissolved silicates. The basis for the colorimetric method is the Beer's Law which describes the relationship between transmission and concentration as follows:

$$I_t = I_0 e^{-k_1 C} \tag{3.1}$$

$$\ln I_t = \ln I_0 - k_1 c \tag{3.2}$$

The above relationship holds in the concentration range zero to 15 ppm for silica solutions analyzed by the silicomolybdate method. The fluid samples had

to be diluted to be brought into the required concentration range. Hatch Chemical Silicomolybdate Colorimetric Method Packets were used to obtain the yellow color in the diluted fluid samples. A Perkin Elmer U.V. spectrophotometer was used for adsorption measurements. The instrument was set at the maximum adsorption wave length which was 343 nm. A calibration curve was constructed by measuring the adsorption of silica solutions of known concentrations. The adsorption of the reacted fluid samples was measured and compared against the calibration curve for concentration measurement.

The atomic absorption method is the most accurate method for total silica measurement since it detects silica in all its forms. The linearity of adsorption for Si holds from 0 up to 100 ppm in the A.A. method. The adsorption of fluid samples was checked against the adsorption of known standard solutions. After each sample a blank was run for zero calibration. After every three samples the adsorption of the standard solutions was measured again to correct for drifts which may have resulted from deposit build-up on the burner or from other possible causes.

3.3.4. X-Ray Diffraction

Some of the core samples were analyzed by X-ray diffraction technique to identify the clays and minerals. During X-ray diffraction analysis, the X-ray beam is deflected from a crystal plane, and the wavelength selected by varying

the angle. The Bragg Equation is applied to measure the distance between adjacent planes in the crystal:[34]

$$n\lambda = 2d\sin\theta \tag{3.3}$$

The angle was varied from zero to 45 degrees. To calculate *d*'s of the observed peaks, Equation 3.3 along with the Θ's were used. The first three significant peaks and their corresponding *d*'s were used to identify the minerals by matching them with the published data.

Chapter 4

RESULTS

Three sets of experiments were performed. Each experiment's initial conditions, procedure and results are discussed separately in the following sections.

4.1. Experiment Set #1

The temperature stayed constant at 180°C throughout the experiment. The pH of the injected caustic solution was 12.87. The caustic solution did not contain NaCl. However, the cores were pre-flooded with brine prior to caustic injection. The initial rate was 0.9 ft/day and was varied down to 0.4 ft/day. It should be noted that all the reported rates in this thesis is calculated by dividing the volumetric flow rate to the cross sectional area.

Figure 4.1 is the plot of pH as a function of pore volume injected. The caustic broke through after 16 pore volumes had been injected. The producing pH stabilized at 11.9. The difference between the injected pH and the stabilized pH is attributed to the sandstone/caustic dissolution.

Figure 4.2 is a plot of effluent silica concentration as a function of pore volumes injected. Silica and caustic breakthrough took place at the same time

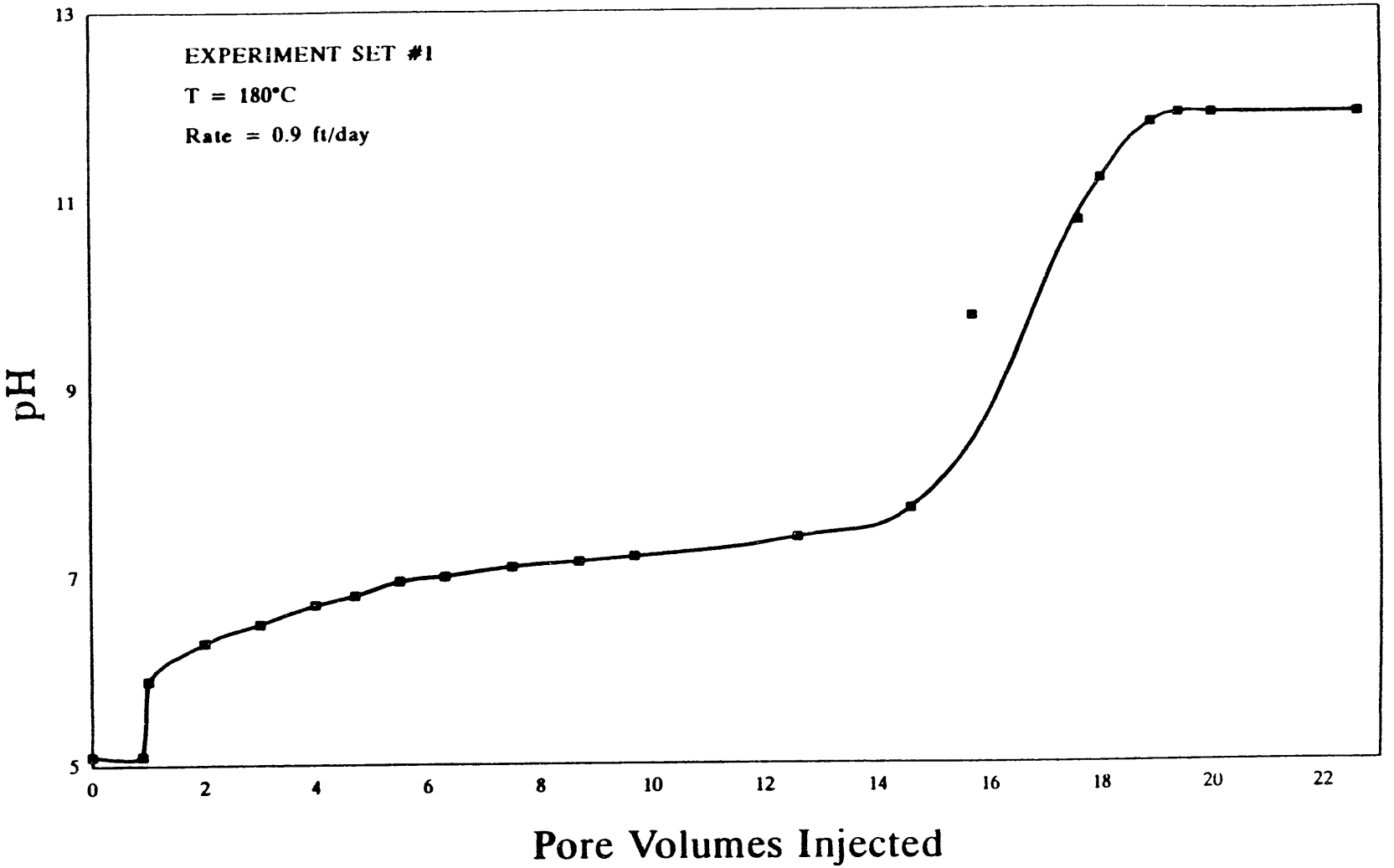

Figure 4.1 Effluent pH as a function of pore volumes injected for Experiment Set #1.

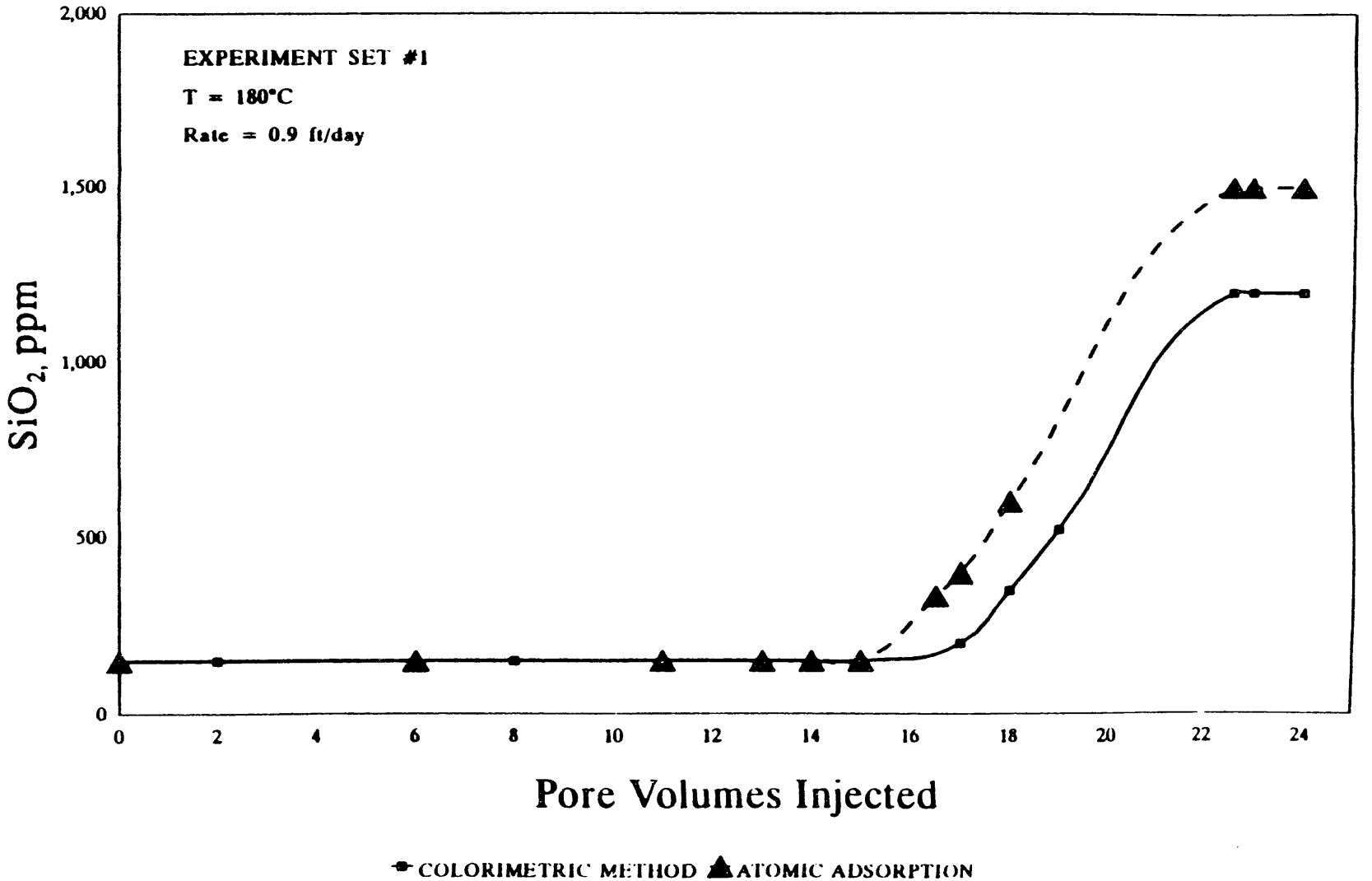

Figure 4.2 Effluent silica concentration vs. pore volumes injected for Experiment Set #1.

and silica concentration stabilized at about 1500 ppm. Both methods of colorimetric and atomic absorption were used for silica concentration measurement. Since a difference in the results by the two methods was observed, atomic absorption, which is the more accurate method, was used in all the subsequent measurements.

After 14.0 pore volumes of caustic injection and at steady state, samples were taken at the effluent end and of the third, second and first cores. The pH and silica concentrations for the samples were measured. After steady state was established at 0.9 ft/day, the rate was reduced to 0.4 ft/day. When the effluent pH had stabilized at the new rate, samples in-between cores were taken. When the flow was diverted for in-between core sampling, enough time was allowed for complete removal of pre-existing solutions in the by-pass lines. The samples were taken after the pH was stabilized.

Figure 4.3 is a plot of pH as a function of dimensionless length. After 14.0 pore volumes, the effluent end pH was about 7.0, while at the end of the first core the pH was measured at 12.2. For steady state at the rate of 0.9 ft/day, the pH dropped to 12.2 rapidly at the end of the first core, and more slowly to 11.9 at the end of the fourth core. For steady state at the rate of 0.4 ft/day, the pH at the end of the first core and the second core did not change relative to that observed at 0.9 ft/day. However, the pH decreased at the end of the third and

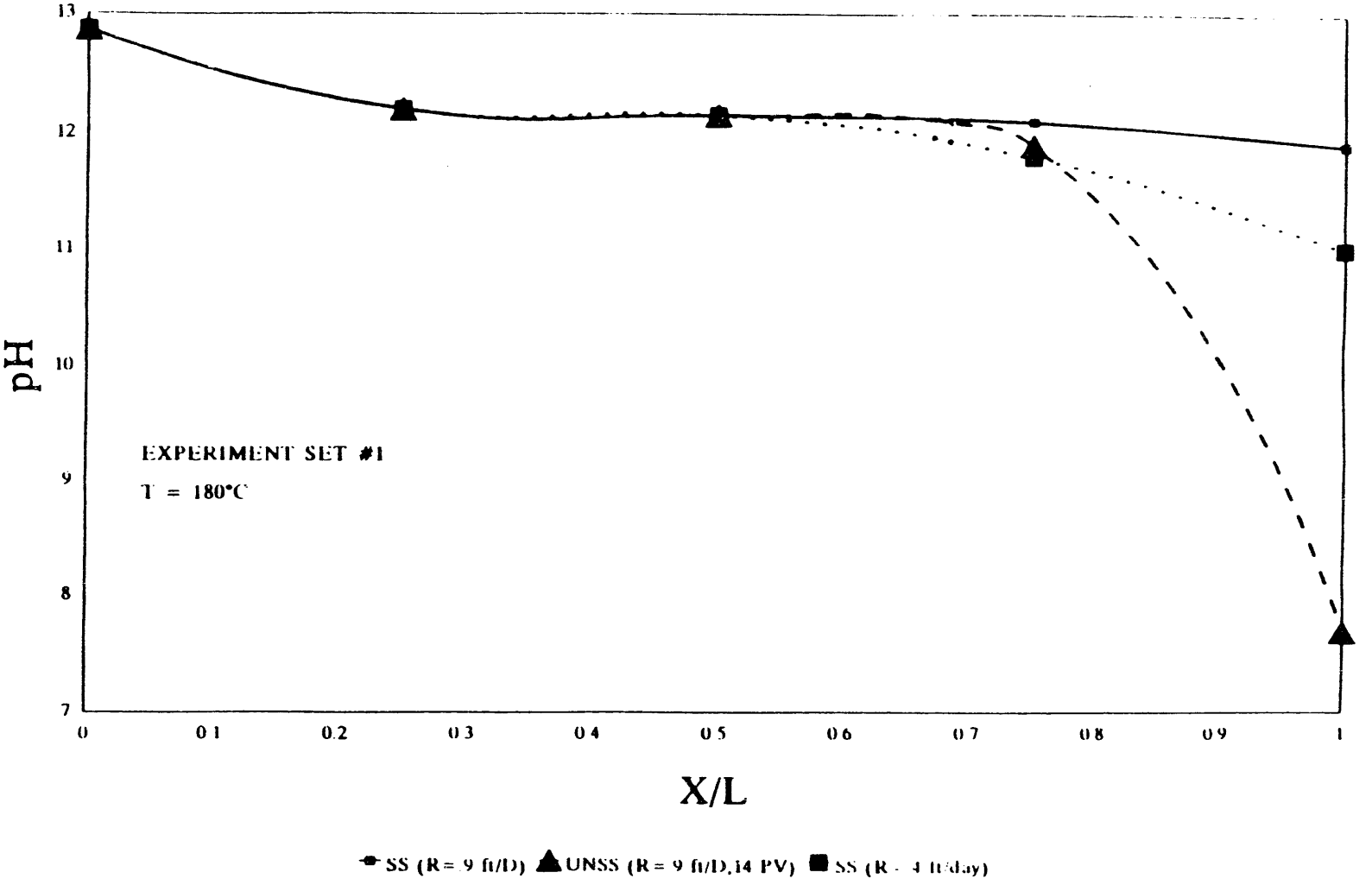

Figure 4.3 pH as a function of dimensionless length for Experiment Set #1

fourth core. The pH was stabilized at 11.0 at the effluent end at the rate of 0.4 ft/day.

The plots of silica concentration as a function of dimensionless length are shown in Figure 4.4. The effluent end silica concentration at unsteady state at the rate of 0.9 ft/day (after 14.0 pore volume), was measured at 150 ppm. At steady state the effluent end silica concentration increased to 1500 ppm. At 0.4 ft/day, the effluent end silica concentration stabilized at 1600 ppm at steady state. In all the plots shown in Figure 4.4 the silica concentration increased from a value of zero at the injection point to values at least as high as what is observed at the end of the first core. All the measured concentrations at the end of the first core in this set of experiments were in excess of 3000 ppm, the highest value being 3800 ppm. It is possible, however, that the silica concentration was even higher than these values between the injection point and the end of the first core. From the end of the first core to the effluent end the silica concentration decreased continuously to the values observed.

4.2. Experiment Set #2

Experiment Set #2 was also conducted at a constant temperature of 180°C throughout. The injected caustic solution had a pH of 12.87. However, the injected solution contained 2% brine. In order to minimize the simultaneous ion exchange and dissolution reaction, the initial rate was increased to 4.8 ft/day,

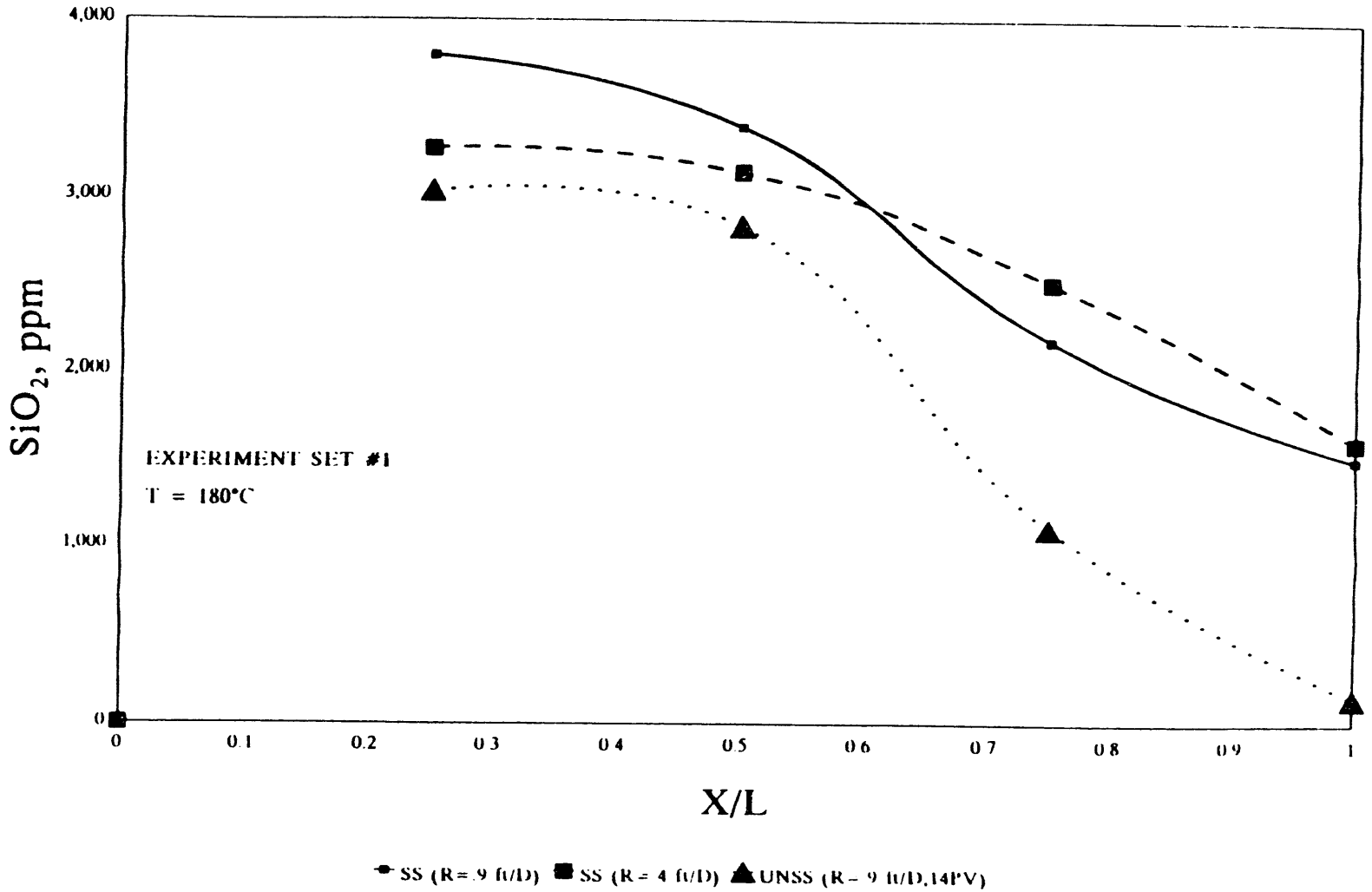

Figure 4.4 Silica concentration as a function of dimensionless length for Experiment Set #1

which was higher than the initial rate in the first set of experiments. The experiment was started by injecting 2% brine solution into the porous medium until the effluent solution pH remained constant near neutral pH. Then the initial rate was set and, after the rate and the pressure across the cores stabilized, the injection of caustic was started.

Figure 4.5 is the plot of the effluent pH as function of pore volumes injected. High pH broke through after 1.5 pore volumes of caustic were injected. The pH stabilized at 11.7. The effluent silica concentration at the steady state was measured at 200 ppm.

When no further change in the effluent pH was observed at the rate of 4.8 ft/day, samples in-between cores were taken for pH and silica concentration measurements. The rate was then reduce to 0.9, 0.4 and 0.2 ft/day, consecutively. At each rate, after the effluent pH had stabilized for a short period of time, samples in-between cores were taken for pH and chemical composition analysis. In order to sample in-between the cores, the flow downstream of where the sample is taken must be interrupted. For instance, if the sample is taken in-between the 3rd and the 4th core (effluent of the 3rd core), the flow to the 4th core must be interrupted. As a result, in some experiments samples were not taken at the end of the first core, in order to minimize the time that caustic injection would be interrupted. Only at the last step of rate reduction were

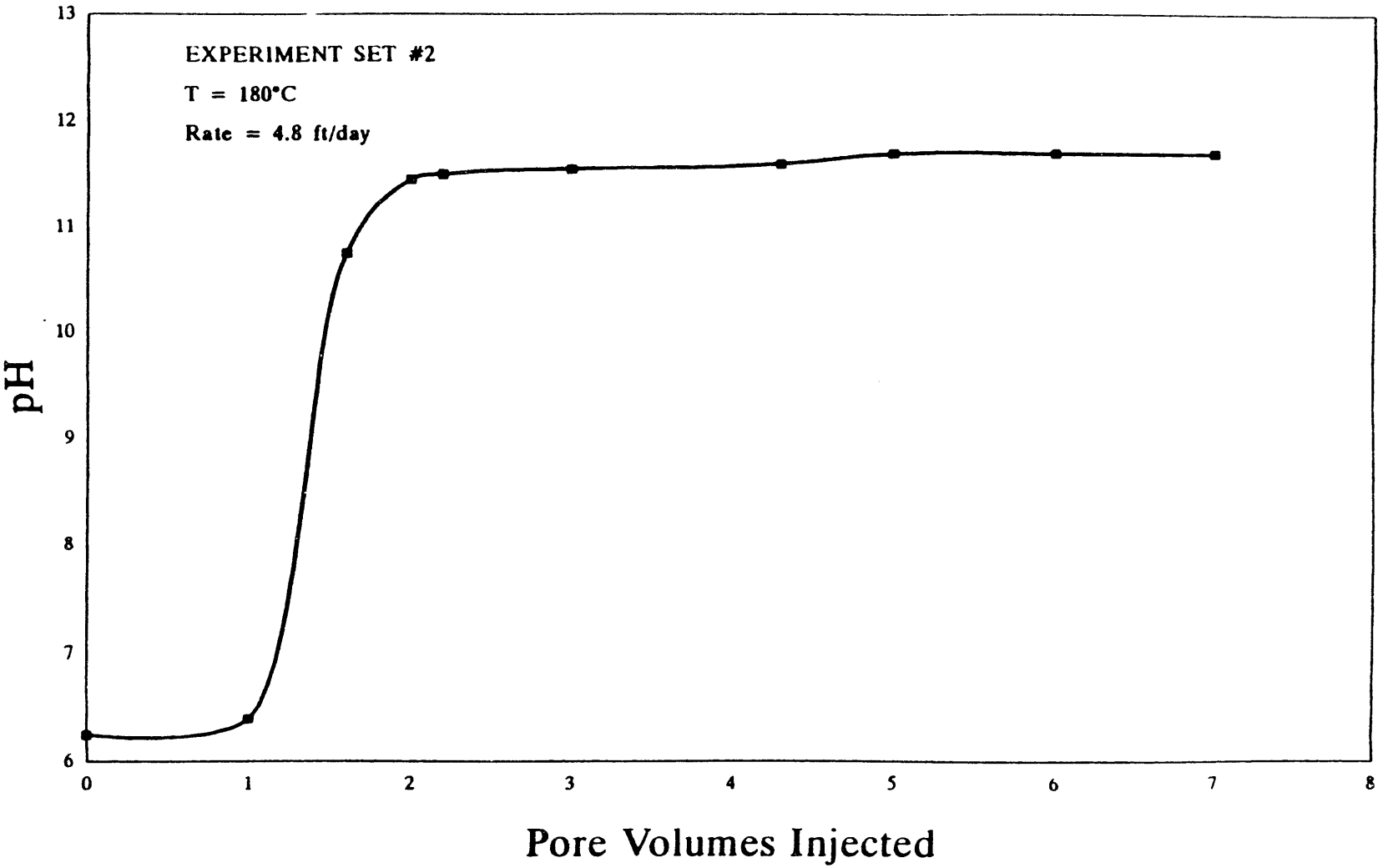

Figure 4.5 Effluent pH vs. pore volumes injected for Experiment Set #2

samples taken at the end of the first core, since afterwards the experiment was terminated.

Figure 4.6 shows the plots of pH as a function of dimensionless length. At lower rates lower effluent pH and lower in-between pHs were observed. The pH profiles are similar in their shapes. From the end of the third core to the effluent, a change in the slope of the profile can be noticed. The effluent pH at 0.9 ft/day was 10.0. At 0.4 ft/day it was 8.7 and at 0.2 ft/day an effluent pH of 7.5 was observed.

Figure 4.7 is the plot of silica as a function of dimensionless length. The effluent end silica concentrations were in the range of 150 to 200 ppm. However, similar to the results of the Experiment Set #1, much higher silica concentrations were measured further upstream in the system. The silica concentration ranges between 550 ppm to 1350 ppm at the end of the second core. The highest concentration was measured at the end of the second core at the rate of 0.4 ft/day. It is possible that higher concentrations of silica also existed between the point of injection and the end of the second core. However, no measurements in this interval were made. The silica profiles indicate that silica concentration increased up to the end of the second core and then decreased from the end of the second core to the effluent end.

Aluminum concentrations were measured using atomic absorption. Figure 4.8 shows the plot of alumina as a function dimensionless length. Concentrations

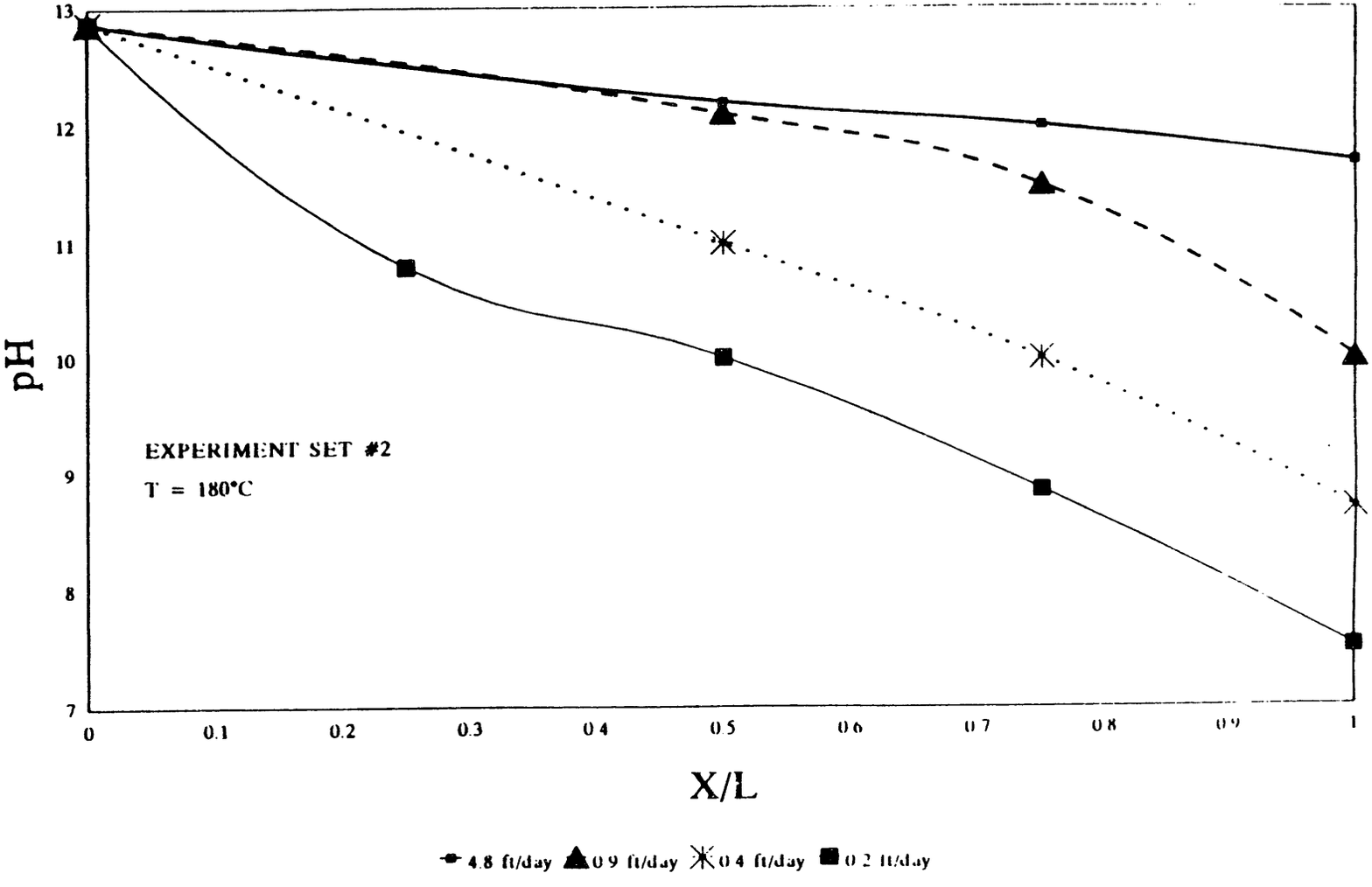

Figure 4.6 pH as a function of dimensionless length for Experiment Set #2.

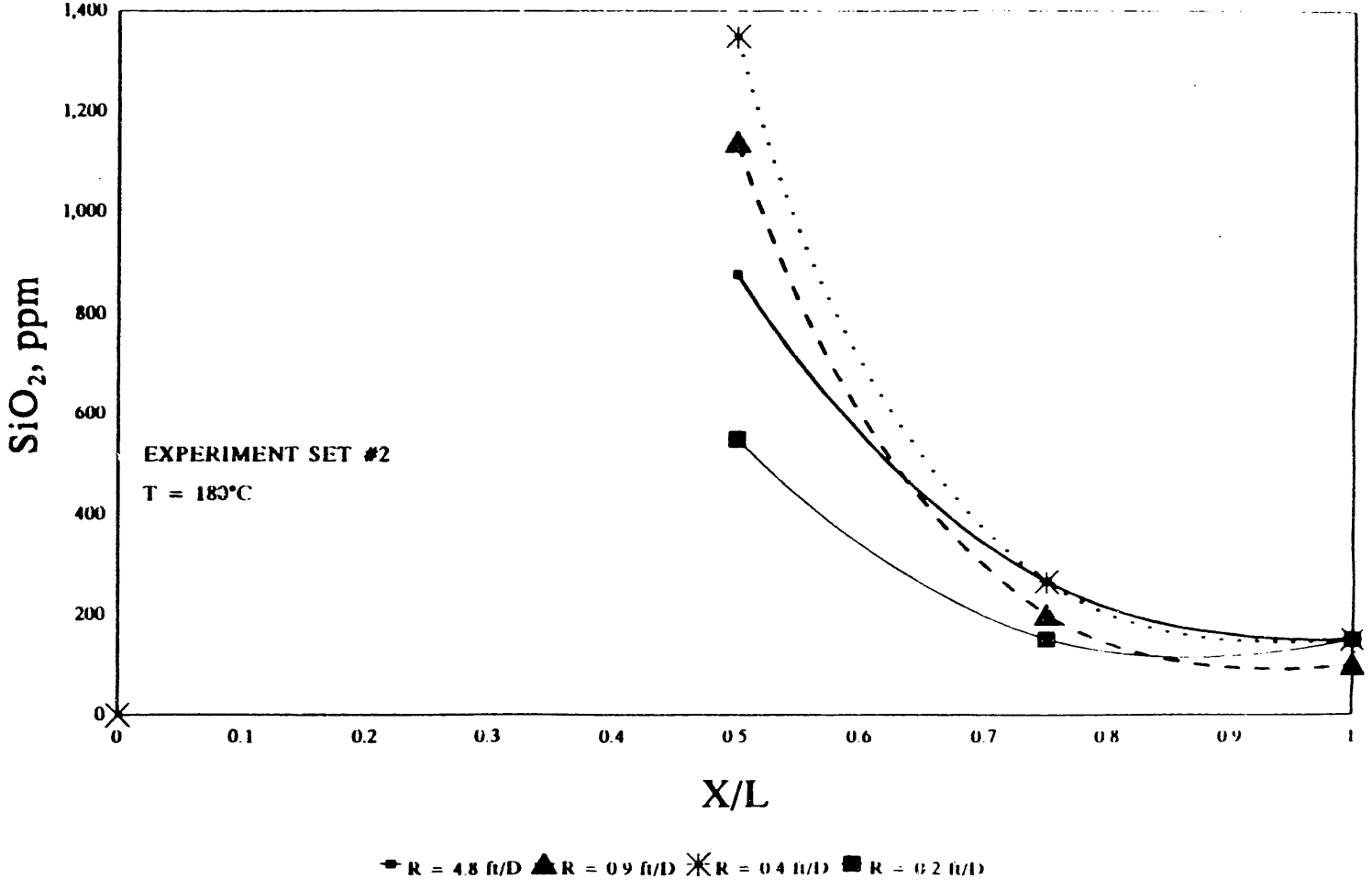

Figure 4.7 Silica concentration as a function of dimensionless length for Experiment Set #2.

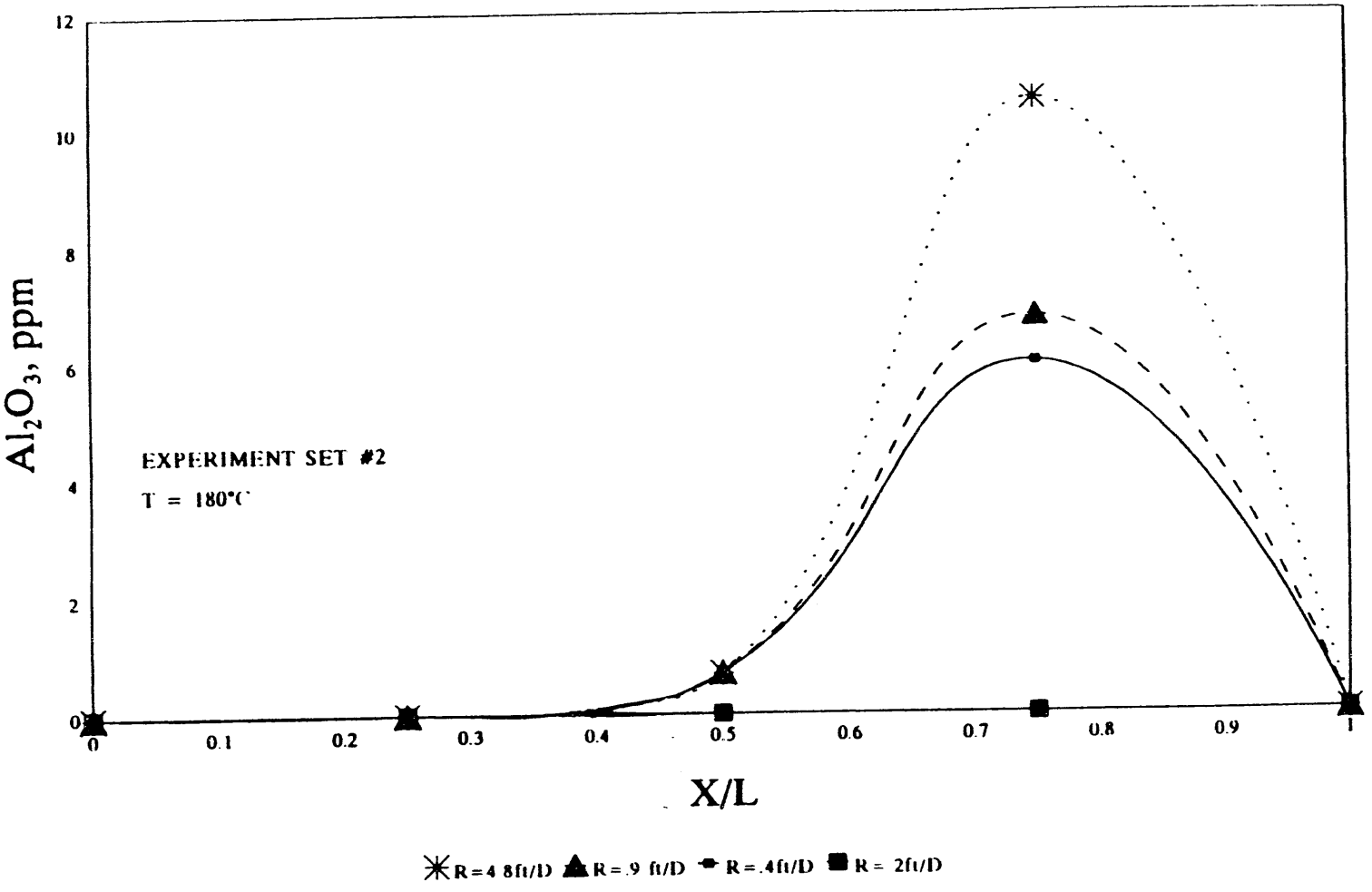

Figure 4.8 Alumina concentration as a function of dimensionless length for Experiment Set #2.

under 1 ppm are not detectable by atomic absorption. At the rate of 0.2 ft/day, none of the samples showed any detectable alumina. At the rates of 4.8, 0.9 and 0.4 ft/day, only the samples taken from the end of the third core showed some alumina in solution. The samples from the ends of the first, second and the fourth cores did not show detectable alumina. The highest concentration was 10.5 ppm, measured at the rate of 4.8 ft/day. Concentrations of 6.8 and 6.0 ppm were measured at rates of 0.9 and 0.4 ft/day at the end of the third core.

The duration of this experiment was 30 days and a total of 22 pore volumes of caustic were injected.

4.3. Experiment Set #3

Experiment Set #3 started at a lower temperature than previous experiments and was increased in steps to 180°C. The injected caustic solution had a pH of 12.87, similar to the other experiments. The injected solution contained 2% brine. Prior to caustic injection, the porous medium was flushed with 2% brine solution until the effluent pH was constant around neutral pH. The effluent pH, silica concentration and alumina concentration as a function of total pore volumes injected for all temperatures and flow rates are plotted in Figure 4.9. The results at each temperature are discussed separately in more detail in the following paragraphs.

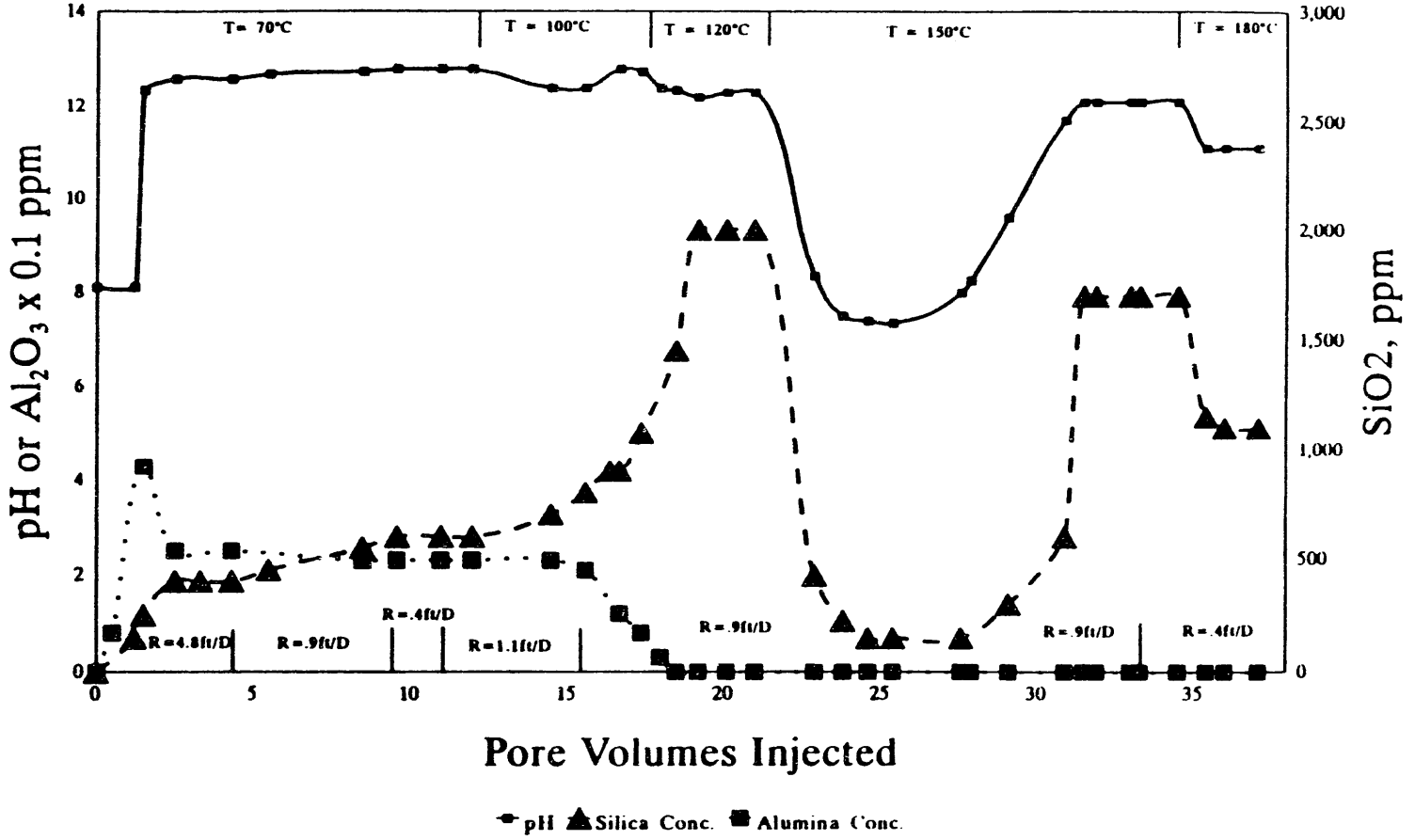

Figure 4.9 Effluent pH, silica and alumina concentration as function of total pore volumes injected, at different temperatures and flow rates for Experiment Set #3.

4.3.1. Results at 70°C

The experiment started at 70°C at the rate of 4.8 ft/day. After steady state was established at this rate, the same procedure was followed as for the previous experiments. The rate was reduced to 0.9 ft/day and 0.4 ft/day. The rate was then increased to 1.1 ft/day.

Initially, at the rate of 4.8 ft/day the caustic broke through after 1.5 pore volumes. The pH stabilized at about 12.6. Then the rate was reduce to 0.9 ft/day. At this rate, the pH stabilized at 12.8. No further drastic change in the pH was noticed following the change in the injection rate. Figure 4.10 shows pH, silica and alumina as a function of pore volumes injected at 70°C. Samples were collected from the end of the second and third cores following the same procedure as for the other experiments. Figure 4.11 shows pH as function of dimensionless length at 70°C at the rate of 0.9 ft/day. As can be noticed, no significant change in the pH was observed.

The samples were analyzed for silica concentration in solution using atomic absorption. Figure 4.10 shows that silica breakthrough occurred at the same time as caustic. Silica concentration at the effluent stabilized around 600 ppm at the rate of 0.9 ft/day. Figure 4.12 shows the plot of silica concentration as a function of dimensionless length. At the rate of 4.8 ft/day the effluent silica concentration was around 400 ppm. It increased continuously from 345 ppm at the end of the second core to 400 ppm at the effluent end. A higher effluent

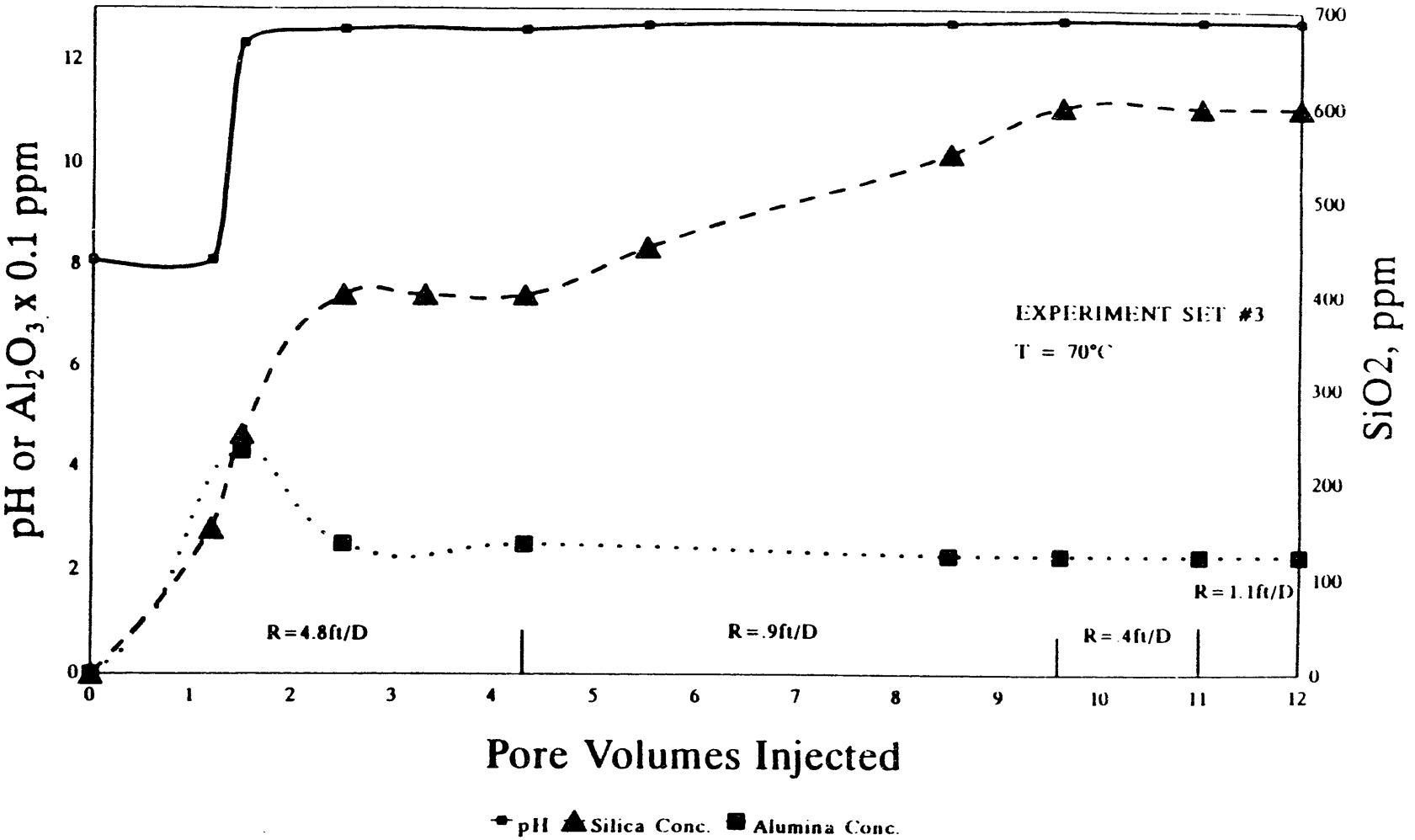

Figure 4.10 Effluent pH, silica and alumina as a function of pore volumes injected, at 70°C for Experiment Set #3.

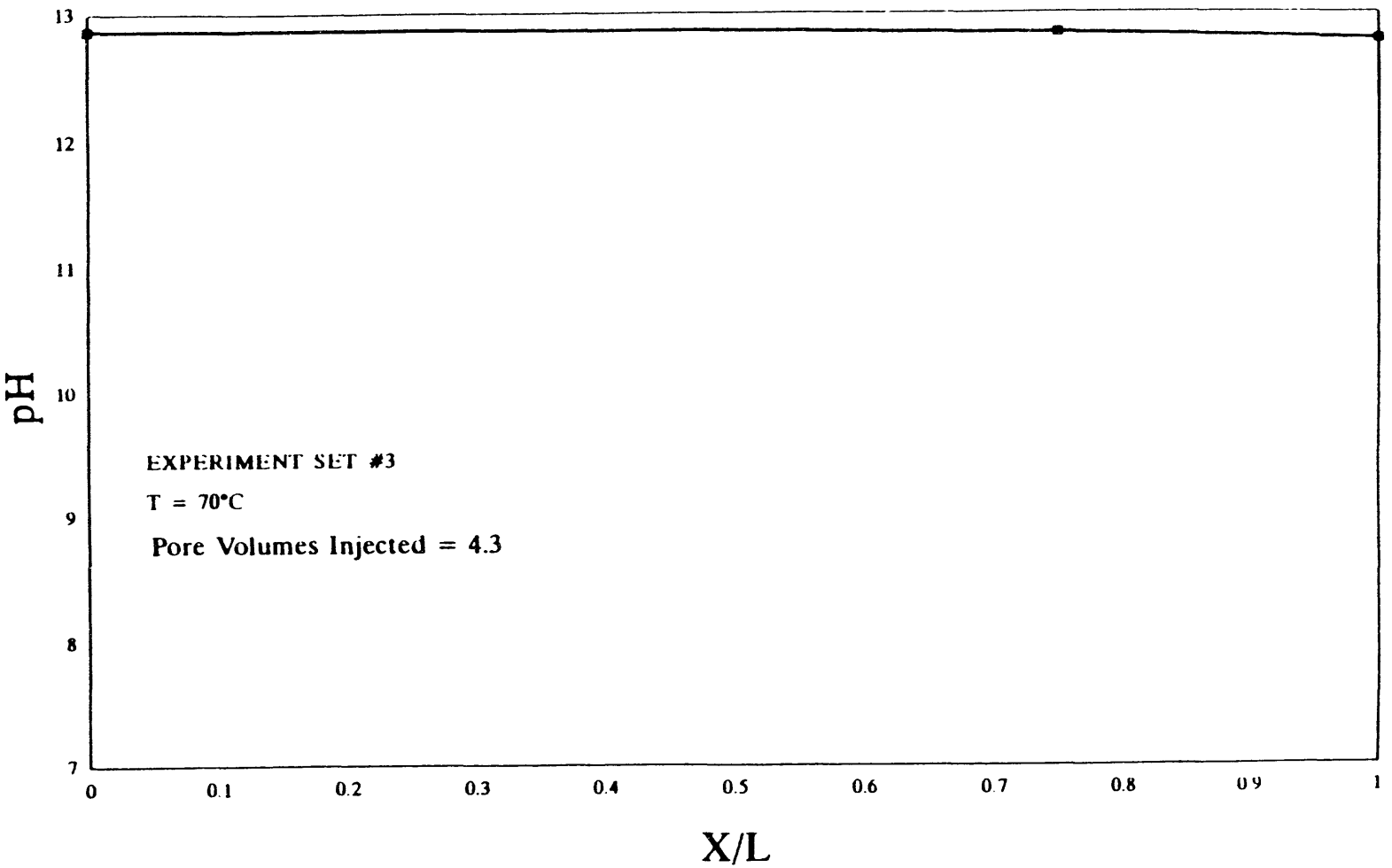

Figure 4.11 pH as a function of dimensionless length, at 70°C for Experiment Set #3.

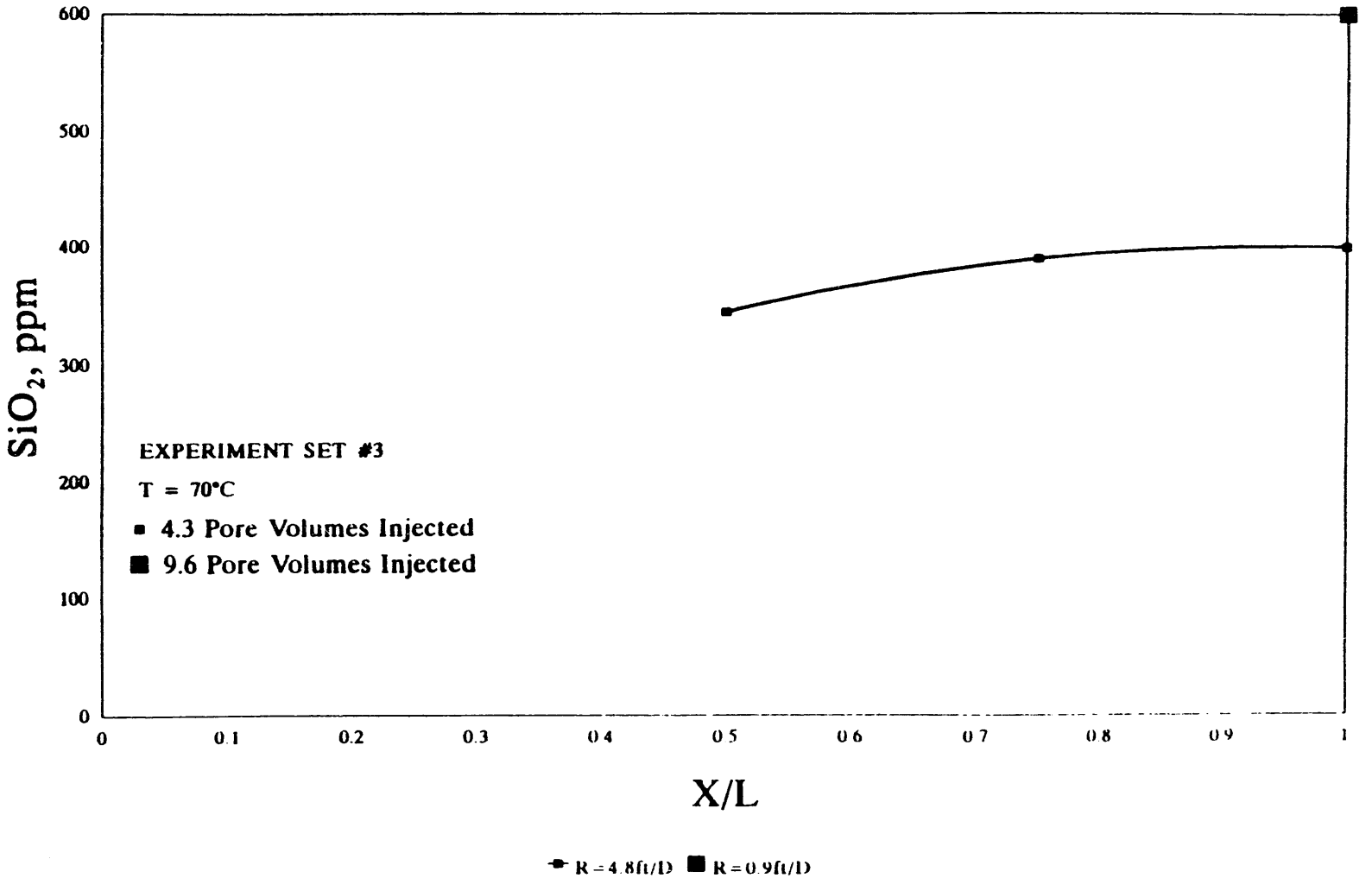

Figure 4.12 Silica concentration vs. dimensionless length at 70°C for Experiment Set #3.

silica concentration was measured when the rate was 0.9 ft/day compared to that measured when the rate was 4.8 ft/day.

The samples were analyzed for alumina concentration in solution using atomic absorption. Figure 4.10 shows that alumina concentration increased from a value of zero at zero pore volumes injected to 43.0 ppm at 1.5 pore volumes. However, the alumina concentration decreased continuously and stabilized at around 23.0 ppm.

4.3.2. Results at 100°C

After completing the experiment at 70°C the temperature was raised to 100°C. Initially the rate was kept constant at 1.1 ft/day. Figure 4.13 shows pH, silica and alumina as a function of pore volumes. As can be seen, following the increase in temperature, there was slight temporary reduction in pH. However, it increased again to 12.8 once the rate was reduced to 0.9 ft/day.

Referring to Figure 4.13, unlike the pH, effluent silica concentration continued to increase when temperature was raised from 70°C to 100°C. This increasing trend continued when the rate was reduced to 0.9 ft/day.

Figure 4.14 is the plot of silica concentration as a function of dimensionless length at 100°C. The only samples from in-between cores was taken at the end of the third core at the rate of 1.1 ft/day. No change was

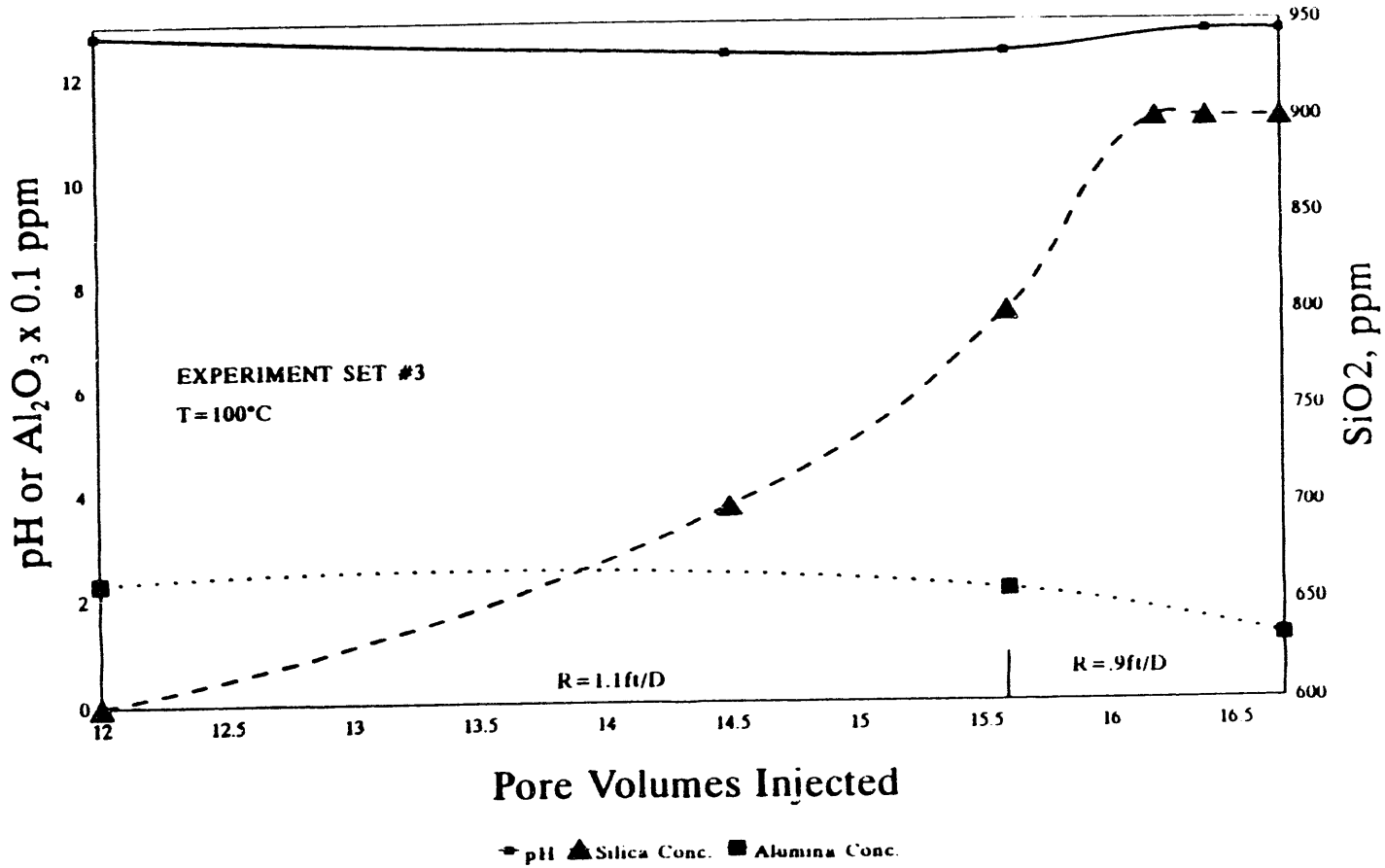

Figure 4.13 Effluent pH, silica and alumina concentrations as function of pore volumes injected, at 100°C for Experiment Set #3.

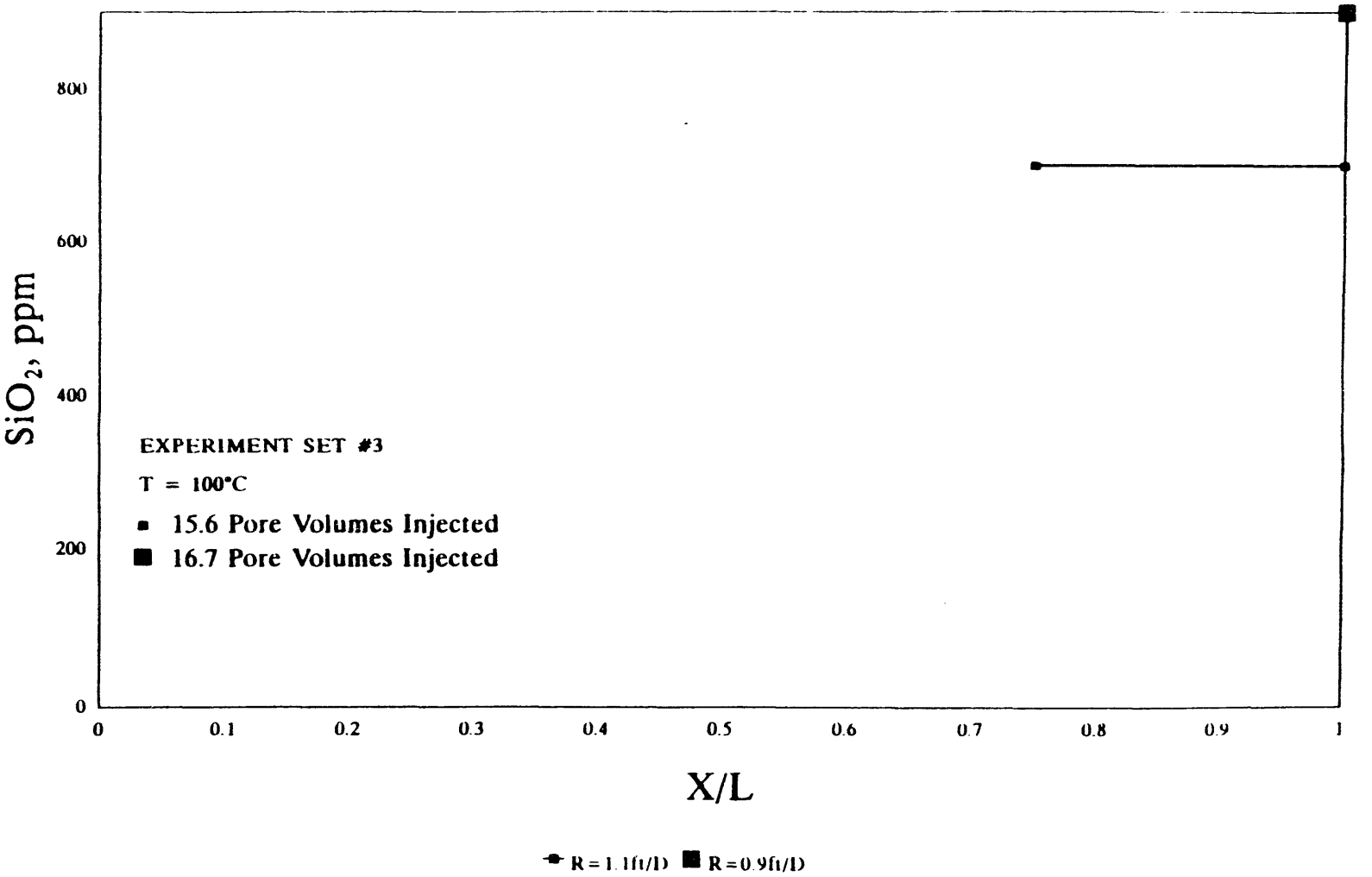

Figure 4.14 Silica concentration vs. dimensionless length at 100°C for Experiment Set #3.

observed compared to what was measured at the effluent end. In Figure 4.13 a slight reduction in effluent alumina concentration at 100°C can be noticed.

4.3.3. Results at 120°C

The temperature was then increased to 120°C while the rate was kept constant at 0.9 ft/day. Figure 4.15 shows the effluent pH, silica and alumina concentration as a function pore volumes injected. As can be seen from Figure 4.15, the pH decreased to 12.3 with an increase in temperature to 120°C.

Figure 4.16 shows the pH continuously decreased from a value of 12.87 at the injection point to 12.3 at the effluent end. Referring to Figure 4.15, the effluent silica concentration was increased drastically to 2000 ppm at the steady state. As can be seen from Figure 4.17, the silica concentration increased from a value of zero at the injection point to 3200 ppm at the end of the third core. However, the silica concentration decreased from 3200 ppm to 2000 ppm at the effluent. In Figure 4.15 the continuous decrease in alumina concentration can be observed. There was no alumina present at the end of the experiment at 120°C.

4.3.4. Results at 150°C

Keeping the rate constant at 0.9 ft/day, the temperature was increased to 150°C. The pH decreased rapidly. After approximately 3.0 pore volumes the pH decreased from 12.3 to around 7.4. The pH stayed at values between 7.4 to 8.0

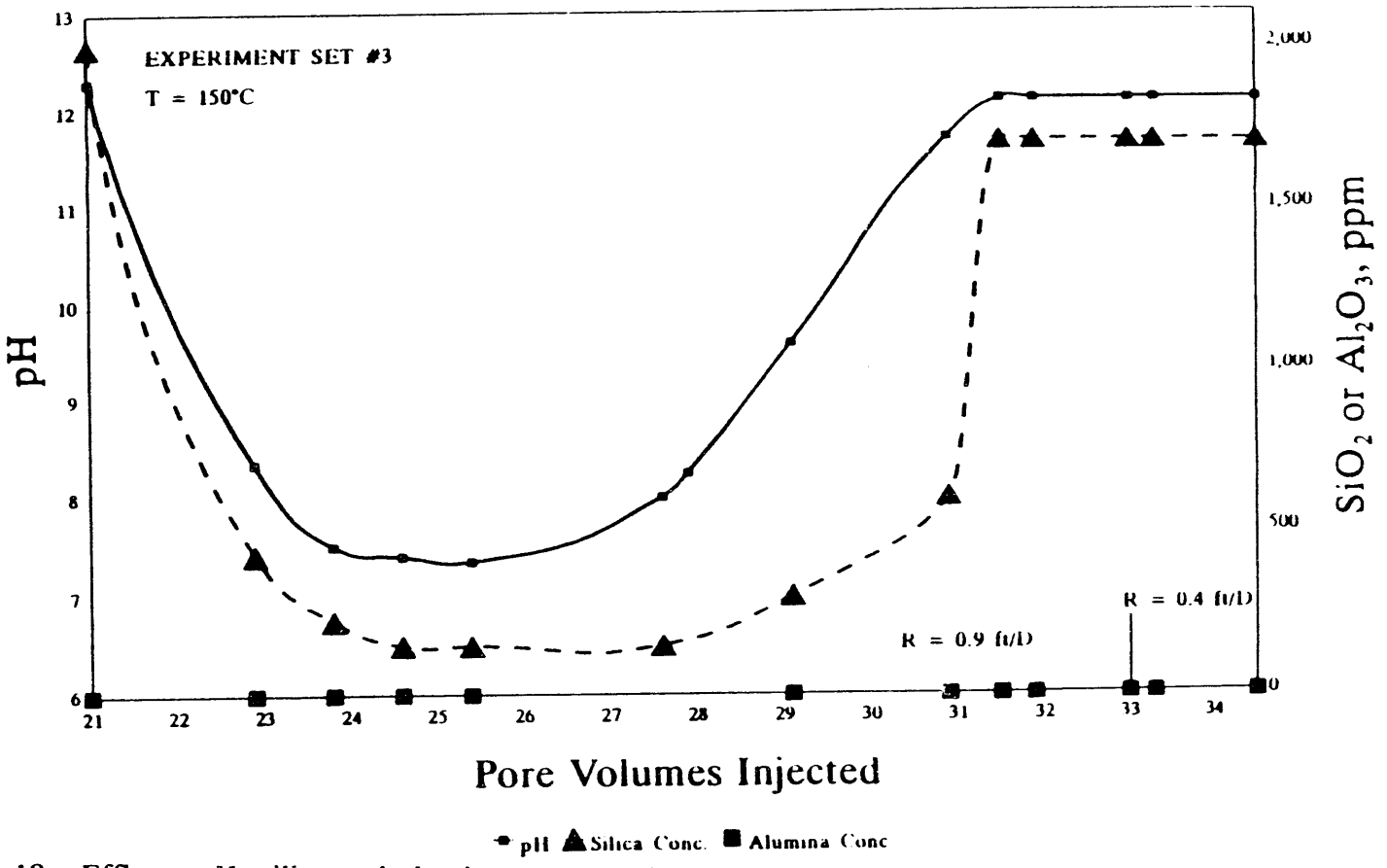

Figure 4.18 Effluent pH, silica and alumina concentration as a function of pore volumes injected, at 150°C for Experiment Set #3.

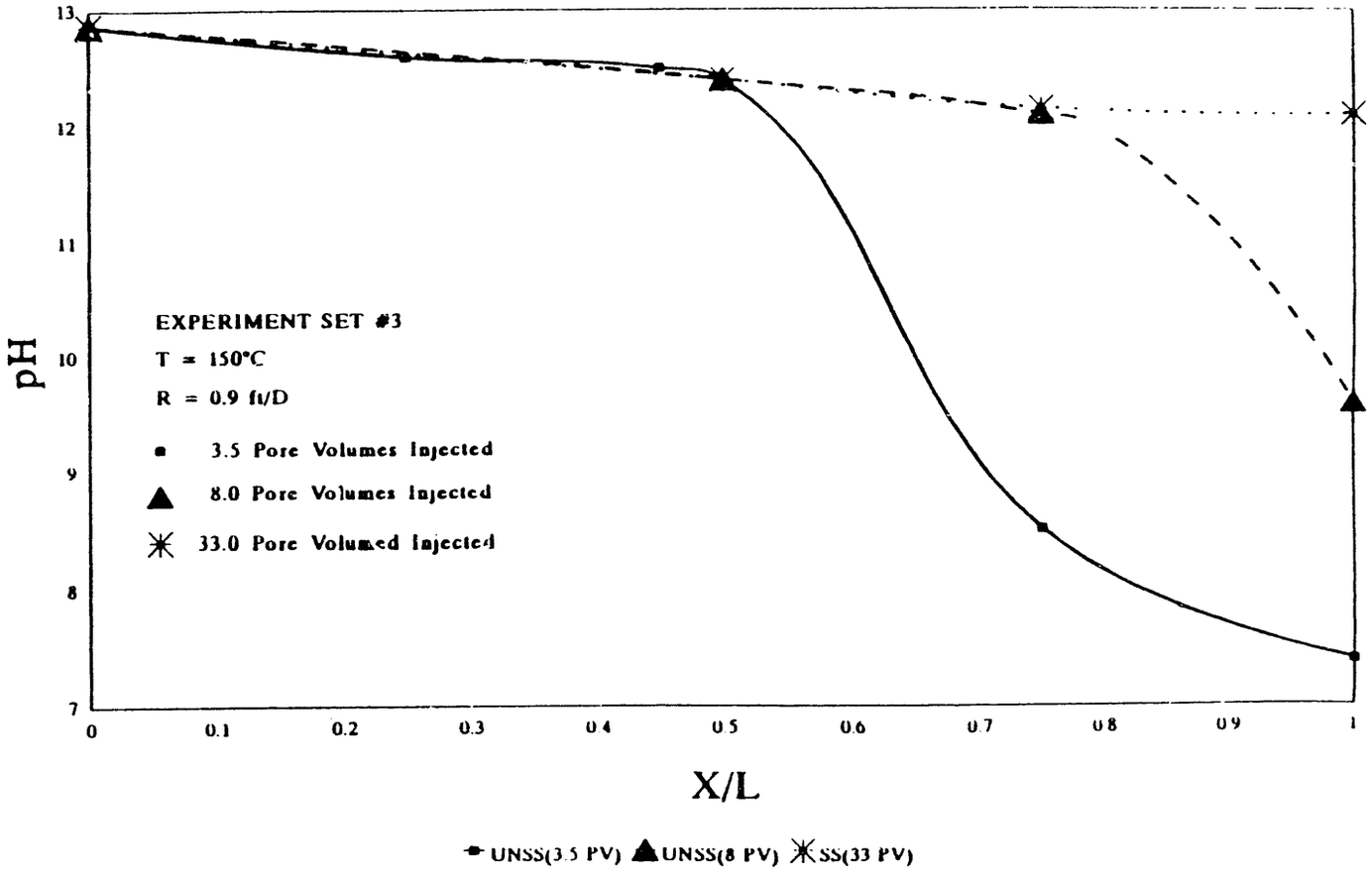

Figure 4.19 pH as a function of dimensionless length at 150°C for Experiment Set #3.

approximately 10 more pore volumes at 150°C, it increased to 1700 ppm. Figure 4.20 is the plot of silica concentration as a function of dimensionless length. The silica concentration increased from a value of zero at the injection point to values at least as high as that measured at the end of the second core. Then from the end of the second core to the effluent end, silica concentration continuously decreased. After injecting 3.5 pore volumes at 150°C, silica concentrations were measured at 150 ppm and 180 ppm at the ends of the third and fourth cores. However, the silica concentration at the end of the second core was measured at 2800 ppm. At steady state higher silica concentrations were measured throughout the porous medium. The observed effluent silica concentration was measured at 1700 ppm. The silica concentration at the ends of the second and the third cores were measured at 3150 and 2300 ppm, respectively.

After completion of the experiment at 0.9 ft/day, the rate was reduced to 0.4 ft/day at constant temperature. Referring to Figure 4.18, no change in the effluent pH was observed. Also the effluent silica concentration stayed the same. Figure 4.21 shows the silica concentration as a function of dimensionless length at the rate of 0.4 ft/day. This profile is slightly different from that shown for the rate of 0.9 ft/day in Figure 4.20. A higher silica concentration was observed at the end of the third core at the rate of 0.4 ft/day than that observed at 0.9 ft/day. At 0.4 ft/day the silica concentration at the end of the third core was measured at 2900 ppm.

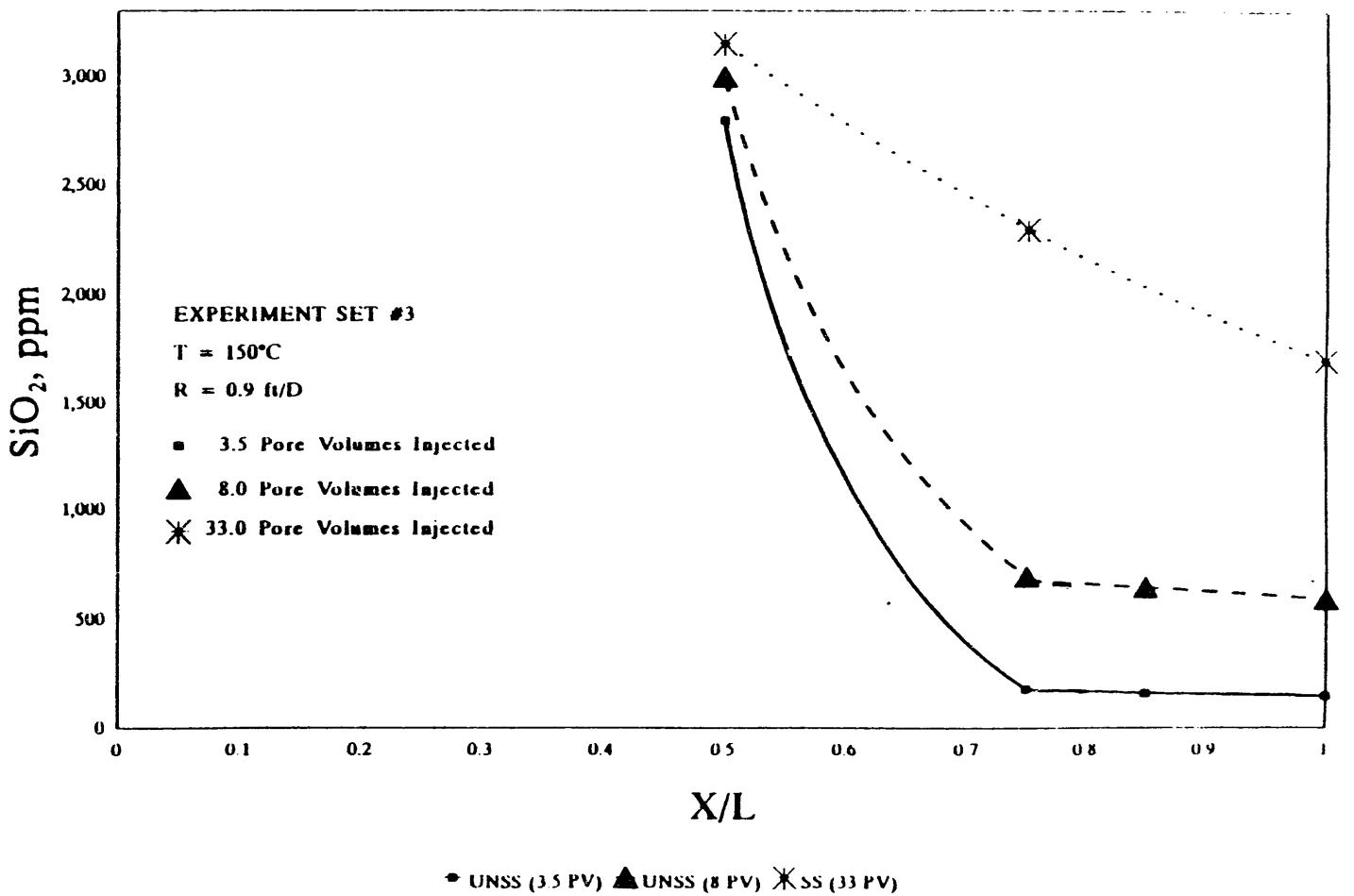

Figure 4.20 Silica concentration as a function of dimensionless length, at 150°C and flow rate of 0.9 ft/D for Experiment Set #3.

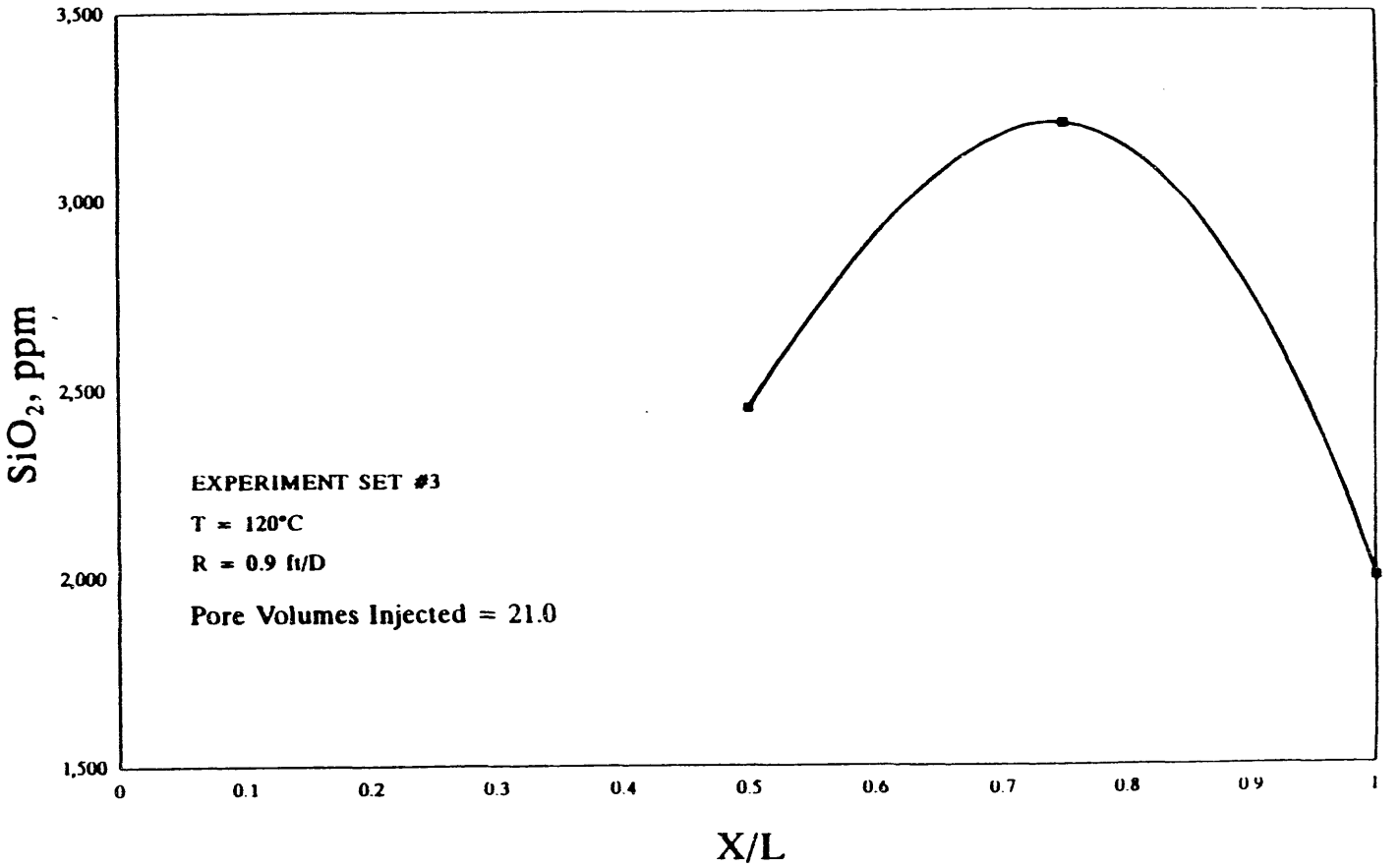

Figure 4.21 Silica concentration as a function of dimensionless length, at 150°C and flow rate of 0.4 ft/D for Experiment Set #3.

The profile of pH as a function of dimensionless length at the rate of 0.4 ft/day was the same as the one at the rate of 0.9 ft/day.

All the collected samples at this temperature and for various rates were analyzed for alumina using atomic absorption method. There was no alumina present in any of the samples.

4.3.5. Results at 180°C

With the rate constant the temperature was raised to 180°C. The effluent pH, silica and alumina as a function of pore volumes injected are shown in Figure 4.22. The effluent pH decreased to 11.1. The effluent silica concentration also decreased to 1150 ppm. As at 150°C, the collected samples did not contain any alumina.

All the collected samples were analyzed for iron and magnesium using atomic absorption. None of the samples contained measurable amounts of the above elements.

X-ray diffraction was performed on the rock samples taken from the middle of the first, second, third and the fourth cores, after completion of the experiment. A sample of the fired Berea sandstone was also analyzed for mineral identification using X-ray diffraction method. Figures 4.23 to 4.26 show the peaks obtained. Figure 4.27 shows the similar results for the unreacted fired Berea sandstone sample.

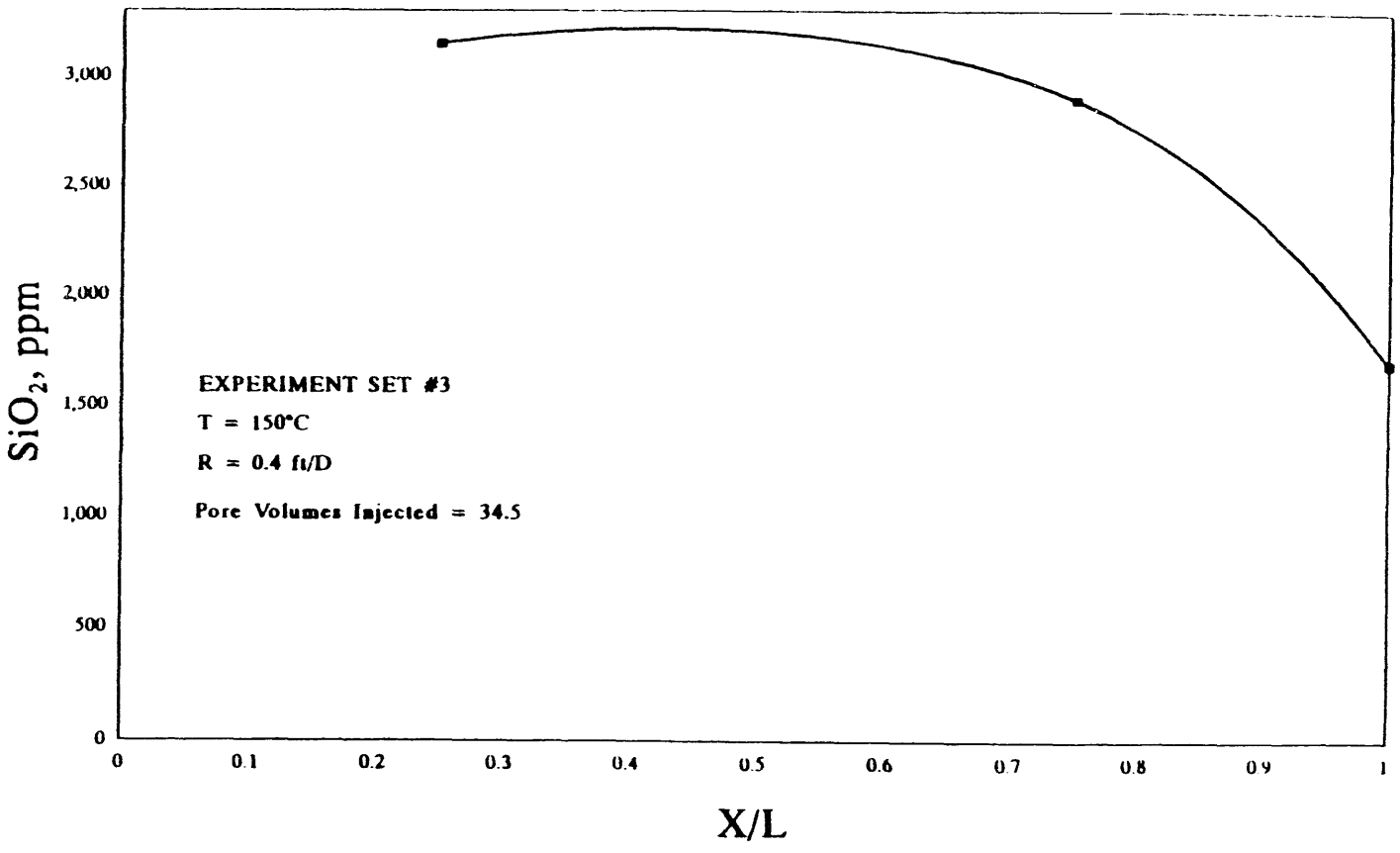

Figure 4.22 Effluent pH, silica and alumina concentration as a function of pore volumes injected at 180°C for Experiment Set #3.

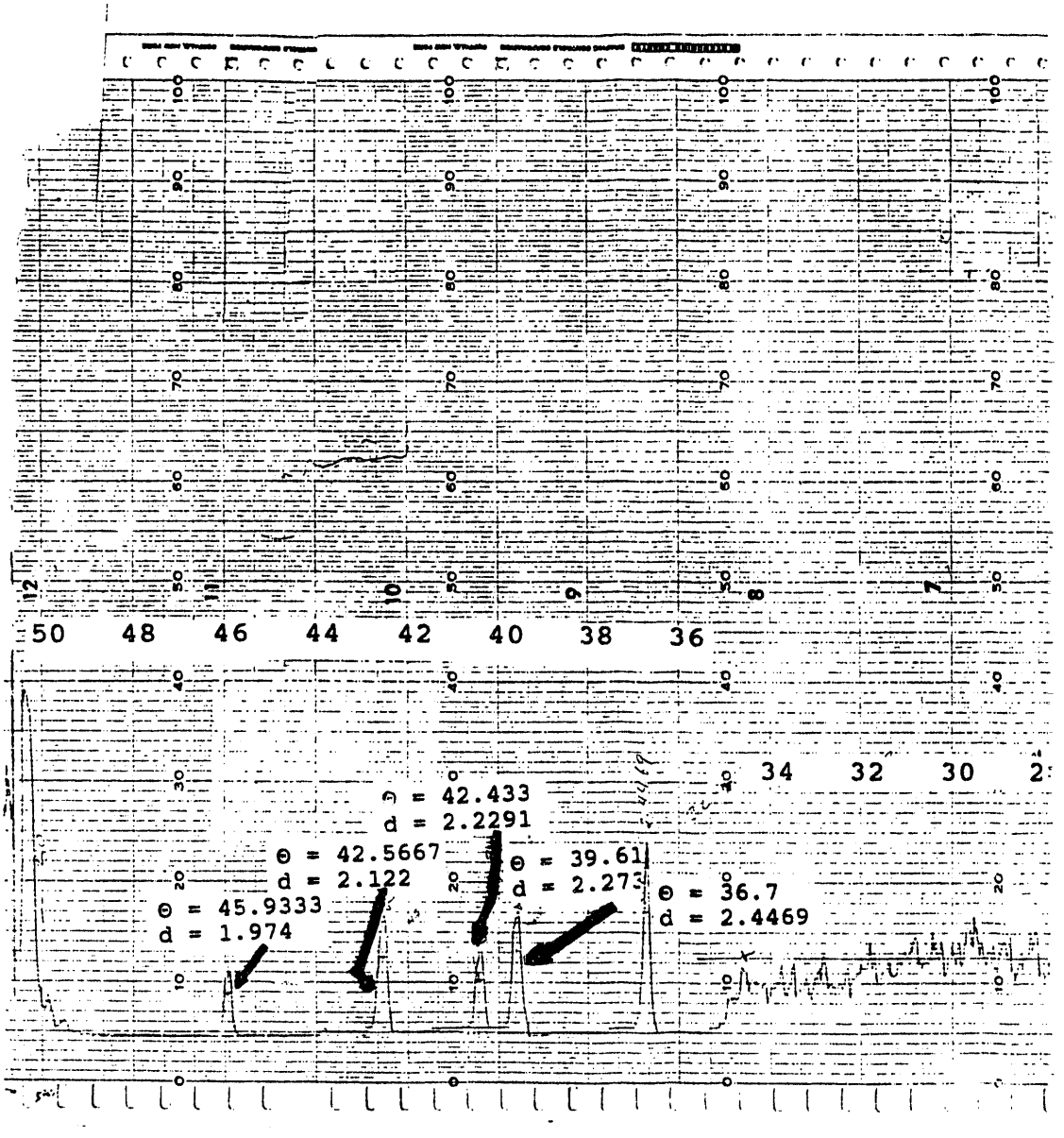

Figure 4.23 X-ray diffraction of the sample from core #1

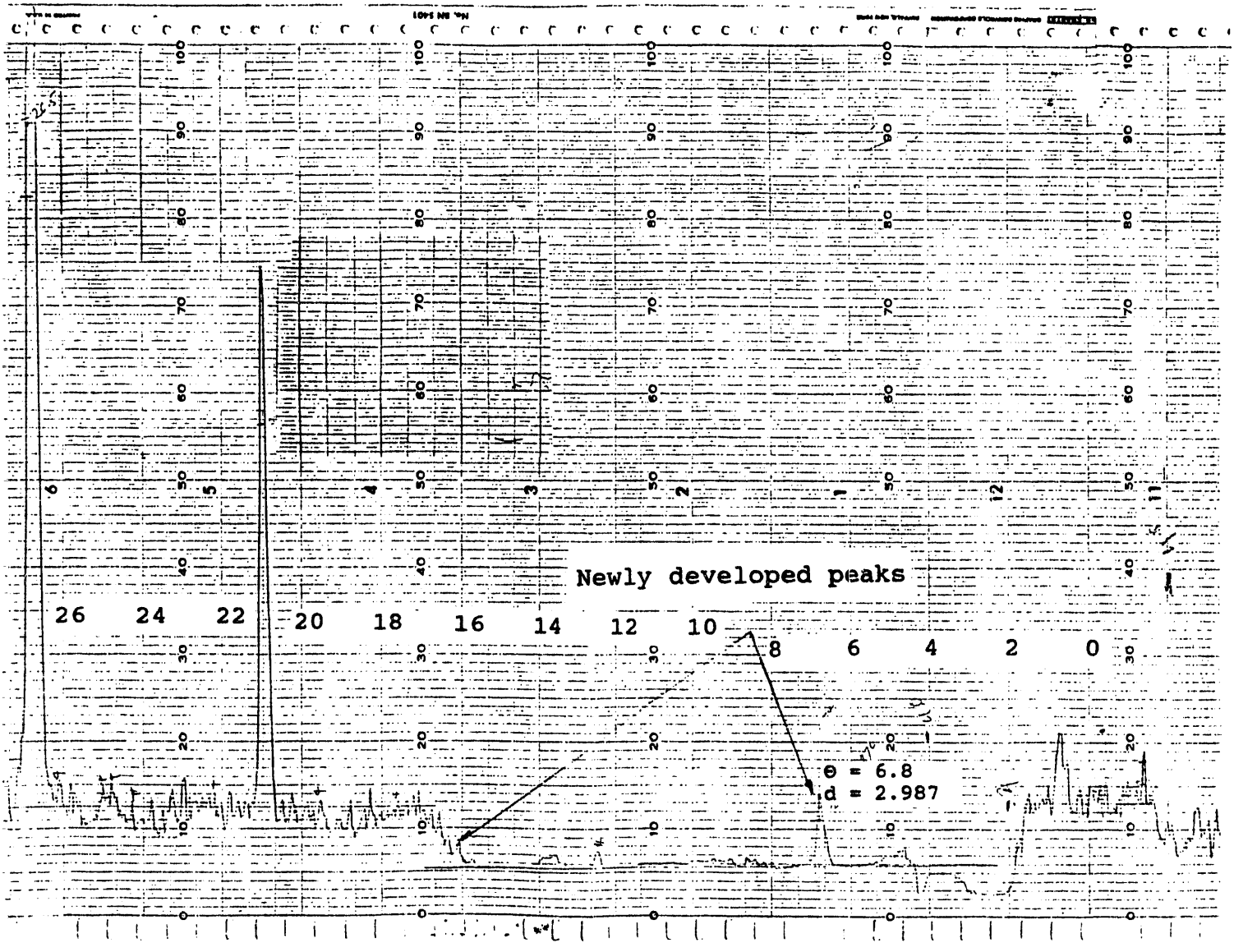
Newly developed peaks
26
24
22
20
18
16
14
12
10
8
6
4
2
0
Θ = 6.8
d = 2.987

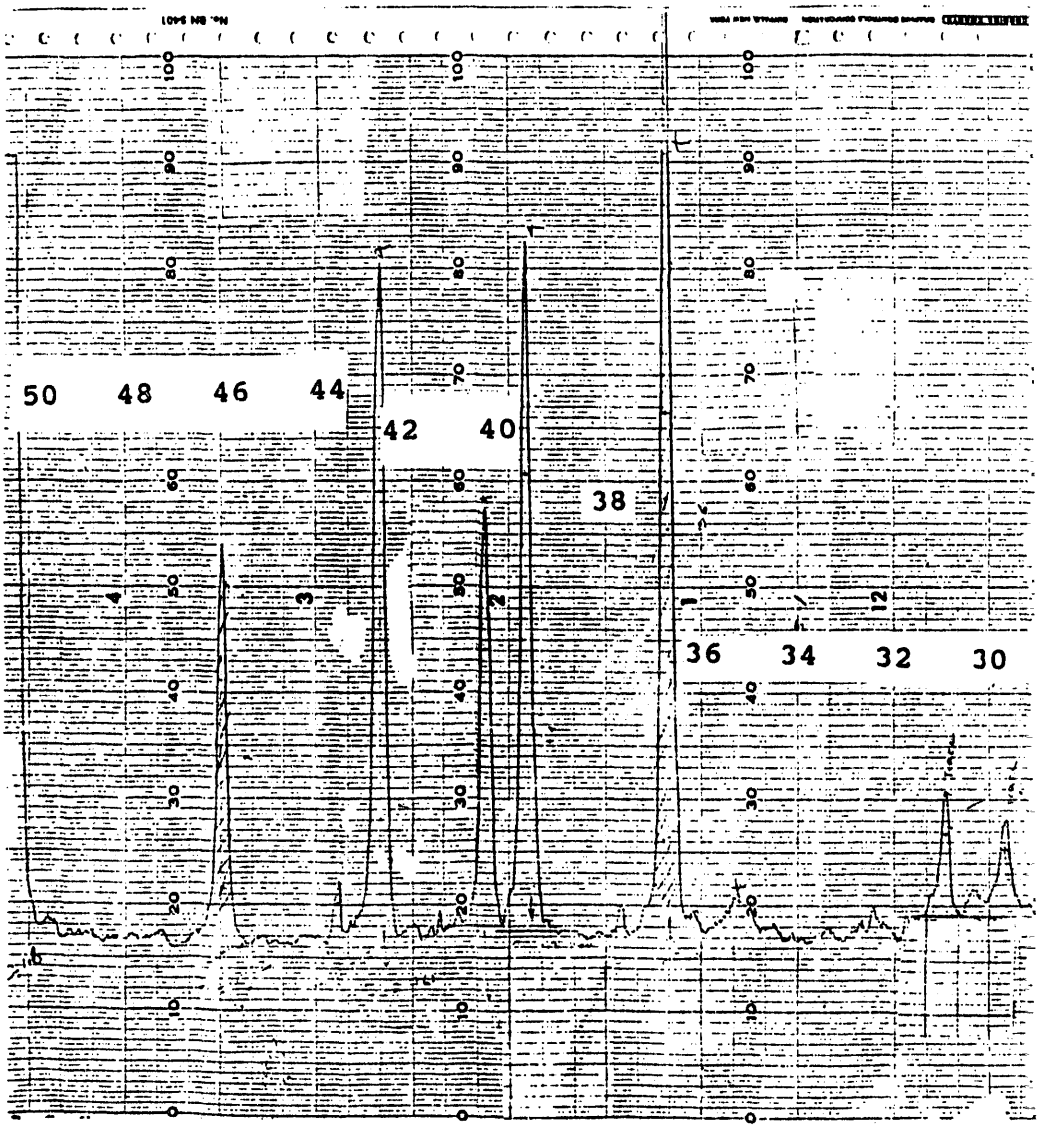

Figure 4.24 X-ray diffraction of the sample from core #2

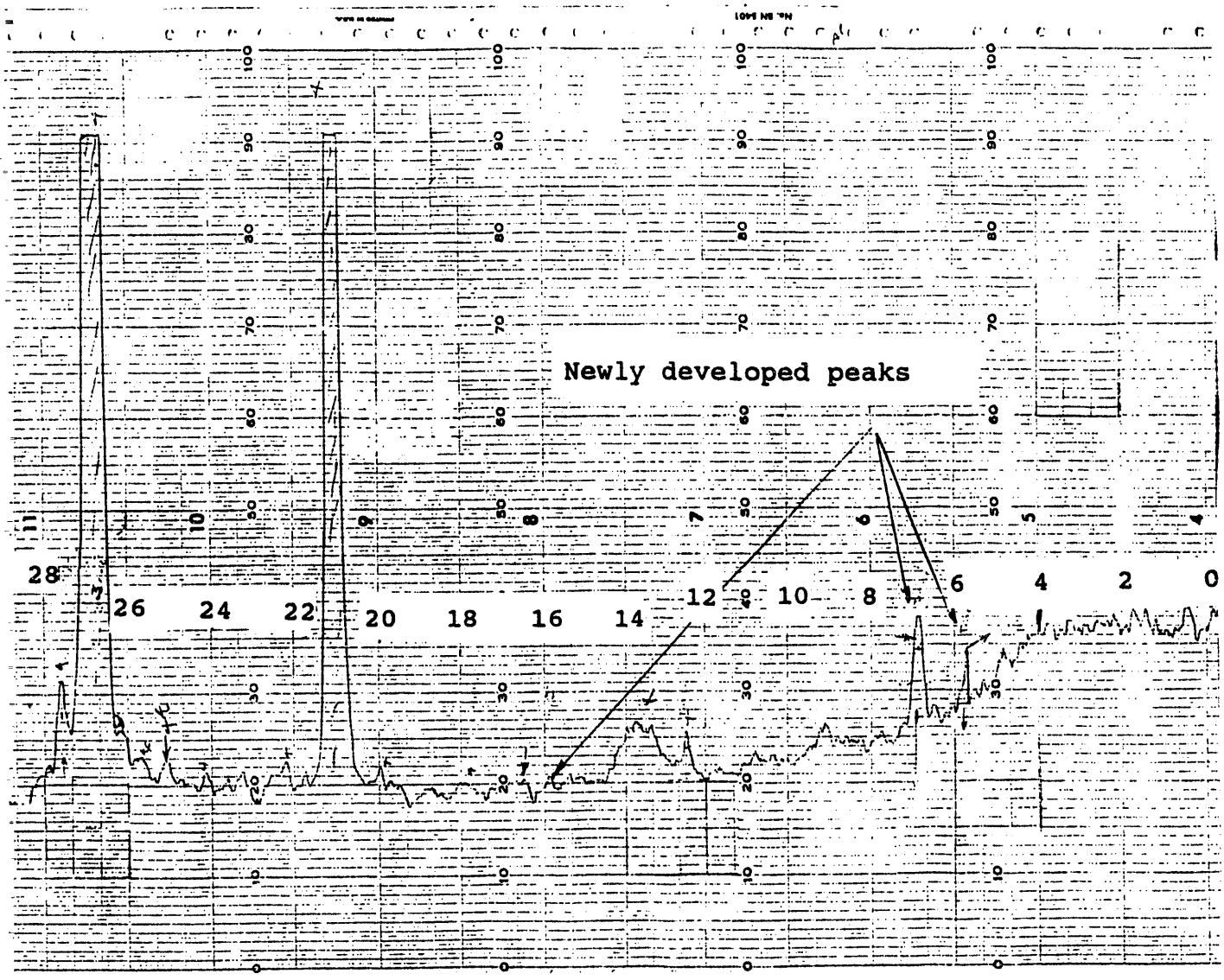
Newly developed peaks
28
26
24
22
20
18
16
14
12
10
8
6
4
2
0

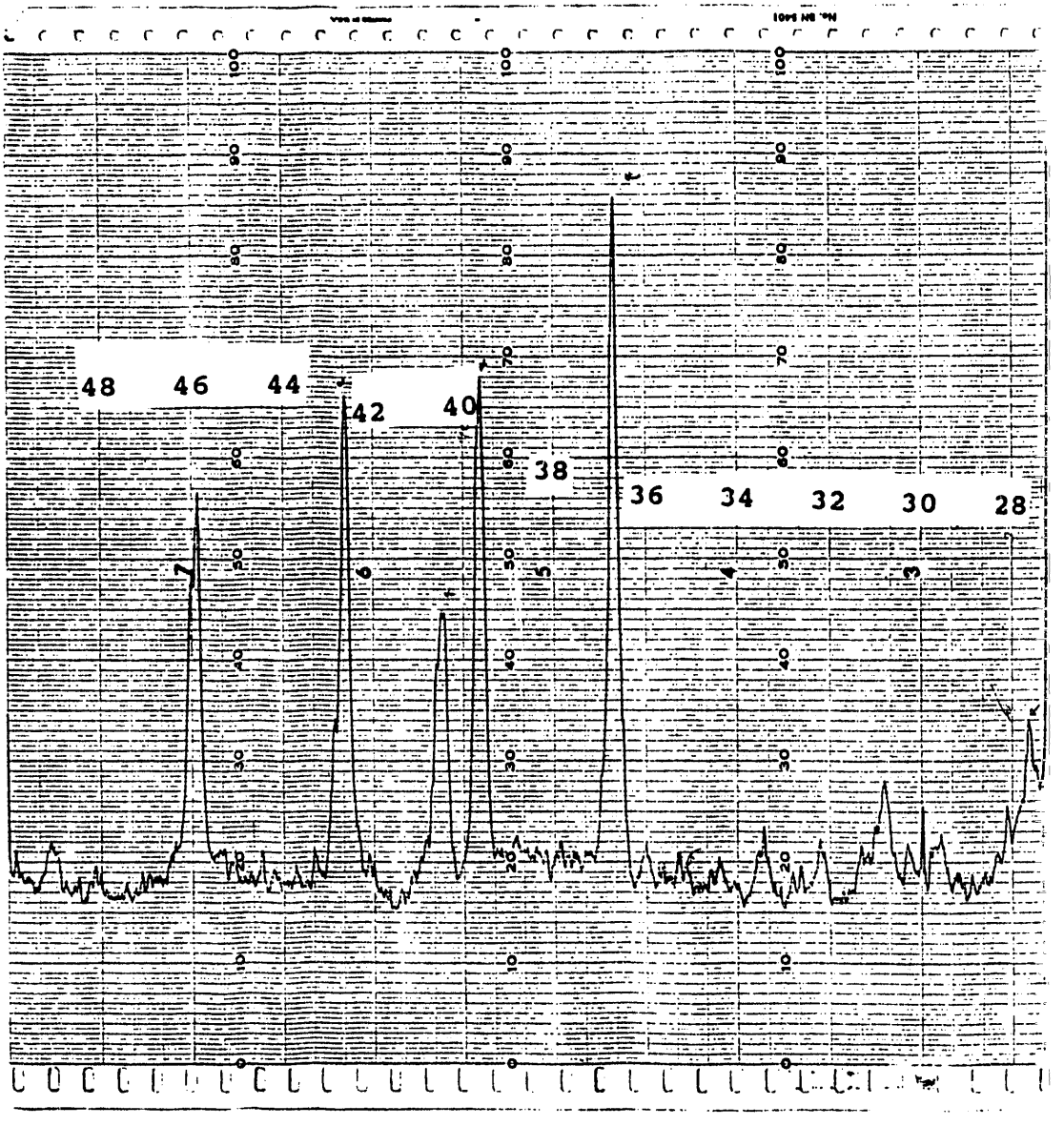

Figure 4.25 X-ray diffraction of the sample from core #3

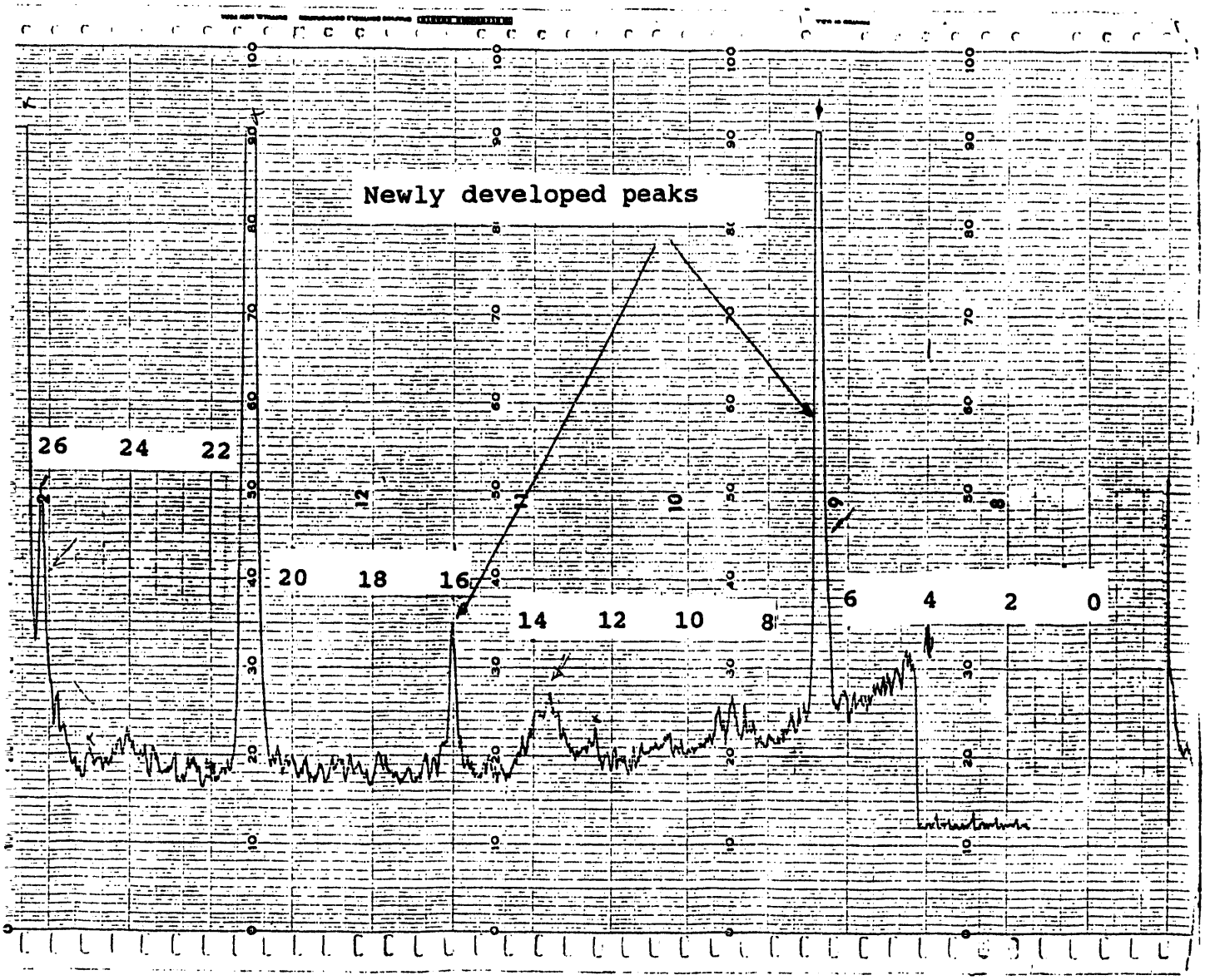
Newly developed peaks
26
24
22
20
18
16
14
12
10
8
6
4
2
0

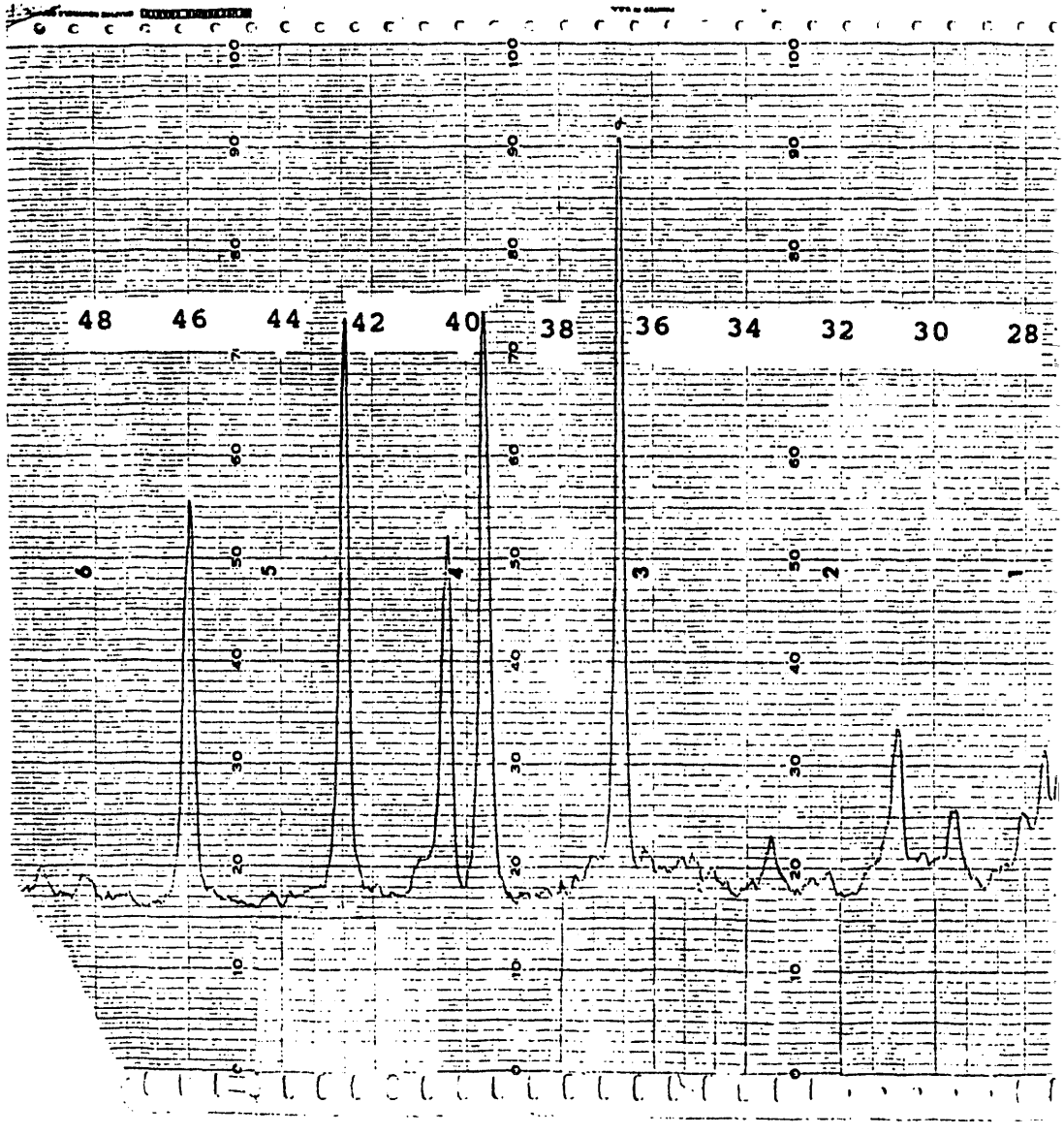

Figure 4.26 X-ray diffraction of the sample from core #4

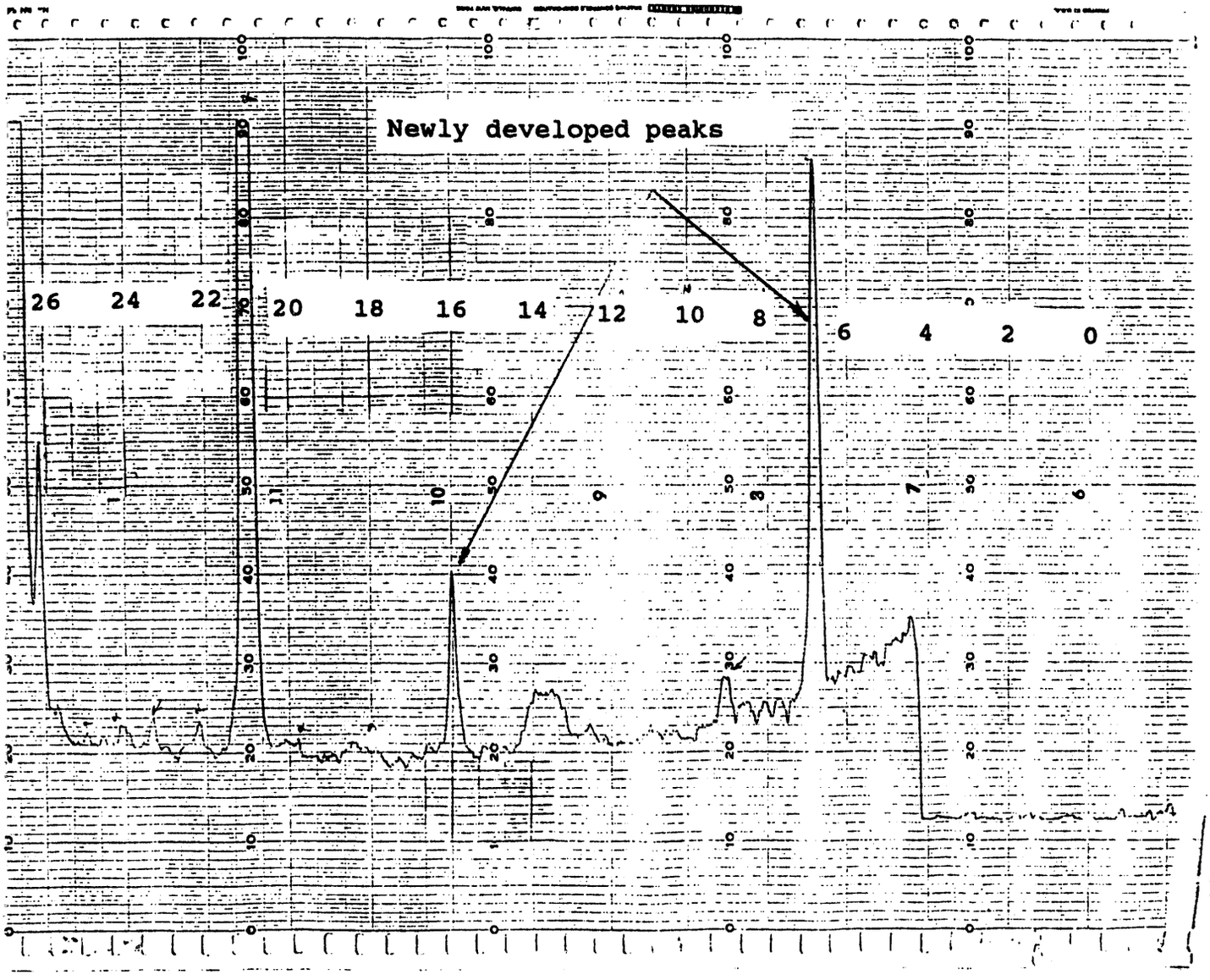
Newly developed peaks
26
24
22
20
18
16
14
12
10
8
6
4
2
0

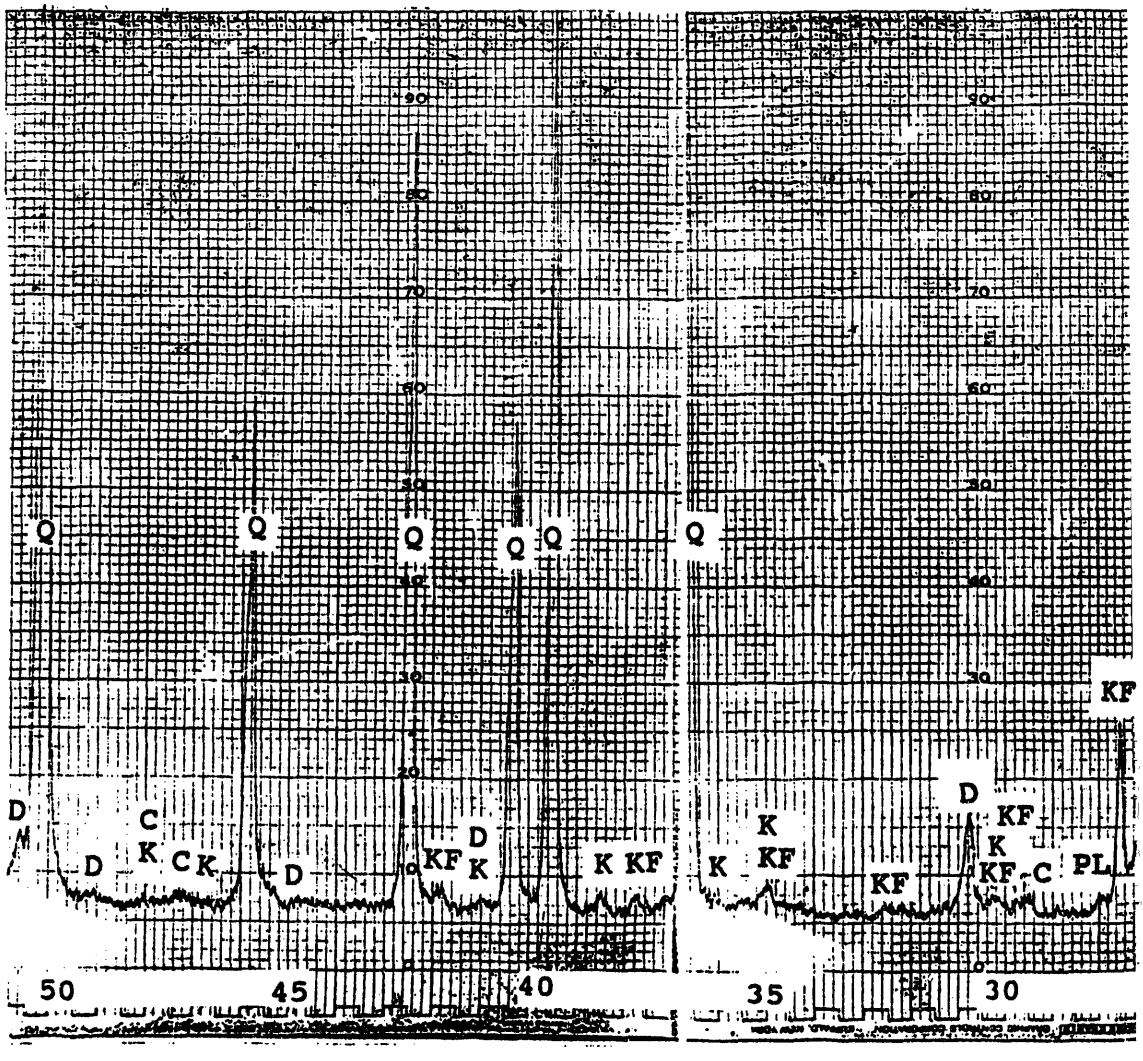

Figure 4.27 X-ray diffraction of the unreacted fired Berea sandstone.

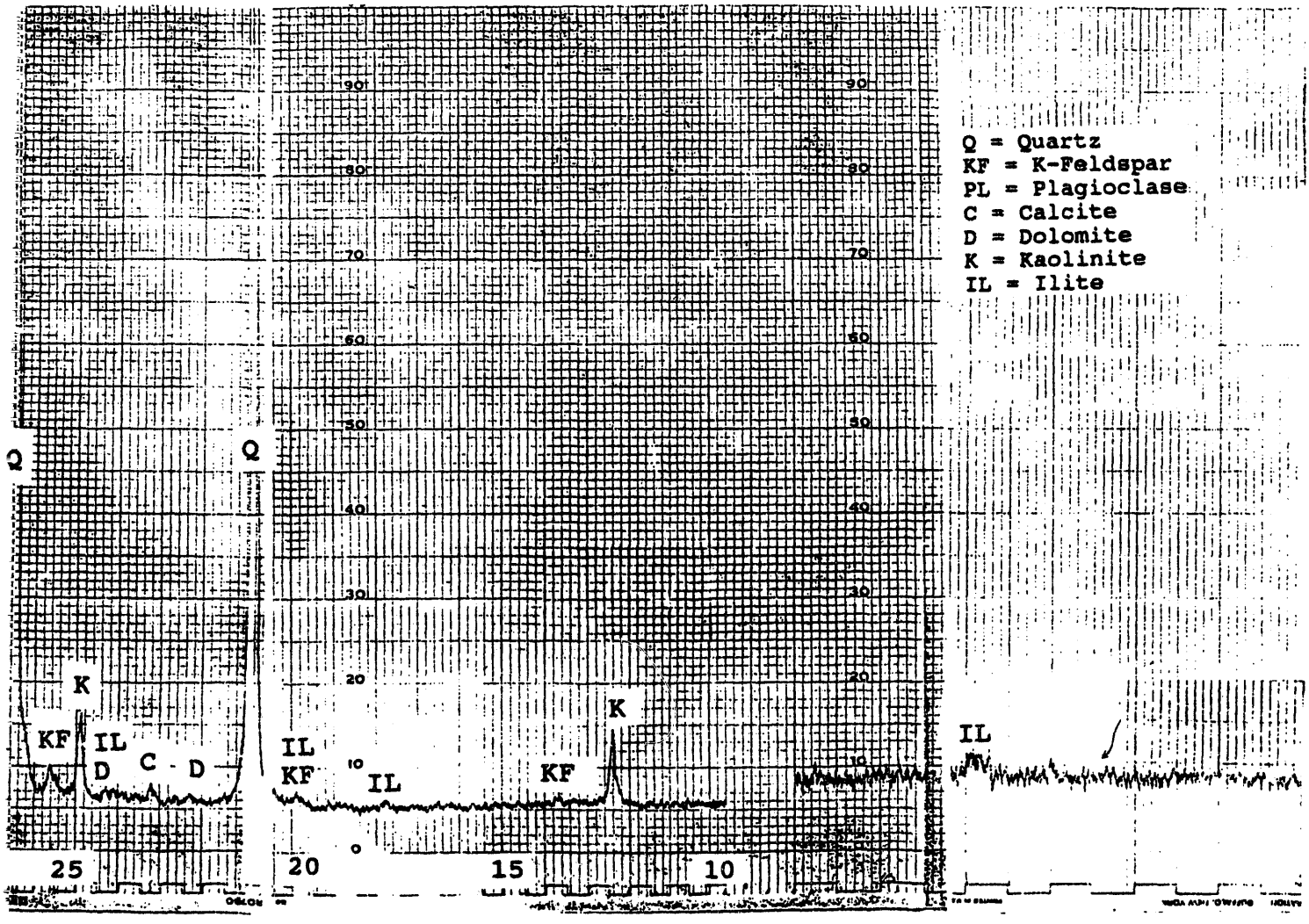
Q = Quartz
KF = K-Feldspar
PL = Plagioclase
C = Calcite
D = Dolomite
K = Kaolinite
IL = Ilite
Q
Q
K
KF
IL
D
C
D
IL
KF
IL
K
KF
IL
25
20
15
10
90
80
70
60
50
40
30
20
10
0

Chapter 5

DISCUSSION

5.1. Discussion of Experiment Set #1 Results

5.1.1. Discussion

Figure 4.1 shows that high pH breakthrough occurred after 16 pore volumes of caustic had been injected. Figure 5.1 shows Dehghani's results under similar conditions.[8] In his work, at the rate of 0.1 ft/day, breakthrough occurred after approximately 2.0 pore volumes had been injected. On Figure 4.3, pH is plotted as a function of dimensionless length. After 14.0 pore volumes of caustic injection, the pH at the end of the third core was measured at 11.9. At the same time, the effluent at the end of the fourth core had a pH of 7.7. Eventually, steady state was attained after 20 pore volumes of caustic injection. The effluent pH stabilized at 11.9. Previous investigations have attributed the lag in pH breakthrough to sodium-hydrogen ion exchange.[6,8,9,11,12,24] However the magnitude of the lag observed in Figure 4.1 is far more than can be explained by ion exchange.

A comparison of Figure 4.1 and 4.2 shows that silica breakthrough occurred at the same time as caustic breakthrough. A comparison of Figure 4.3 and 4.4 shows also that the high pH front and high silica concentration coincide.

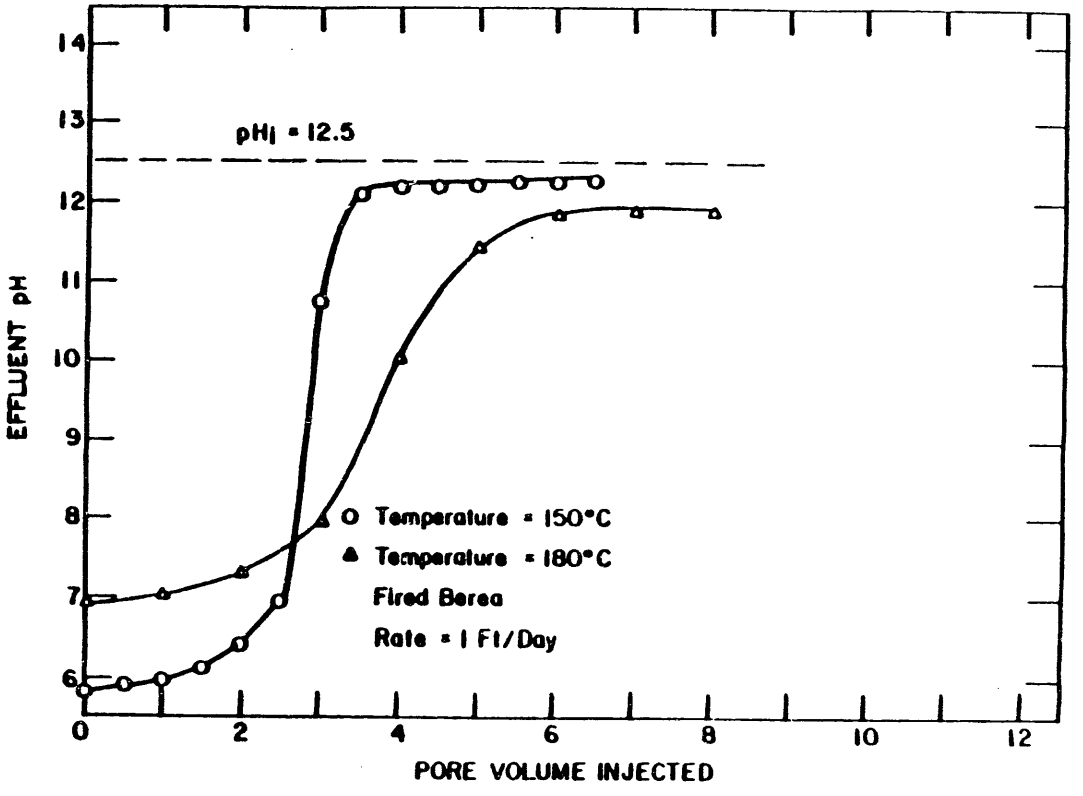

Figure 5.1 Effluent pH as a function of pore volumes of 0.0316 N hydroxide injected in fired Berea sample at 150°C and 180°C with a rate of 1 ft/day. (Reference: 8)

Another hydroxyl ion consuming reaction, in addition to ion exchange, is the dissolution reaction. As indicated by Equations 2.9 to 2.18, the silica concentration in solution should increase as hydroxyl ion is consumed. As can be seen in Figure 4.4, the silica concentration increased from a value of zero at the point of injection to values at least as high as that measured at the end of the first core, and then decreased steadily with distance through the core. Silica entered the solution through the dissolution reactions. A comparison of Figure 4.3 and 4.4 shows, however, that the rapid decline in pH or hydroxyl ion concentration coincides with a decline in the silica concentration. It is expected that the pH and silica fronts travel with a rate that depends on the injection flow rate and the reaction rate. In this experiment the fronts moved slowly and 16 pore volumes were injected before the pH and silica fronts reached to the effluent end. A comparison of the results of Saneie's analytical model with the results of this experiment indicates that the fronts in this experiment travelled significantly slower than that of the analytical model. The profiles in Figures 4.3 and 4.4 indicate that the hydroxyl ion and silica in solution were left behind while the fronts moved ahead. Saneie's[24] analytical model considers only ion exchange and dissolution reactions. Therefore, another reaction other than dissolution or ion exchange caused the silica to be removed from solution. Since the pH decreases this reaction must consume hydroxyl ion. The silica could be removed from solution as SiO_2 through a condensation reaction that is the reverse of the

dissolution reaction. Such a condensation reaction would occur when the silica concentration in solution exceeds the solubility limit of the silica under the experimental conditions. A state of silica supersaturation in solution would occur if the solution temperature is decreased sufficiently. The condensation reaction would release hydroxyl ion back into solution. Since the experimental results of this work suggest that the silica removal from solution caused consumption of hydroxyl ion, the condensation reaction as a mechanism for silica removal from solution is ruled out. Furthermore, the highest silica concentrations measured are much below the saturation concentrations at 180°C. Silica also can be removed from solution through reaction with dissolved metallic ions and formation of insoluble silicates. The insoluble silicates precipitate from solution when the equilibrium limit of the insoluble silicate is exceeded. Jepson[41] also proposed the adsorption of silica on an aluminum substrate as a mechanism for the removal of silica from solution. These reactions will be further discussed in the section 4 of this chapter. Figure 4.3 and 4.4 indicate that when the rate of injection was reduced to 0.4 ft/day further changes in the pH and silica concentration took place. Therefore, it can be concluded that final equilibrium was not achieved in this experiment. It should be noted that the measured pHs are not the true pHs. The pHs were measured at the effluent end and at room temperature while the experiments were performed at 180°C. All the pHs reported herein are at room temperature and must be used for comparison only. The other source of error is

the reverse silicate ionization reactions that take place upon cooling of the solution at the effluent end. These reactions release hydroxyl ion back into solution. Therefore, the measured pH may be higher than the true pH. Dehghani[8] suggested using Van Lier's equation along with the measured total silica concentration to obtain the fraction of silicic acid in solution. Then, using the silica species distribution curve for the working temperature, such as Figure 2.1, the hydroxyl ion concentration can be obtained. Hydroxyl ion concentration can be converted to pH by using the water ionization constant at the working temperature. The silica distribution curves have been developed by considering only the silica dissolution reaction and dissociation reactions. Since the results of this work indicate that reactions other than silica dissolution and dissociation can affect the hydroxyl ion and silica concentrations in solution, a true pH can not be obtained using this method. However, the measured pH can serve as a useful guide for comparison and also as a measure of attainment of steady state.

5.1.2. Summary

The results of Experiment Set #1 can be summarized as follows:

- Silica enters the solution through the dissolution reaction. A competing reaction removes silica from solution. Silica removal from the solution by this reaction causes hydroxyl ion consumption. This results in a significant lag in the hydroxyl ion

and silica breakthrough. The pH and silica breakthrough in this experiment occurred after 16 pore volumes of caustic were injected.

5.2. Discussion Of the Experiment Set #2 Results

5.2.1. Discussion

In order to minimize the effect of slow reactions, the initial rate was increased to 4.8 ft/day in Experiment Set #2. Since ion exchange reactions are fast and reversible, the increased flow rate does not alter hydroxyl ion consumption due to ion exchange. At higher rates, caustic consumption by the slow and rate dependent reactions such as silica dissolution and silica removal from solution is less significant due to shorter residence time. The injected caustic solution in this experiment contained 2% NaCl unlike Experiment Set #1. However, in both experiments the porous medium was pre-flushed with the 2% brine prior to caustic injection. As discussed in Section 2.1 and shown in Equations 2.1 and 2.2, adding salt or increasing the sodium ion concentration causes a shift to the right in the hydrogen/sodium ion exchange reaction and increases the amount of ion exchange and caustic consumption. Consequently, one would expect a later breakthrough of a high pH in Experiment Set #2 than that observed in Set #1. On the contrary, however, as can be seen in Figure 4.5, caustic breakthrough took place considerably earlier in Set #2 than in Set #1.

Therefore, a comparison of the results from Set #1 and Set #2 confirms that the delayed breakthrough in Set #1 was not due to the ion exchange reaction. The effect of salt on the rate of dissolution and the solubility of quartz have not been fully investigated. However, Saneie[24] in her model assumed that the silica sites where sodium/hydrogen ion exchange has taken place will not contribute to the dissolution. Consequently, a higher salt concentration leads to less dissolution. The effluent pH stabilized at 11.7 at the rate of 4.8 ft/day. Figure 4.7 shows that although the effluent solution had a silica concentration of 150 ppm, the silica concentration was about 1350 ppm at the end of the second core. Higher effluent pH and silica concentrations would have been observed as in Experiment Set #1, if injection had been continued. Therefore, it can be concluded that the steady state was not established in this experiment, although the variations in the effluent pH were not significant. Similar to Experiment Set #1, significant amount of caustic should have been injected, in order for steady state to be established.

Upon reduction of the injection rate, the pH dropped significantly throughout the core, as indicated in Figure 4.6. At the rate of 0.2 ft/day the effluent end pH was measured at around 7.5. Also in Figure 4.7 the drop in silica concentration can be seen throughout the porous medium as a result of the injection rate reduction. The silica profile in Experiment Set #2 is similar to that observed in Set #1. Silica removal from the solution accompanied by an increase in hydroxyl ion consumption, suggests the domination of the silica removal

reaction. When the rate was reduced, the removal of silica from solution increased and lower silica concentrations and pHs were observed at the end of the third core. Therefore, it can be concluded that silica removal is dominant and that the silica removal reaction is rate dependent. Lower rates or higher residence times increase the amount of silica and hydroxyl ion removed from the solution. Similarly, the pH and silica concentration breakthrough occurred earlier in Set #2 than in Set #1 due to the higher initial rate and the insignificant amount of silica removed from the solution in Set #2.

As mentioned in Section 2.3, silica removal from solution and caustic consumption through the clay/caustic interaction have been reported by others.[28,29,30,31] The most reactive clay has been reported to be kaolinite. Silica removal from solution is believed to occur through the formation and subsequent deposition of insoluble aluminosilicates.[28,29,30,31] In order to examine the extent and the nature of these interactions, alumina concentrations of the collected samples were measured. Figure 4.8 shows that alumina was detected only at the end of the third core. The alumina concentration had increased from a value of zero at the injection point to values at least as high as that measured at the end of the third core. In the first three section of the porous medium aluminum bearing minerals were dissolved, increasing the alumina concentration in solution. Since alumina was not detected at the effluent end, it must have been deposited out of the solution from the end of the third core to the effluent end. Reducing

the rate increased the amount of alumina deposition and at the lowest rate (0.2 ft /day) alumina was not detected in any of the collected samples. From these results it can be concluded that alumina is deposited out of solution and deposition is rate dependent. If enough residence time is allowed, the solubility of the aluminum bearing minerals can approach zero. The maximum alumina concentration measured in this set was 10.5 ppm. This is considerably less than that observed for silica.

5.2.2. Summary of Experiment Set #2

From the results of the Experiment Set #2 the following can be concluded:

1. The silica removal from solution observed in Experiment Set #1 was confirmed. The profiles indicate that silica and high pH front lag behind and significant amount of caustic must be injected before these fronts are produced at the effluent end.
2. The silica removal from solution is rate dependent. Lower rates result in an increase in the amount of silica removed from solution and in higher hydroxyl ion consumption.
3. Aluminum bearing minerals dissolve increasing the aluminum concentrations in solution.

4. Alumina deposition out of solution was observed.

5. Solubility of alumina can approach zero, if sufficient residence time is allowed. In this experiment, at the lowest flow rate, alumina was not detected in any of the samples collected from the effluent of the cores.

5.3. Discussion of the Experiment Set #3 Results

5.3.1. Discussion

5.3.1.1. Discussion of Results at 70°C

A third set of experiment was run to examine the effect of temperature. This set of experiments started at 70°C. The initial rate was 4.8 ft/day, and the caustic solution contained 2% NaCl. As can be seen in Figure 4.10, after 1.5 pore volumes were injected caustic breakthrough occurred. The effluent pH stabilized at around 12.8. Upon reducing the rate, further increase in the effluent pH was noticed. Eventually, the effluent pH stabilized at around the injected pH. It should be noted that the Fisher Scientific pH probe shows small fluctuations with rate changes. Simple experiments were run to evaluate the rate sensitivity of the probe. Buffered solutions with a pH of 9.0 were injected through straight tubing at different rates. The measured effluent pH increased from 9.0 to 9.3 when the rate was reduced from 4.8 ft/day to 0.9 ft/day. Therefore, if the changes in the effluent pH are not significant (within 0.5 Standard Unit) and the rates are

varying, the measured effluent pHs can not be compared. At 70°C changes in the effluent pH are not significant.

At the rate of 4.8 ft/day samples in between cores were collected for pH and silica measurements. Figure 4.11 shows pH as a function of dimensionless length at 4.8 ft/day and 70°C. The measured pH was constant throughout the porous medium. Figure 4.10 shows that the silica concentration gradually increased after the rate was reduced. At an injection rate of 4.8 ft/day, it increased from a value of zero at zero pore volumes injected and stabilized at 390 ppm after 4.3 pore volumes were injected. It further increased to 600 ppm when the rate was reduced to 0.9 ft/day. The silica concentration also increased slightly throughout the porous medium at 4.8 ft/day, as can be seen from Figure 4.12. This increasing trend in the silica concentration is an indication of an increase in the amount of dissolution. The increase in dissolution should cause a lower effluent pH and higher hydroxyl ion consumption. However, the measured effluent pH does not reflect the increased dissolution. This can be attributed to the difference between the measured effluent pH and the true pH. As was mentioned earlier, due to the lower temperature at the effluent, the silicate ionization reactions are reversed. Consequently, silicic acid and hydroxyl ion are released into solution. As a result, while the total silica concentration remains constant, the effluent pH increases. Therefore, the changes in the measured effluent pH are insignificant. As can be seen in Figure 4.12, no silica

removal from solution was observed at this temperature.

As shown in Figure 4.10, the effluent alumina concentrations initially increased from a value of zero at zero injected pore volumes to 43.0 ppm. The alumina concentration then decreased and stabilized at 23.0 ppm. Alumina initially went into solution by dissolution of aluminum bearing minerals. Then, aluminum precipitated out of solution, apparently forming a new aluminum mineral for which the solubility limit was less than the solubility of the original aluminum bearing minerals. In order for the solubility limit to be less than that of the original, the new precipitate must have a Si/Al ratio larger than that of the original aluminum bearing minerals. Sydansk[22] in his work noticed a very similar trend in the effluent alumina concentration. He also attributed this behavior to the formation of new aluminosilicate minerals of the zeolite family. His SEM and XRD results supported these conclusions.

Upon decreasing the rate to 0.4 ft/day no further changes in the effluent pH, silica concentration or alumina concentration was noticed. The rate was then increased to 1.1 ft/day. As can be seen from Figure 4.9 no change in the effluent concentrations occurred because of the rate change. It can be concluded that a state of final equilibrium at the effluent end was established at 70°C.

5.3.1.2. Discussion of Results at 100°C

The temperature was then increased to 100°C while the rate was kept at 1.1 ft/day. Referring to Figure 4.13 the effluent pH dropped and stabilized at around 12.4. As can be seen, the effluent silica concentration increased continuously. The effluent silica concentration was measured at 700 ppm when the rate was 1.1 ft/day. The lower effluent pH and higher effluent silica concentration indicate higher dissolution and higher caustic consumption. As Figure 4.13 indicates the effluent alumina concentration decreased and was measured at 21.0 ppm when the rate was 1.1 ft/day. This indicates further deposition of alumina out of solution. Therefore, it can be concluded that increasing temperature increases alumina deposition out of solution and reduces effluent alumina concentrations.

The rate was then reduced to 0.9 ft/day. As one would expect for lower rates and higher residence time, the effluent silica concentration increased and was measured at 900 ppm, which is higher than that observed at the rate of 1.1 ft/day. However, the effluent pH also showed a small increase. This contradiction, as was seen at 70°C also, can be due to the rate sensitive nature of the pH probe. It must also be noted, that an increase in temperature will result in an increase of the ion exchange capacity. Consequently, a temporary decrease in the effluent pH may be observed due to the additional ion exchange. Figure 4.14 shows silica concentration as a function of dimensionless length at 100°C.

The alumina concentration was further reduced and measured at 12.0 ppm, as can be seen in Figure 4.13. It can be concluded that the deposition of alumina out of a silica solution is flow rate dependent.

5.3.1.3. Discussion of Results at 120°C

The temperature was then increased to 120° C, keeping the rate constant at 0.9 ft/day. Figure 4.15 shows that the effluent pH decreased and stabilized at 12.3. Approximately 4.5 pore volumes of caustic were injected before steady state was established. The silica concentration increased significantly and stabilized at 2000 ppm. Figure 4.17 shows that silica deposition occurred along the fourth core. The silica concentration dropped from 3200 at the end of the third core to 2000 ppm at the end of the fourth core. The effluent alumina concentration decreased steadily to zero. This indicates that the solubility of the new aluminum bearing minerals eventually approaches zero. These results are similar to those observed in Experiment Set #2. Compared to the results for lower temperatures, the changes which occurred in the effluent as a result of increasing the temperature from 100°C to 120°C, were more significant. Therefore, the temperature dependencies of the dissolution reaction and silica removal from the solution are greater above 100°C.

5.3.1.4. Discussion of Results at 150°C

The temperature was raised to 150°C. As can be seen from Figure 4.18, an immediate and substantial drop in the effluent pH was observed. The effluent pH decreased to values as low as 7.35. The effluent pH stayed at neutral levels for a few pore volumes. After 4.5 pore volumes of caustic solution had been injected at 150°C, the effluent pH started increasing. A total of 10 pore volumes of caustic were required before the effluent pH stabilized at 12.1. This is similar to the significant lag in the pH breakthrough observed in the Experiment Set #1. When the temperature was raised to 150°C, a decrease in the silica concentration was observed indication silica removal from solution, which caused an increase in the hydroxyl ion consumption. The effluent pH stayed at the neutral level for a few pore volumes before high pH breakthrough occurred.

As shown on Figure 4.18, the effluent silica concentration dropped significantly corresponding with the drop in the effluent pH. The effluent silica concentration dropped to 150 ppm before it increased to higher concentrations. The effluent silica concentration stabilized at 1700 ppm. These results are also consistent with what was observed in Experiment Set #1. The high pH breakthrough coincided with the high silica concentration breakthrough. The silica removal from solution coincided with hydroxyl ion consumption, indicating a silica removal mechanism that is also hydroxyl ion consuming. Once this reaction is completed, higher levels of hydroxyl ion and silica concentrations were

produced at the effluent end. The profiles of pH as a function of dimensionless length (Figures 4.3 and 4.7) are similar to those of previous sets of experiment, as can be seen from Figure 4.19. Figure 4.20 shows that the silica profiles as a function of dimensionless length are also consistent with what was observed in the previous experiments. The change in the slope of the pH profile and the change in the slope of the silica profile coincide. Where the pH was in the neutral region (between 7 and 8), the silica concentration was close to the observed quartz solubility limits (around 150 ppm). This behavior is similar to an ion exchange reaction. As the silica removal reactions were completed, higher silica concentrations were measured. The removal of silica from solution has been observed in batch experiments.[28,29,30] However, an increase in the silica and hydroxyl ion solution concentration were not observed following the silica removal from the solution, since in a batch experiment the amount of available hydroxyl ion is limited.

When rate was reduced to 0.4 ft/day, the effluent pH and the pH profile as a function of dimensionless length did not change. The effluent silica concentration also stayed the same. Figure 4.20 shows that silica concentration at the end of the third core at the rate of the 0.4 ft/day was slightly higher than that at 0.9 ft/day. This indicates that final equilibrium was not achieved at this temperature. Furthermore, the silica removal reaction was not complete. For longer residence times, higher effluent silica and hydroxyl ion concentrations

would have been observed.

5.3.1.5. Discussion of Results at 180°C

The temperature was raised to 180°C. As Figure 4.21 shows, the effluent pH and silica concentration both dropped. The effluent measurements were the same as the ones observed in the Experiment Set #1 under similar conditions. The profiles as a function of dimensionless length were also similar to those of Experiment Set #1.

The alumina measurement at 180°C and 150°C did not indicate any alumina in solution. The solubility of the aluminum bearing minerals approached zero. Nevertheless, silica removal took place in the absence of any alumina in solution.

5.3.2. Summary

From the results of the Experiment Set #3 the following can be concluded:

1. Silica dissolution and hydroxyl ion consumption are insignificant at temperatures up to 100°C.
2. Silica removal from solution is temperature dependent and the amount of silica removed from solution increases with increasing temperature. Significant silica removal from solution occurred when the temperature was increased from 120°C to 150°C.

3. The silica removal reaction is hydroxyl ion consuming. At 150°C, the significant removal of silica from solution coincides with the significant drop in pH.

4. The silica removal reaction manifests itself in a manner similar to ion exchange reactions. Once the sites of reaction are satisfied, higher silica and hydroxyl ion concentrations breakthrough.

5. Alumina deposition reactions are temperature dependent. At higher temperatures lower effluent alumina concentrations were observed. This indicates that the new alumina silicate deposited on the rock surface has lower solubility than the original silicate. Solubility of alumina in solution can decrease to zero, due to alumina deposition reactions.

6. Silica deposition reactions can take place in the absence of any alumina in solution.

In the following paragraphs the mechanism of the proposed reactions are discussed.

5.4. Mechanism of Silica and Alumina Deposition

The deposition of alumina and silica has been observed by other investigators also.[28,29,30,31] Sydansk's[22] results at 185°F shown in Figure 5.2 are

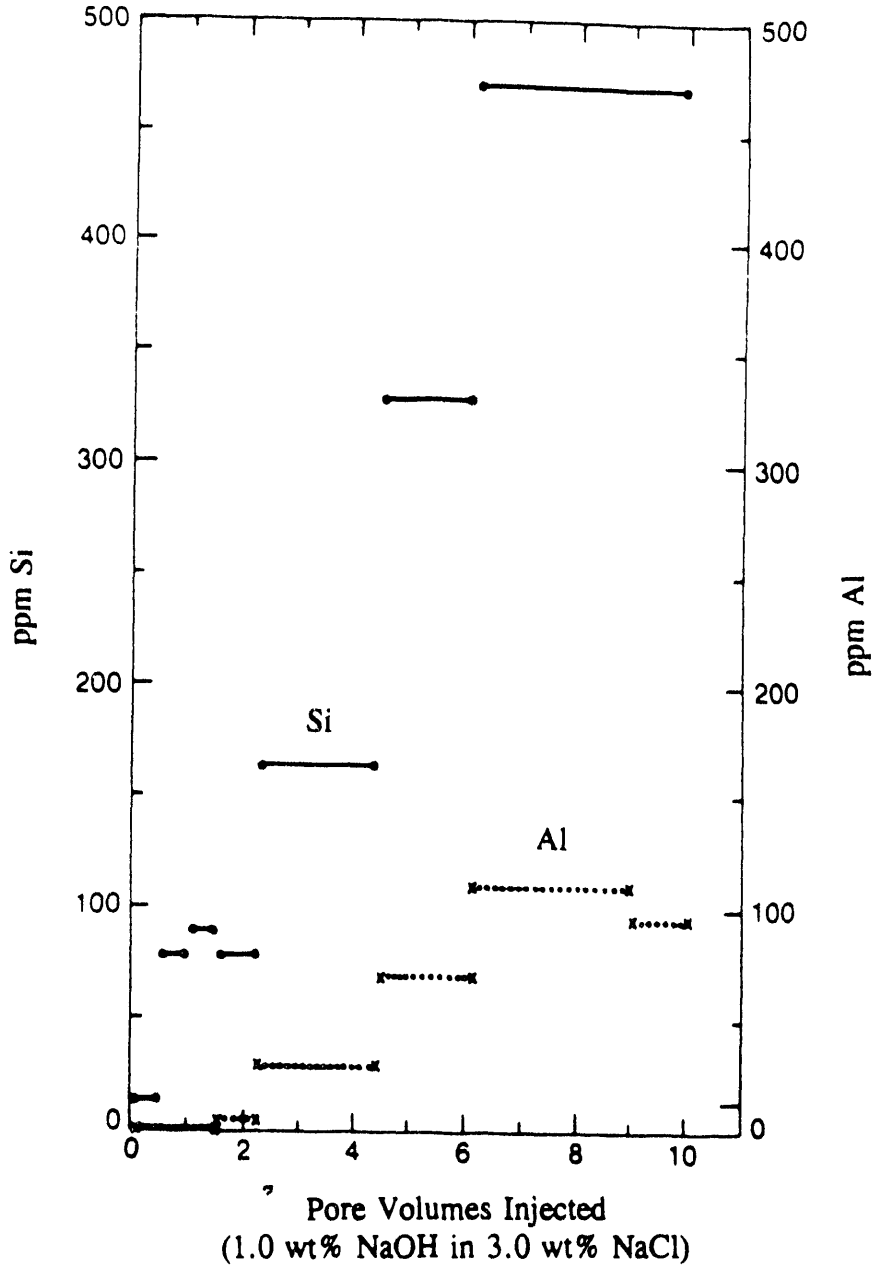

Figure 5.2 Silicon and aluminum concentrations in effluent samples for 1.0 wt% NaOH flooded at 185°F in a Berea sandstone plug. (Reference: 22)

similar to the results of the Experiment Set #2 and #3. These results were rationalized as follows:

1. Clays were dissolved initially and silica and alumina were propagated by the caustic solution;
2. As the caustic, alumina and silica concentrations increased steadily, new aluminosilicate minerals began to precipitate in accordance with the equilibrium-constant considerations of the newly precipitated minerals.

According to Sydansk the new precipitates belonged to a zeolite family that has a higher silicon to aluminum ratio than the dissolved clays. Due to the higher *Si/Al* ratio, the solubility of alumina in the presence of precipitate was less than in the presence of the original clay.

Thornton et al.[29] developed a chemical model to extrapolate the laboratory data on mineral-alkali reactions to reservoir time scales. During bottle tests, deposition of sodium, aluminum and silica from the solutions was observed. Figure 5.3 shows some of these results. These results were also explained by the formation of new minerals. The products of the deposition reaction were assumed to be pure phillipsite and pure gibbsite. The deposition reactions were written as follow:

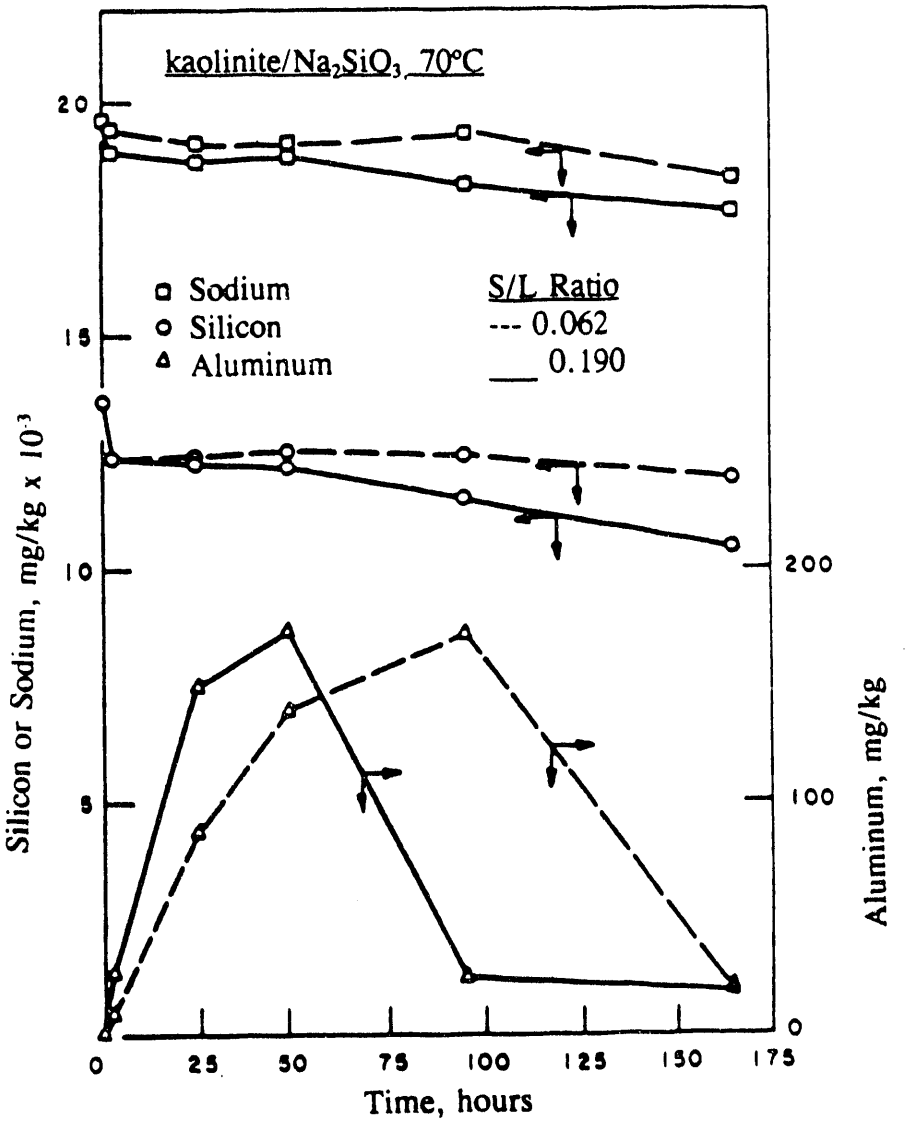

Figure 5.3 Consumption of Na_2SiO_3, by kaolinite at 70°C. (Reference: 29)

$$10kaolinite + 20OH^- + 15H_2O \rightarrow 10H_3SiO_4^- + Al(OH)_4^- \quad (5.1)$$

$$6Na^+ + 10H_3SiO_4^- + 6Al(OH)_4^- \rightarrow 2phillipsite + 10(OH)^- \quad (5.2)$$

$$4Al(OH)_4^- \rightarrow 4gibbsite + 4OH^- \quad (5.3)$$

$$10kaolinite + 6Na^+ + OH^- + 5H_2O \rightarrow 2phillipsite + 4gibbsite \quad (5.4)$$

Mohnot et al.[28] studied the mineral-alkali reactions through a series of static bottle tests. During kaolinite dissolution by alkali, dissolved *Si* and *Al* reached high values quickly, but decreased later. The large drop in silica concentration accompanied the large and fast drop of hydroxide ion. These results are shown in Figure 5.4 and 5.5. The new mineral formation is believed to be the cause of silica and hydroxyl ion consumption. Mohnot[28] proposed in his paper that the minerals are dissolved incongruently. The new minerals will precipitate when the concentration of dissolved species exceed their solubility products. Precipitation reactions are also incongruent. Of the many possible incongruent reactions Mohnot presented the following reactions which consume both hydroxyl ion and silica.

$$Al_2Si_2O_5(OH)_4 + 2Na^+ + 2OH^- + 4Si(OH)_4 \rightarrow 2NaAlSi_3O_8 + 11H_2O \quad (5.5)$$

$$Al_2Si_2O_5(OH)_4 + 2Na^+ + 2OH^- + 2Si(OH)_4 \rightarrow NaAlSi_2O_6.H_2O + 5H_2O \quad (5.6)$$

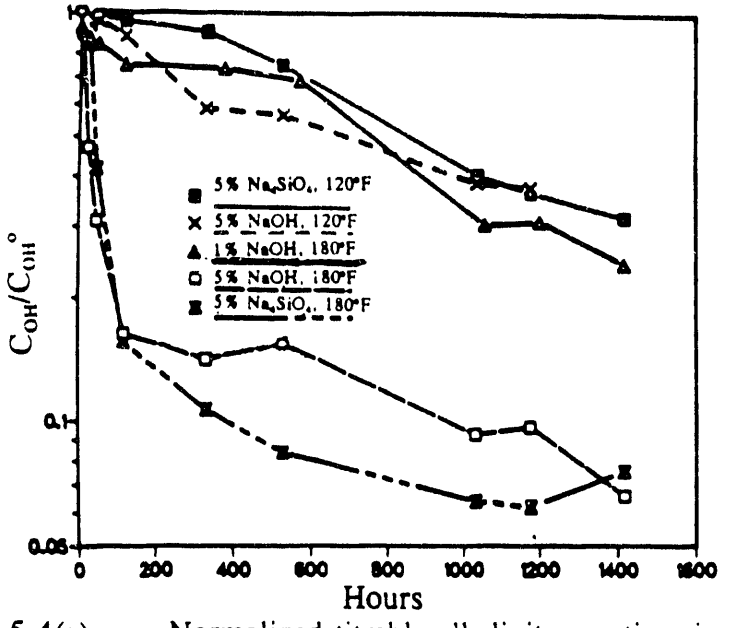

Figure 5.4(a) Normalized titrable alkalinity vs. time in kaolinite-alkali reactions. (Reference: 28)

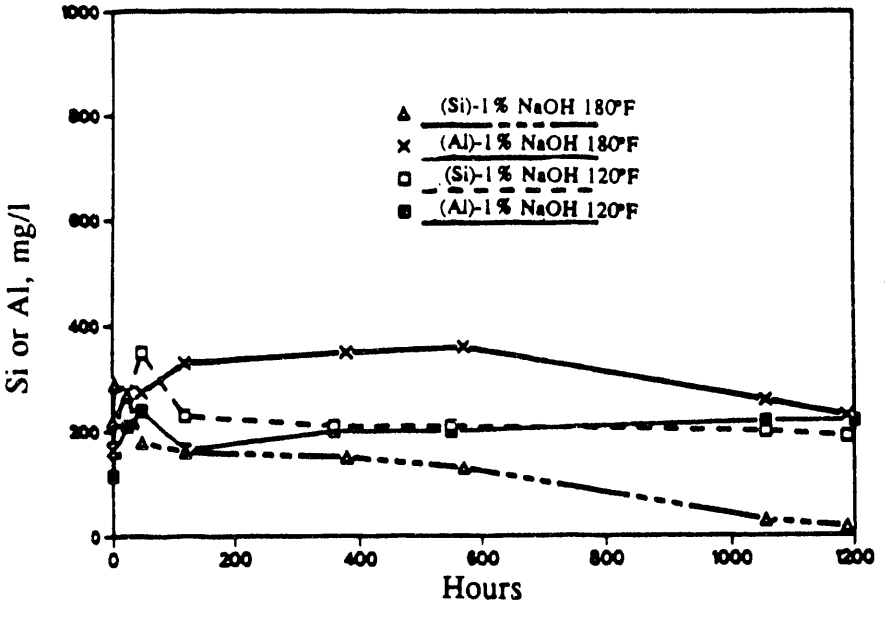

Figure 5.4 (b) Concentration of dissolved silicon and aluminum vs. time in kaolinite-1% NaOH reactions. (Reference: 28)

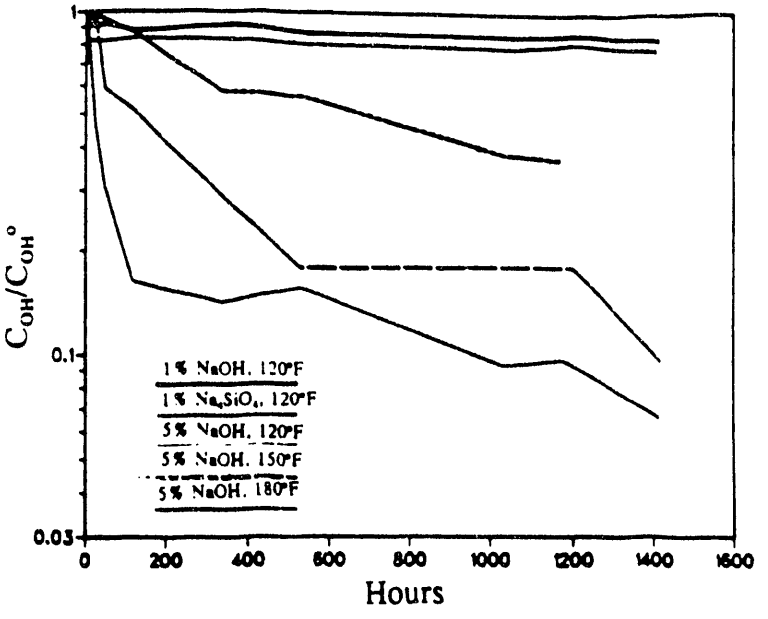

Figure 5.5(a) Kinetic data in 1% alkali - and effect of temperature in kaolinite-alkali reactions. (Reference: 28)

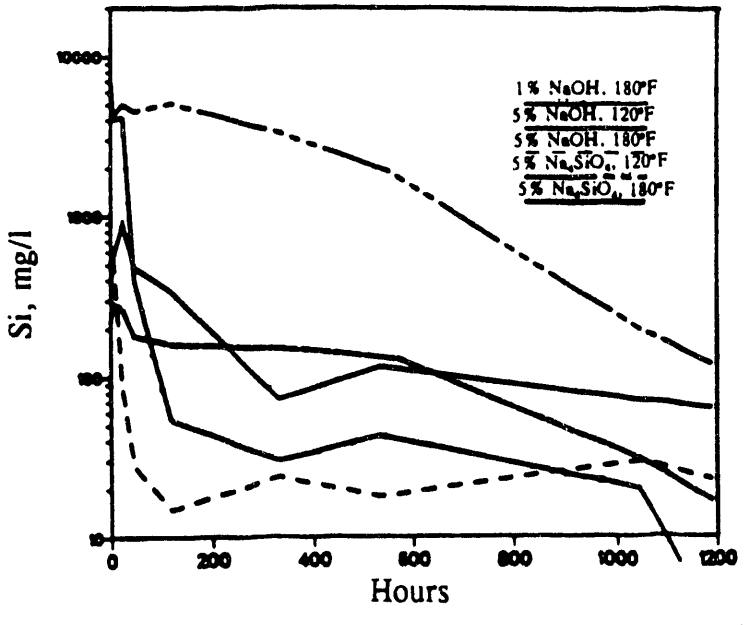

Figure 5.5(b) Dissolved silicon concentration vs. time in kaolinite-alkali reactions. (Reference: 28)

Diallo et al.[30] observed similar results in static bottle tests performed with mixtures of quartz and kaolinite. Small amounts of dissolved aluminum added during quartz dissolution reduced the silica concentration significantly. Adding dissolved silica reduced the steady state equilibrium concentrations for both aluminum and silicon in kaolinite dissolution. The concentration of *Si* and *Al* in the binary mixtures of kaolinite and quartz were both reduced as compared to pure quartz and kaolinite. Some of the results are shown in Figures 5.6 and 5.7.

The sorption of silica from sea water by clays had been reported to be the mechanism by which the oceans maintain their composition.[35,36,37,38] Mac Kenzie et al.[35] demonstrated that sorption of silica from sea water is a function of pH and dissolved SiO_2. Siever et al.[39] performed a series of bottle tests consisting of adsorption of silica from aqueous solution by kaolinite. The pH was varied between 5.0 and 10.0. Similar to the results of this work, no aluminum in solution was observed. This was attributed to the strong pH dependency of solubility of aluminum species. In their work, the solubility of kaolinite in presence of water at pH 5 or higher was shown by the following reaction:

$$Al_2Si_2O_5(OH)_4 + 5H_2O \rightleftharpoons 2\,Al(OH)_3 + 2\,H_4SiO_4 \qquad (5.7)$$

where $Al(OH)_3$ can be considered as gibbsite or amorphous aluminum hydroxide surfaces created as tetrahedral layers of SiO_2 are leached from the dissolving

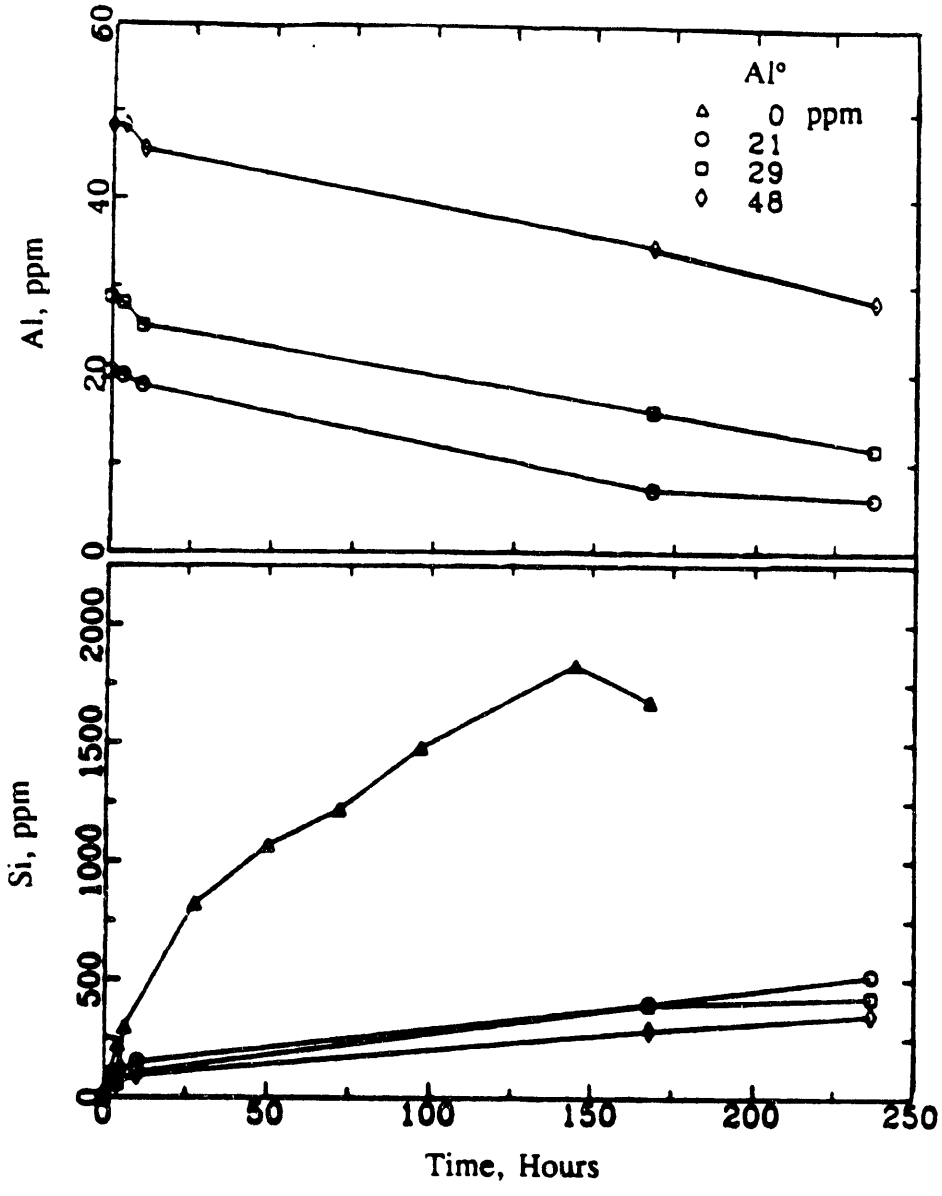

Figure 5.6 Silicon and aluminum concentration as a function of time from quartz dissolution in the presence of added soluble aluminum. (Reference: 30)

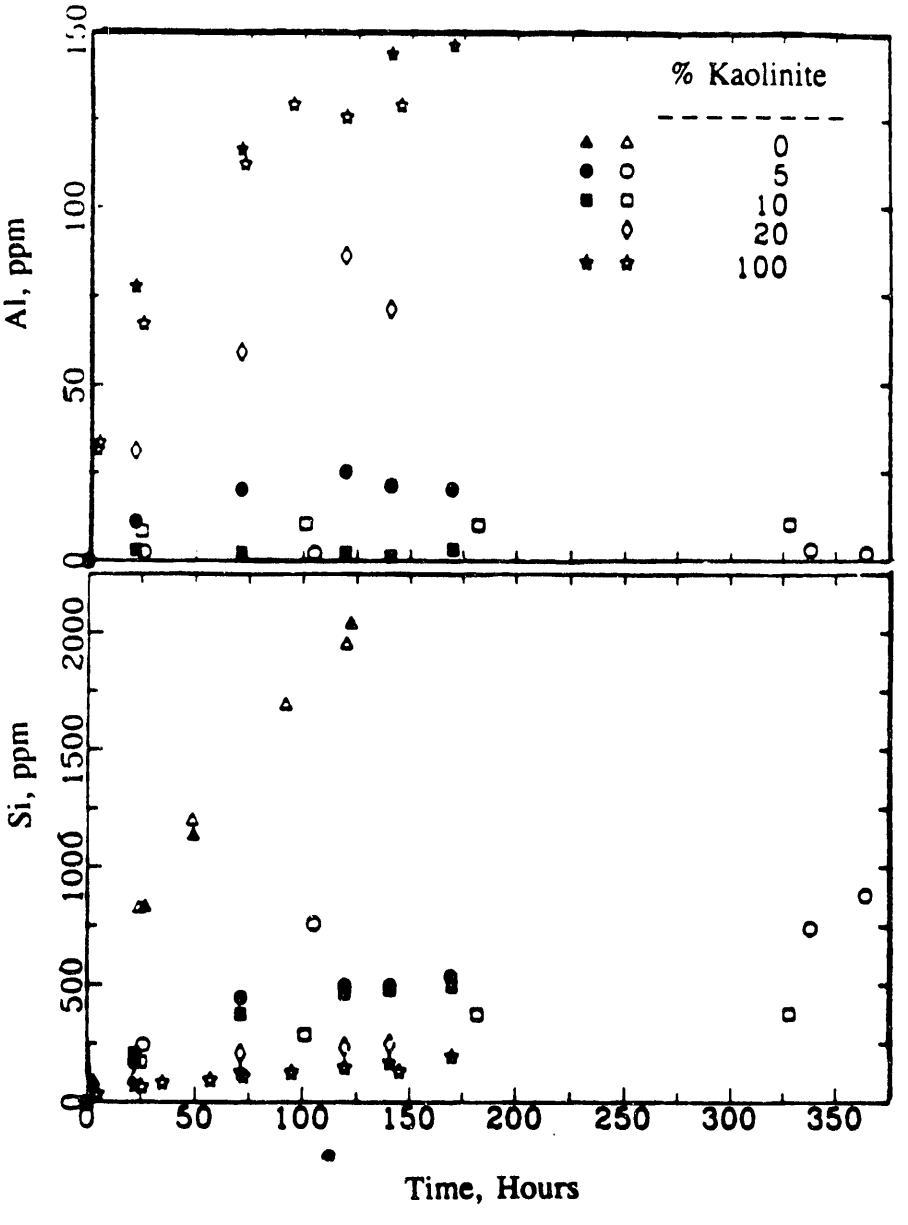

Figure 5.7 Silicon and aluminum concentration as a function of quartz and kaolinite in 0.1 N NaOH. (Reference 30)

minerals. The SiO_2 sorbed from solution or dissolved into solution were plotted against initial SiO_2 in solution. Figure 5.8 shows a typical plot. Each point represents one run. The point at zero sorbed silica is referred to as a crossover point. The runs showing dissolution represent reactions tending towards equilibrium between the clay surface, the solution and a surface leached of silica. The runs showing sorption represent reactions tending towards equilibrium between the clay surface, the solution and the surface enriched in silica. The value of the crossover point is a function of pH, temperature and the electrolyte concentration and type. It decreases with decreasing pH and increases with increasing temperature. Sorption increases with increasing electrolyte concentration. Sorption is also a function of kaolinite preparation. Acid washing and grinding both enhance sorption. However, it was shown that heat treatment of kaolinite, similar to the core firing in this work, does not alter the extent of the reactions greatly. It was concluded that SiO_2 sorption is incongruent and the sorption continues until the surface is saturated. Siever et al.[39] suggested the following simplified reactions for the adsorption of silica on the kaolinite surface:

$$Al_2Si_2O_5(OH)_4 + 2SiO_2 \rightarrow Al_2Si_4O_{10}(OH)_2 + H_2O \qquad (5.8)$$

$$Al_2Si_2O_5(OH)_4 + SiO_2 \rightarrow Al_2Si_3O_7(OH)_4 \qquad (5.9)$$

$$5Al_2Si_2O_5(OH)_4 + 4SiO_2 + 2K^+ \rightarrow 2KAl_5Si_7O_{20}(OH)_4 + 2H^+ + 5H_2O \qquad (5.10)$$

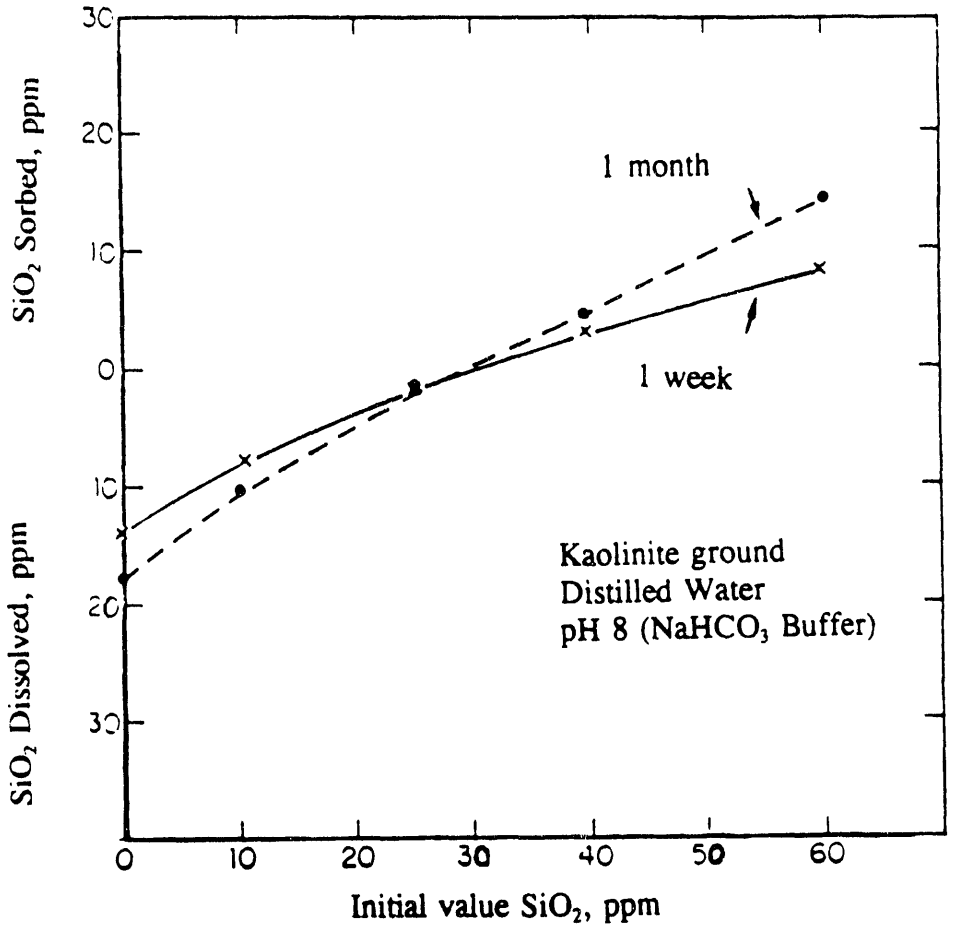

Figure 5.8 Sorption and dissolution of kaolinite in distilled water at pH 8 at one week and one month. (Reference: 39)

$$Al_2Si_2O_5(OH)_4 + K^+ + 4SiO_2 \rightarrow KAl_2Si_6O_{14}(OH)_3 + H^+ \qquad (5.11)$$

Reactions 5.10 and 5.11 explain hydroxyl ion consumption through silica adsorption. In their study potassium chloride was the dominant electrolyte. Similar reactions can be written in the presence of sodium chloride as electrolyte.

Iler studied the effect of adsorbed alumina on the solubility of amorphous silica.[40] It was shown that alumina adsorbs on the surface of silica and reduces both the solubility and the rate of solution of silica significantly, even when much less than a monolayer of aluminum is present. The aluminum is adsorbed from both saturated and unsaturated silica solutions. Therefore, while aluminum is being adsorbed, the silica concentration in solution can either increase or decrease, depending on equilibrium solubility. Nevertheless, the equilibrium solubility is more if no aluminum is adsorbed on the surface. This is attributed to the negative aluminosilicate ions absorbed on the surface that prevent the approach of hydroxyl ions which are required to catalyze the dissolution of silica. Consequently, the solubility depends on the proportion of silica and aluminum on the surface at equilibrium.

Jepson et al.[41] studied the adsorption of silicic acid on gibbsite suspended in *NaCl* solution over the pH range 4 to 11. The adsorption increased with increasing pH up to 9 and then decreased. The adsorption in some cases exceeded the maximum monolayer coverage. The adsorption was not reversible.

With increasing silica adsorption, Cl^- counterion adsorption decreased and Na^+ counterion adsorption increased leading to charge reversal over most of the pH range. Adsorption also occurred through a condensation reaction with the new surface, meaning silica condensed on the silica adsorbed on the gibbsite surface. The maximum coverage was observed at pH of 9. The rate of polymerization of silica is greater at this pH. Consequently, the amount of silica condensed and the coverage are the largest. Jepson's results suggest a chemisorption mechanism for silica removal from the solution. The following reactions (5.12 and 5.13) were proposed to demonstrate the chemisorption mechanism at pH of 6.

The silicic acid reacts with the gibbsite surface according to:

$$Surface\text{-}OH_2^+ ... Cl^-, OH^- + Si(OH)_4 \rightarrow Surface\text{-}O\text{-}Si(OH)_3 + HCl + 2H_2O \quad (5.12)$$

Following reaction 5.12 a portion of the silicic acid is ionized and *Na* ions enter the double layer:

$$Surface\text{-}O\text{-}Si(OH)_3 + Na^+ \rightarrow Surface\text{-}O\text{-}Si(OH)_2O^- ... Na^+ + H^+ \quad (5.13)$$

For every silica adsorbed on the surface two hydrogen ions are released into solution. At pH of 9 the experimental results showed that for every three SiO_2 adsorbed one H^+ is released into the solution.

In summary, the above mentioned investigations confirm the removal of silica from solution in the presence of alumina surfaces. Similarly, the removal of alumina from silicate solutions has also been observed.[22,28,29,30,31,40,41] The

suggested silica or alumina removal mechanisms are:

1) precipitation of insoluble minerals; or

2) adsorption on the surface of silica or alumina

Silica and alumina must be present in solution at a high enough concentration for precipitation to occur. The results of the present work indicate that silica removal from the solution can take place even when alumina is not present in the solution. Therefore, the reactions 5.10 and 5.11 proposed by Siever et al. and reactions 5.12 and 5.13 proposed by Jepson are consistent with the results of this work. Figure 5.9 shows the picture of the first core in Experiment Set #2 after termination of the experiment. Approximately, an inch of the core had been dissolved from the end where caustic was injected. In the absence of silica adsorption, large amounts of silica should be produced at the effluent end. However, the silica dissolved from the rock was never recovered. The alumina concentrations in solution were not sufficient to explain the lag in the silica breakthrough. Similar results were observed in the other experiment sets. These observations confirm that silica is adsorbed on the rock surface, mainly on clays, and the adsorption can be explained by reactions similar to 5.10, 5.11, 5.12 and 5.13.

The results of the aforementioned experimental work did not predict the performance of a caustic flood influenced by the silica adsorption reaction. Although additional hydroxyl ion consumption through the silica removal reaction

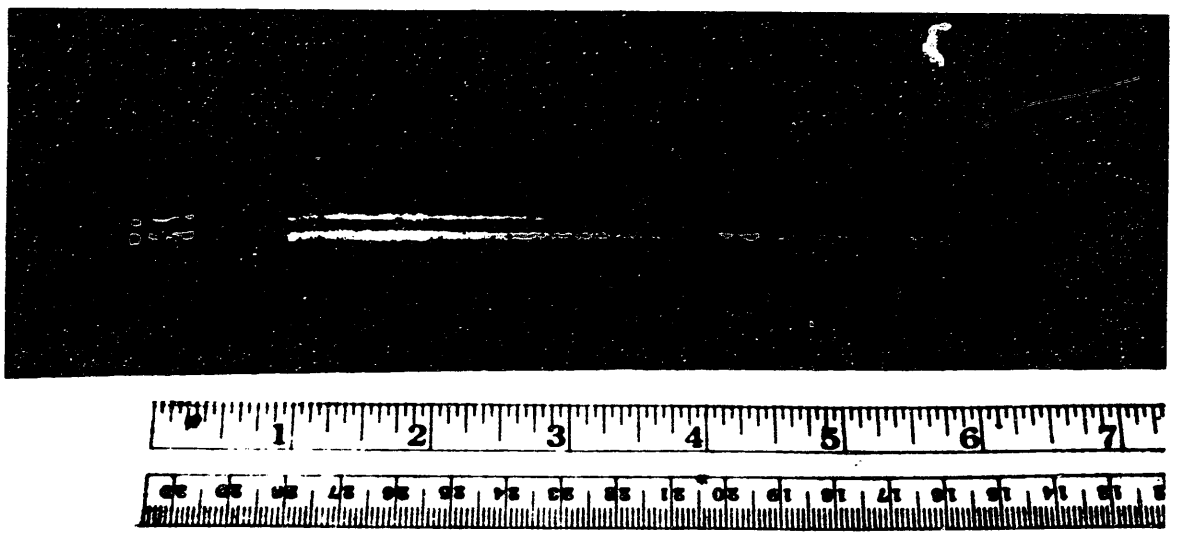

Figure 5.9 The first core in Experiment Set #2, after termination of the experiment.

was observed, the extent of it in a dynamic system is not fully understood. Once the silica adsorption sites are satisfied, high levels of silica concentration and pH breakthrough. Although, adsorption of silica and alumina on the surface consume hydroxyl ion, the final equilibrium pH is increased.

The X-ray diffraction analysis in Table 3.1 shows the minerals and their corresponding bulk percentages for a fired Berea sandstone prior to caustic injection. Figures 4.23, 4.24, 4.25, and 4.26 show the X-ray analysis results for first, second third and fourth cores from the Experiment Set #3. A comparison of the results of the reacted sandstone to that of the unreacted, shows that a family of peaks is present in some of the reacted sandstone results that is not present in the results for the unreacted sandstone. This suggests the development of a new surface. The new peaks could not be identified. This is not surprising since the adsorption of silica according to reactions such as 5.9 and 5.10 does not indicate formation of any known mineral. On the other hand, reactions proposed by Thornton[29] and Mohnot[28] do lead to the formation of known aluminosilicate minerals.

In summary silica removal occurs through an adsorption reaction. Adsorption is dependent on pH, temperature and rate.

Chapter 6

CONCLUSIONS

Caustic flooding experiment were performed in long porous medium with extended residence times. The porous medium consisted of four Berea sandstone cores (8" in length and 1" in diameter) which were placed in series. Experiments were ran at temperatures up to 180°C and flow rates were varied from 4.8 to 0.2 ft/day. Samples were taken from in-between the cores and were analyzed for pH, silica concentration and alumina concentrations. The results of these samples were used to establish pH and chemical composition variations along the porous medium. The conclusions from the results of this work are summarized as follows:

1. Consistently, significant lags in high pH and high silica concentration breakthrough were observed. These lags were considerably larger than those observed in previous work.[8,22] Silica and pH profiles indicate that a decline in pH is accompanied by a decline in silica concentration in solution. As a result, the delay in breakthrough is attributed to a silica removal reaction that can be characterized as follows:

a. A silica removal reaction consumes both silica and hydroxyl ion.

b. The reaction is flow rate dependent. At lower rates, the amount of silica removed from the solution increases and the delay in breakthrough is greater.

c. The silica removal reaction is temperature dependent. At higher temperatures, the amount of silica removed from solution increases.

d. This reaction manifests itself in a manner similar to that of an ion exchange reaction. Once the sites of reactions are satisfied, high silica concentration and pH breakthrough occurs.

2. Alumina deposition out of solution was observed. The alumina deposition reaction can be characterized as follows:

a. An alumina deposition reaction can cause the solubility of alumina to reach zero.

b. The alumina deposition reaction is flow rate dependent. At lower flow rates, higher amounts of alumina are deposited.

c. The alumina deposition reaction is temperature dependent. Higher temperatures enhance alumina deposition.

3. Silica removal from solution was observed even in the absence of alumina in solution. As a result, the observed removal of silica from solution is not caused by formation of insoluble aluminosilicates.

4. A chemisorption mechanism is suggested for the silica removal from solution. Chemisorption of silica onto the rock surface is independent of the concentration of alumina in solution. The proposed mechanism suggests that chemisorption of silica consumes hydroxyl ion. The proposed mechanism is consistent with the results of this work.

5. The X-ray diffraction analysis shows that new peaks are developed indicating formation of new minerals. However, these peaks do not correspond to any known compound.

6. Hydroxyl ion consumption is not significant for temperatures up to 100°C. Caustic may maintain a pH above an effective level necessary for caustic flooding for temperatures up to 100°C.

7. The temperature dependency of the silica removal reaction is greater above 100°C. A temperature change from 70°C to 100°C, did not cause any silica removal from solution. When temperature was raised from 100°C to 120°C, silica removal from solution was observed, however, it was not significant. Changing temperature

from 120°C to 150°C caused significant drop in effluent pH and silica concentration. The high pH and silica fronts lagged behind. Approximately, eight pore volumes of caustic were injected before the high silica and pH front were produced at the effluent end.

8. For temperatures above 100°C, which would be incurred in steam flooding, caustic flooding may not be feasible, due to the large amounts of caustic required to be injected before a high pH level can be maintained throughout the reservoir.

Chapter 7

SUGGESTED FUTURE WORK

In order to quantify silica removal from solution in an alkali flooding process, it is necessary to perform more dynamic and batch experiments at elevated temperatures. Experiments must be performed on pure silica, and pure minerals and known mixtures of silica and minerals. A similar set-up, such as the experiments discussed in this thesis, is recommended for obtaining pH and chemical composition profiles. Silica removal from solution can be further studied through comparison of the pH and concentration profile of the pure rock and clay and their mixtures. The extent of silica removal in each system will determine the dominant surface for silica adsorption. Batch experiments must be performed under conditions similar to those in the dynamic system to obtain the pH and concentration of the solution at equilibrium. The impact of silica removal on an alkali flooding process can then be analyzed by examining how far the pH and concentration of the solutions in dynamic experiment are from the equilibrium conditions.

At temperatures above 100°C, the process of caustic flooding is hindered by the significant lag in high pH breakthrough and by the large number of pore volumes of caustic that must be injected before a high level of pH can be

established throughout the porous medium. As was mentioned earlier, this lag in caustic breakthrough is due to silica removal from solution which consumes the hydroxyl ion. Once the pH breakthrough occurs, a high level of pH exists throughout the porous medium. The results of this work indicate that the concentration of silica in solution must reach a high level before silica removal from solution takes place. In a caustic flooding process, silica enters the solution through a dissolution reaction. It can be postulated that if instead of caustic a saturated alkali silicate solution was injected, dissolution reaction would not occur. However, silica removal from solution would take place similar to the observations of this work. Further studies are needed to examine alkali silicate flooding experiments in a similar set up as in this work, at temperatures above 100°C. The alkali solution must remain saturated with respect to silica. This will require the silicate solution to be prepared at the same pressure and temperature as the experiment. Experiments can be performed in a similar set up as in this work, where a saturated alkaline silicate solution is injected in a pure silica system. The results of such a study will determine the extent of silica removal from solution in a pure silica system as well as the movement of silica and pH fronts in a pure silica system when a saturated alkaline solution is injected.

Jepson's[41] results indicate that at 25°C, silica removal from solution is highest at a pH of 9. Furthermore, silica removal from solution is also dependent on electrolyte concentration. At 25°C, optimum *NaCl* concentration for silica

removal is 2%. Similar data are not available for higher temperatures. In this work, the measured pHs are not true pHs. Since the mechanism of silica removal from solution and the rate of reaction is not known, these measured pHs can not be converted to true pHs. Furthermore, from the results of this study no conclusion can be drawn on the impact of *NaCl* concentration on the silica removal reaction. A series of batch tests should be performed to determine optimum pH and *NaCl* concentration for silica removal at higher temperatures.

The results of this work indicate that a high level of pH can be maintained at temperatures up to 100°C. The lag in caustic breakthrough at these temperatures is not significant. Previous experiments on caustic flooding with residual oil in place were performed in short porous medium and consequently small residence times. Experiments with extended residence time must be performed to examine the oil recovery in these temperatures.

REFERENCES

1. Squires, F.: "Method of Recovering Oil and Gas," U.S. Patent 1,238,3551 (Aug. 28, 1917).

2. Nutting, P.G.: "Chemical Problems in the Water Drilling of Petroleum from Oil Sands," Ind. & Egg. Cem-(1925)17,1035-1036; also "Soda Process for Petroleum Recovery," Oil And Gas J. (1927) 25 NO. 50, 32 and 106; Petroleum Recovery by Soda Processes," ibid (1928) 27 No.22, 146 and 238.

3. Atkinsons, H.: "Recovery of Petroleum from Oil Bearing Sands," U.S. Patent 1,651,311 (Nov. 29, 1927).

4. Robinson, R.J., Bursell, C.G., and Restine, J.L.: "A Caustic Steamflood Pilot-Kern River Field," SPE 6523, Presented at California Regional Meeting of SPE of AIME, Bakersfield, CA (April 1977).

5. Mayer, E.H., Berg, R.L., Carmichael, J.D., Weinbrand, R.M.: "Alkaline Injection for Enhance Oil Recovery - A Status Report," J. of Petroleum Engineering (Jan. 1983) 209-221.

6. Bunge, A. and Radke, C.J.: "Migration of Alkaline Pulses in Reservoir Sands," SPEJ. (Dec. 1982) 998-1012.

7. Reed, M.G.: "Gravel Pack and Formation Sandstone Dissolution During Steam Injection," J of Petroleum Technology (June 1980) 941-949.

8. Dehghani, K.: "Caustic Consumption by Reservoir Rock at Elevated Temperatures," PhD Dissertation, University of Southern California, Los Angeles, CA. (1983).

9. Somerton, W.H. and Radke, C.J.: "Role of Clays in Enhanced Oil Recovery of Petroleum from Some California Sands," J. of Petroleum Technology (March 1983) 643-654.

10. de Zabala, E.F., Vislocky, J.M., Rubin, E., and Radke, C.J.: "A Chemical Theory for Linear Alkaline Flooding," SPEJ. (April 1982) 245-258.

11. Bunge, A.L. and Radke, C.J.: "The Origin of Reversible Hydroxide Uptake on Reservoir Rock," SPE 11798, Presented at the International Symposium of Oilfield and Geothermal Chemistry, Denver, CO, June 1-3, 1983.

12. Bunge, A.L. and Radke, C.J.: "Divalent Ion Exchange With Alkali," SPEJ. (Aug. 1982) 657-668.

13. Jenning, H.Y.Jr.: "A Study of Caustic Solution Crude Oil Interfacial Tension," SPEJ. (June 1975) 197-202.

14. Ramakrishnan, T.S. and Wasan, D.T.: "A Model for Interfacial Activity of Acidic Crude Oil/Caustic System for Alkaline Flooding," SPEJ. (Aug. 1983) 602-612.

15. Nelson, R.C., Lawson, J.B., Thingpen, D.R. and Stegemeier, G.L.: "Cosurfactant - Enhance Alkaline Flooding," Presented at the Fourth SPE/DOE Symposium on Enhance Oil Recovery, Tulsa, April 15-18th, 1984.

16. Holt, P.F., and King, D.T.: "The Chemistry of Silica Surfaces," J. Chem. Soc. (London) (1955)(a), 733.

17. Stober, W.: "Formation of Silica Acid in Aqueous Solution Suspension of Different Silica Modifications," (Equilibrium Concepts in Natural Water Systems), Adv. Chem. Ser. (1967)(67), 1961.

18. Kpeykin, V.A. and Mikhaylov, A.S.: "Solubility and Form of Occurrence of Silica in Normal Dilute Solution," Doklady Academii Nauk SSR, (1970)(191), 917-920.

19. Southwick, J.G.: "Solubility of Silica in Alkaline Solutions; Implications for Alkaline Flooding," SPEJ. (1985)(25), 857-864.

20. Iler, R.K.: The Chemistry of Silica, John Wiley and Sons, New York, (1979).

21. Goto, K., J.: Chem. Soc. Jap. Pure Chem. Sect., 76, 1364 (1955).

22. Sydansk, R.D.: "Elevate-Temperatures Caustic/Sandstone Interaction; Implication for Improving Oil Recovery," SPEJ. (Aug. 1982) 453-462.

23. Van Leir, J.A., de Bruyn, P.L. and Overbeek, J.Th.G.: "The Solubility of Quartz," J.Phys.Chem. (1960) 64(9), 1975.

24. Saneie, S. and Yortsos, Y.C.: "Kinetics of Silica Dissolution and Hydroxyl Ion Consumption In Alkaline Flooding," SPE 17410, Presented at California Regional Meeting of SPE, Long Beach, CA (March 1988).

25. Strelko. V.V.: "On the Dissolution Mechanism of Dispersed Silica," Teor. Eksp. Khim., 100, 359 (1973) [Engl.Trans. p.277].

26. Stober, W.: "Formation of Silica Acid in Aqueous Solution Suspension of Different Silica Modification," (Equilibrium Concepts in Water Systems), Adv.Chem.Ser. (1967)(67), 1061.

27. Ehrlich, R. and Wygal, R.J.Jr.: "Interrelation of Crude Oil and Rock Properties With the Recovery of Oil by Caustic Flooding," SPEJ. (Aug. 1976) 263-270.

28. Mohnot, S.M., Bae, J.H. and Foley W.L.: "A Study of Mineral-Alkali reactions" SPE 13032, Presented at the 59th Annual Technical Conference and Exhibition Of SPE, Texas, September 16-19, 1984.

29. Thornton, S.D. and Lorenz, P.B.: "Role of Silicate and Aluminate Ions in the Reaction of Sodium Hydroxide With Reservoir Minerals," SPE 16277 Presented at the SPE International Symposium on Oilfield Chemistry, San Antonio, Texas, Feb 4-6, 1987.

30. Diallo, M.S., Jenkins-Smith, N.L. and Bunge, A.L.: "Dissolution Rates for Quartz, Aluminum-Bearing Minerals, and Their Mixtures in Sodium and Potassium Hydroxide," SPE 16276, Presented at the SPE International Symposium on Oilfield Chemistry, San Antonio, Texas, February 4-6, 1987.

31. Johnson, J.R.: "Caustic Consumption By Kaolinite At Temperatures to 120°C," M.S. Thesis, University of Alaska, Dec. 1987.

32. Meites, Louis,: Handbook of Analytical Chemistry, New York, McGraw Hill Section 11, Page 7.

33. Torabzadeh, S.J.: "The Effect of Temperature and Interfacial Tension on Water-Oil Relative Permeabilities of Consolidated Sands," PhD Dissertation, University of Southern California (December 1984)

34. Erwing, G.M.: Instrumental Methods of Chemical Analysis, McGraw Hills Book Company (1975).

35. Mac Kenzie, F.T. and Garrels, R.M.: "Silica-Bicarbonate Balance in the Ocean and Early Diagenesis," J. Sediment. Petrol. 36, 1075-1084.

36. Mac Kenzie, F.T., Garrels, R.M., Bricker, D.P. and Bickley, F.: "Silica in Sea Water: Control by Silica Minerals," Science 155, 140401405 (1966).

37. Siever, R., Beck, K.C. and Bernar, R.A.: "Composition of Interstitial Waters of Modern Sediments," J. Geol. 73, 39-73 (1965).

38. Sillen, L.G.: "The Physical Chemistry of Sea Water," Amer. Assoc. Adv. Sci. 67, 549-581 (1961).

39. Siever, R. and Woodford N.: "Sorption of Silica by Clay Minerals," Geochimica et Cosmochimics Acta, 37, 1851-1880 (1973).

40. Iler, R.K.: "Effect of Adsorbed Alumina on the Solubility of Amorphous Silica in Water," Journal of Colloid and Interface Science, 43,399-408,(1973).

41. Jepson, W.B., Jeffs, D.G. and Ferris, A.P.: "The Adsorption of Silica on Gibbsite and Its Relevance to the Kaolinite Surface," Journal of Colloid and Interface Science, 35-2, 454-461, (1976).

*U.S.GPO:1992-761-027/60063

END

DATE FILMED

4/12/93